



OLLSCOIL NA
GAILLIMHE
UNIVERSITY
OF GALWAY



Synthesis and Characterisation of New Metal-organic Frameworks as Carriers of Antibacterial Agents

Aileen Kelly BSc

Supervisor: Dr Constantina Papatriantafyllopoulou

Head of School: Prof. Olivier Thomas

Thesis submitted for the degree of Master of Science

School of Biological and Chemical Sciences

College of Science and Engineering

University of Galway

31st August 2023

Table of Contents

1	Table of Figures	3
2	Table of Tables	5
3	Abbreviations	6
4	Affadavit	7
5	Acknowledgements.....	8
6	Abstract	10
7	Introduction	11
7.1	Metal Organic Frameworks	11
7.2	Secondary Building Units	11
7.3	Organic Linkers.....	13
7.4	Properties.....	15
7.4.1	Porosity	16
7.4.2	Surface Area.....	16
7.4.3	Crystallinity	17
7.5	Synthesis of Metal Organic Frameworks	17
7.5.1	Solvothermal Synthesis.....	18
7.5.2	Microwave Synthesis	19
7.6	Stilbene ligands in MOF synthesis	19
7.7	Mixed Metal MOFs	20
7.8	Biomedical Applications of Metal Organic Frameworks.....	22
7.9	Multi Drug Resistant Tuberculosis	25
7.10	Multimodal MOFs	28
7.10.1	Combined MOF therapeutic delivery	28
8	Aims and Objectives.....	30
9	Results and Discussion	32
9.1	Cyanostilbene dicarboxylic acid synthesis	32
9.2	Compound A	35
9.3	Stilbene tricarboxylic acid synthesis	37
9.4	Azodisalicylic Acid MOFs.....	38
9.4.1	Azodisalicylic Acid Linker	38
9.4.2	Azodisalicylic Acid MOFs.....	40
9.4.3	Copper-Zinc Mixed Metal MOF.....	43
9.4.4	Dissolution Studies.....	47
9.4.5	MOF Activation	49

9.4.6	Antibiotic Encapsulation	50
9.4.7	Antibacterial Assays	59
10	Conclusion & Future work.....	60
11	Experimental	62
11.1	General Synthesis	62
11.2	Tricyanostilbene synthesis.....	62
11.3	Cyanostilbene dicarboxylic acid synthesis	63
11.4	Stilbene tricarboxylate synthesis.....	63
11.5	Compound A synthesis	64
11.6	Azodisalicylic acid ligand synthesis.....	64
11.7	Zn ₂ (AZA) synthesis	65
11.8	Co ₂ (AZA) synthesis	65
11.9	Mg ₂ (AZA) synthesis	65
11.10	Mixed Metal Zn ₂ Cu ₂ (AZA) synthesis.....	65
11.10.1	Solvothermal Synthesis	65
11.10.2	Reflux Heated Synthesis	66
11.11	Microwave Synthesis.....	66
11.12	MOF Activation.....	67
11.13	Isoniazid Encapsulation	67
11.14	Rifampicin Encapsulation	67
11.15	Ciprofloxacin Encapsulation	68
11.16	In-situ Zn ₂ (AZA) rifampicin loading.....	68
11.17	Dissolution studies.....	68
12	Bibliography	70
13	Appendix	74

1 Table of Figures

Figure 1: The assembly of MOF building blocks to form a porous structure. Image made using Biorender.	11
Figure 2: Common SBU geometries. ⁶	12
Figure 3: The various SBU nets afforded by combining different building units and coordination numbers are illustrated. ⁸	13
Figure 4: The bdc ligand has been extended using aromatic rings, thus increasing overall porosity of the MOF. Image made using Chemdraw.	13
Figure 5: Interpenetration of multiple MOFs, reducing the pore sizes. ¹¹	14
Figure 6: Multidentate ligands used in the synthesis of MOFs. ¹³	14
Figure 7: The synthesis of a MOF using solvothermal techniques, followed by the removal of solvent guest molecules resulting in the activated MOF. ²³	19
Figure 8: Microwave assisted MOF synthesis. ²⁴	19
Figure 9: <i>Trans-cis</i> isomerisation of stilbene ligand.....	20
Figure 10: The synthesis of a Mixed Metal MOF using different metal precursors, resulting in the formation of a heterometallic, synergistic MOF. ²⁷	21
Figure 11: Some of the most commonly used DDS, including micelles, liposomes, dendrimers and mesoporous silica. ⁴⁰	23
Figure 12: The larger BET surface area and pore volumes attributed to MOF's enables a far superior inulin loading in comparison to that of mesoporous silica. ⁴¹	24
Figure 13: Structure of Isoniazid. Made using Chemdraw.....	26
Figure 14: Structure of Rifampicin. Made using Chemdraw.....	27
Figure 15: Structure of Ciprofloxacin. Made using Chemdraw.....	27
Figure 16: Combined delivery system; MOF made up of three different APIs with antimicrobial properties. ⁵²	28
Figure 17: Scheme of the metabolism of olasalazine to PAS. Made using Chemdraw.	29
Figure 18: Structure of Azodisalicylic acid. Made using Chemdraw.	31
Figure 19: The synthesis of tricyanostilbene. This condensation reaction of 4-formyl benzonitrile and 4-cyanophenylacetonitrile at 130°C, with the addition of piperidine to precipitate the tricyanostilbene ligand.....	32
Figure 20: The synthesis of cyanostilbene dicarboxylic acid. The hydrolysis of the precursor tricyanostilbene at 130°C, with the addition of acetic acid in excess and a catalytic amount of sulfuric acid to precipitate the cyanostilbene dicarboxylic acid ligand.	33
Figure 21: IR spectrum of cyanostilbene dicarboxylic acid ligand.	33
Figure 22: The ¹ H NMR obtained from the synthesis of cyanostilbene dicarboxylic acid, with DMSO-d ₆ used as a solvent.	34
Figure 23: IR of Compound A pre-cooling.....	36
Figure 24: IR of Compound A post-cooling.	36
Figure 25: Scheme of the hydrolysis of the nitrile group in cyanostilbene dicarboxylic acid to form the ligand stilbene tricarboxylic acid.....	37
Figure 26: Needle crystals of stilbene tricarboxylic acid under the microscope (x 10 magnification) ..	37
Figure 27: The IR spectrum of stilbene tricarboxylic acid compared to cyanostilbene dicarboxylic acid.	38
Figure 28: Metabolic degradation pathway of Azodisalicylic acid via Azoreductase to the prodrug PAS	39
Figure 30: IR spectrum of AZA linker.	40
Figure 31: PXRD patterns of Mg ₂ (AZA), Zn ₂ (AZA), Co ₂ (AZA) and Cu ₂ (AZA). ⁶²	40

Figure 32: The crystal structure of Mg ₂ (AZA) along 001 crystallographic axis, and its rod SBU on the right. ⁶²	41
Figure 33: IR spectra of Mg ₂ (AZA), Zn ₂ (AZA), Cu ₂ (AZA) and Co ₂ (AZA) respectively.	42
Figure 34: Graph indicating the % prodrug release of Zn ₂ (AZA) and Cu ₂ (AZA) in both water and PBS over 72 hours. ⁶²	43
Figure 35: The EDX spectrum and data for solvothermally synthesised Zn:Cu 3:1.	44
Figure 36: Elemental mapping and EDX data for refluxed Zn:Cu 3:1.....	46
Figure 37: Elemental mapping and EDX data for refluxed Zn:Cu 4:1.....	46
Figure 38: Dissolution of 3:1:1 zinc and copper sample in water over 1 hour.	48
Figure 39: Dissolution of 4:1:1 zinc and copper sample in water over 1 hour.	48
Figure 40: Dissolution of 3:1:1 zinc and copper sample in PBS over 1 hour.....	49
Figure 41: Dissolution of 4:1:1 zinc and copper sample in PBS over 1 hour.....	49
Figure 42: ¹ H NMR of isoniazid in DMSO-d ₆ and DCl.	51
Figure 43: ¹ H NMR of Zn ₂ (AZA) loaded with isoniazid, solvents used were DMSO-d ₆ and DCl.	51
Figure 44: ¹ H NMR of Mg ₂ (AZA) loaded with isoniazid, solvents used were DMSO-d ₆ and DCl.	52
Figure 45: ¹ H NMR of Co ₂ (AZA) after undergoing isoniazid loading, solvents used were DMSO-d ₆ and DCl.....	52
Figure 46: ¹ H NMR of rifampicin in DMSO-d ₆	54
Figure 47: ¹ H NMR of Zn ₂ (AZA) rifampicin loading, solvents used were DMSO-d ₆ and DCl.	54
Figure 48: ¹ H NMR of Zn ₂ (AZA) in situ rifampicin loading, solvents used were DMSO-d ₆ and DCl.....	55
Figure 49: ¹ H NMR of Mg ₂ (AZA) rifampicin loading, solvents used were DMSO-d ₆ and DCl.	55
Figure 50: ¹ H NMR of Co ₂ (AZA) rifampicin loading, solvents used were DMSO-d ₆ and DCl.	56
Figure 51: ¹ H NMR of ciprofloxacin, solvents used were DMSO-d ₆ and DCl.....	57
Figure 52: ¹ H NMR of Zn ₂ (AZA) ciprofloxacin loading, solvents used were DMSO-d ₆ and DCl.....	57
Figure 53: ¹ H NMR of Mg ₂ (AZA) ciprofloxacin loading, solvents used were DMSO-d ₆ and DCl.	58
Figure 54: ¹ H NMR of Co ₂ (AZA) ciprofloxacin loading, solvents used were DMSO-d ₆ and DCl.	58
Figure 55: ¹ H NMR on tricyanostilbene in d-CDCl ₃	74
Figure 56: IR spectra of tricyanostilbene ligand.	74
Figure 57: ¹ H NMR of AZA linker, using DMSO-d ₆ as solvent. ⁶²	75
Figure 58: SEM image of solvothermally synthesised 3:1:1 zinc to copper to AZA.	75
Figure 59: SEM image of solvothermally synthesised 4:1:1 zinc to copper to AZA.	76
Figure 60: SEM image of solvothermally synthesised 5:1:1 zinc to copper to AZA.	76
Figure 61: SEM image of solvothermally synthesised 6:1:1 zinc to copper to AZA.	76
Figure 62: IR spectrum of mixed metal 3:1 zinc and copper MOF synthesised under reflux.	77
Figure 63: IR spectrum of mixed metal 4:1 zinc and copper MOF synthesised under reflux.	77
Figure 64: IR spectrum of mixed metal 5:1 zinc and copper MOF synthesised under reflux.	77
Figure 65: IR spectrum of mixed metal 6:1 zinc and copper MOF synthesised under reflux.	78
Figure 66: The IR spectra of microwave synthesised 3:1:1 zinc to copper to AZA, from 30 mins to 120 mins.....	78
Figure 67: Elemental mapping of Microwave synthesised 3:1:1 zinc to copper to AZA, 1 hour.	79
Figure 68: Elemental mapping of Microwave synthesised 3:1:1 zinc to copper to AZA, 1.5 hours.	79
Figure 69: Elemental mapping of Microwave synthesised 3:1:1 zinc to copper to AZA, 2 hours.	79
Figure 70: Solid state UV/Vis spectra carried out on the 3:1:1 zinc to copper to AZA 2 hour microwave synthesis, alongside that of the AZA ligand, and both metal sources.	80

2 Table of Tables

Table 1: Parameters and synthesis conditions trialled during attempted MOF synthesis using cyanostilbene dicarboxylic acid.	35
Table 2: Unit cell parameters of AZA MOFs. ⁶²	41
Table 3: The % abundance of zinc and copper present in each refluxed mixed metal sample.....	45
Table 4: The growth of <i>P. aeruginosa</i> and <i>S. aureus</i> after 18 hours of exposure to each sample. ⁶²	59
Table 5 Instrument Information	62

3 Abbreviations

MOF	Metal Organic Framework
SBU	Secondary Building Unit
bcc	Body centred cubic
pcu	Primitive cubic unit
bdc	Benzene-1,4-dicarboxylic acid
BPY	Bipyridine
BET	Brunner-Emmett-Teller
XRD	Single crystal X-ray diffraction
PXRD	Powder x-ray diffraction
TGA	Thermo gravimetric analysis
DMF	Dimethylformamide
DEF	Diethyl formamide
DMA	Dimethylacetamide
NMP	N- Methyl-2-pyrrolidone
IRMOF	Isorecticular Metal organic framework
MM MOF	Mixed metal Metal organic framework
PSM	Post synthetic modification
WHO	World Health Organisation
DDS	Drug Delivery System
API	Active Pharmaceutical Ingredient
MDR TB	Multi Drug Resistant Tuberculosis
XRD TB	Extensively Drug Resistant Tuberculosis
RNA	Ribonucleic acid
DNA	Deoxyribonucleic acid
PAS	Para-Aminosalicylic acid
AZA	Azodisalicylic acid
UV	Ultraviolet
NMR	Nuclear Magnetic Resonance
IR	Infrared Microscopy
DMSO	Dimethyl Sulfoxide
PBS	Phosphate Buffer Solution
EDX	Energy Dispersive Xray
SEM	Scanning Electron Microscopy

4 Affidavit

Student Declaration on Plagiarism, Collusion or Copying

This declaration is to be completed and signed by the student. It must be included in the essay, first and final draft of the project reports.

I declare that this material, which I now submit for assessment, is my own work and that any assistance I received in its preparation is fully acknowledged and disclosed in the document. To the best of my knowledge and belief, all sources have been properly acknowledged, and the assessment task contains no plagiarism.

I understand that plagiarism, collusion, and/or copying are grave and serious offences and am aware that penalties could include a zero mark for this assessment, suspension or expulsion from NUI Galway. I have read the NUI Galway code of practice regarding plagiarism at www.nuigalway.ie/plagiarism.

I acknowledge that this assessment submission may be transferred and stored in a database for the purposes of data-matching to help detect plagiarism. I declare that this document was prepared by me for the purpose of partial fulfilment of requirements for the programme for which I am registered with the AUA. I also declare that this assignment, or any part of it, has not been previously submitted by me or any other person for assessment on this or any other course of study or another college.

A handwritten signature in black ink, reading "Aileen Kelly", is written over a horizontal dashed line.

Signed: Aileen Kelly

Date: 31st of August 2023

5 Acknowledgements

Firstly, I would like to thank my supervisor Dr Constantina Papatriantafyllopoulou for the help and support she gave me throughout my masters. Her knowledge and input was invaluable and she helped me to improve my chemistry skills and knowledge exponentially over the year. I am extremely grateful for the understanding and patience she had, and I really appreciate the time she dedicated to meetings, and corrections throughout the year, especially in the last few months, despite her busy schedule.

I would like to thank all the members, past and present of Galway Porous Materials. Darragh was a fantastic mentor to me in the lab and a great friend outside of it. I am incredibly thankful for how generous he was with his time in helping me whenever I needed it. I will miss our lab discussions and coffee breaks and everything in between dearly. I also want to thank Ahmed, who provided the lab with immense knowledge and many laughs. He was a fantastic help, despite being so busy when finishing up. I would like to thank Foteini, for being a lovely lab mate who always brought a positive atmosphere to the lab and was great help whenever I had any questions. I would also like to thank previous members of the group, Emily, Mona, and Waleed.

Thanks to Dr Constantinos Efthymiou for being so open to help with any questions I had throughout my masters and for always being such a friendly and welcoming person whenever our paths crossed on campus.

I would like to thank Lamis who was a great help in running any XRD samples. I enjoyed all our coffees and chats whenever we needed a break from the lab. I also want to thank Seán for his help in running solid state UV/Vis and for all of his help, and musical writing inspiration for my thesis.

Grazie mille to Federica, Karolina and Simona for all of the coffees and laughs we shared throughout the year. I was lucky to be surrounded by such supportive and kind friends.

Thank you to the academic and technical staff and to the School of Biological and Chemical Sciences, for their hard work they put into everything throughout the year.

I would like to extend a huge thanks to all of my fellow postgraduate students. From Carna to Cologne, Westport to Wednesday pints - the year was full of great memories. I wish you all the best in the remainder of your studies.

Big thanks to all of my housemates- past and present, and all of my friends, who always were there for me through all ups and downs, and for the 5 star dinners that were waiting for me at home after a long day.

I want to thank my parents, my sisters, and Monty, for the continued support and encouragement they gave me throughout the year, and for always being there when I needed it.

6 Abstract

Metal Organic Frameworks are highly porous, crystalline materials that have been used for a multitude of applications, with drug delivery and sensing at the forefront. These frameworks are extremely versatile and can be applied to multimodal applications, allowing for combined therapies and treatments to be developed.

In this project, multimodal MOFs and mixed metal MOFs capable of antibacterial significance and a novel organic linker with the capability to form a theranostic MOF for luminescence and drug delivery was synthesised.

Multi Drug Resistant Tuberculosis (MDR TB) is a disease that has become a threat to global health, killing 1.6 million people yearly thus being the second leading cause of human death via infectious disease. First and second line therapies are beginning to lose their efficacy as more drug resistant strains are on the rise. Additionally, the drugs that are currently on the market to treat MDR TB entail solubility issues, side effects and undergo rapid metabolism. To overcome the API issues alongside preventing the development of drug resistance, the multimodal MOFs, $[Zn_2(AZA)]$, $[Mg_2(AZA)]$ and $[Co_2(AZA)]$, were synthesised. These MOFs combined a prodrug organic linker azodisalicylic acid (AZA) as the organic component of the MOF, the antimicrobial metals Zn^{2+} , Mg^{2+} , Co^{2+} & Cu^{2+} and the APIs isoniazid, rifampicin, and ciprofloxacin. The MOFs successfully encapsulated isoniazid and ciprofloxacin and antibacterial assays were performed.

A mixed metal MOF, $[Zn_2Cu_2AZA]$, using the AZA prodrug linker and the metals Zn^{2+} and Cu^{2+} was synthesised. These metals were chosen in the hopes of achieving a controlled release of drug, while also combining the synergistic antimicrobial properties of each metal. These MOFs are currently undergoing MIC antibacterial studies to determine their efficacy.

A stilbene-based ligand, cyanostilbene dicarboxylic acid, was synthesised with the potential of synthesising a MOF capable of both chemotherapeutic delivery and bioimaging. Alongside this, a second stilbene linker stilbene tricarboxylic acid was synthesised with the aim to produce a highly porous MOF capable of high drug loading and luminescence.

7 Introduction

7.1 Metal Organic Frameworks

Metal-organic frameworks (MOFs) are a class of porous, crystalline materials that have emerged as a platform for many promising biomedical and environmental applications, with drug delivery, catalysis, sensing and gas storage at the forefront.¹ This array of applications owes largely to their highly desirable properties, including stability, high surface area, porosity and facile synthesis.¹ The term “Metal Organic Framework” was first coined in a paper by Yaghi in 1999, who reported the synthesis of MOF-5, which acted as a blueprint for the decades of research on MOFs that followed.² MOFs are composed of two main building blocks, shown in Figure 1. The first are inorganic metal clusters, also known as secondary building units (SBUs). The second are organic ligands, which act to bridge the SBUs to form a highly robust porous framework. The choice of both metal source and organic linker can have a significant influence on the structure and properties of the MOF.³

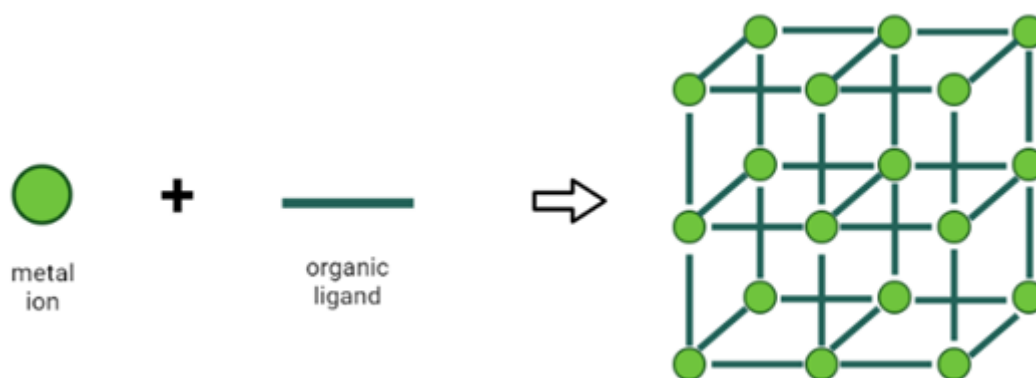


Figure 1: The assembly of MOF building blocks to form a porous structure. Image made using Biorender.

7.2 Secondary Building Units

Secondary building units (SBUs) are inorganic metal clusters with specific coordination modes which allow them to be bridged by polytopic ligands to form porous networks.⁴ Polytopic ligands are a diverse range of ligands varying from ditopic to hexatopic and can contain various different functional groups.⁵ These are used as they can aggregate the metal ions to form an SBU, whereby the individual ions are secured into the cluster formation, thus coordinating with multiple bridging ligands to allow the assembly of a porous framework.⁴

SBUs are responsible for determining the overall structure and topology of a MOF. Depending on the geometry of the linker and its binding mode, an SBU can have different geometries, including square planar, trigonal, tetrahedral and paddlewheel.³ An example of common SBU geometries is observed in Figure 2.

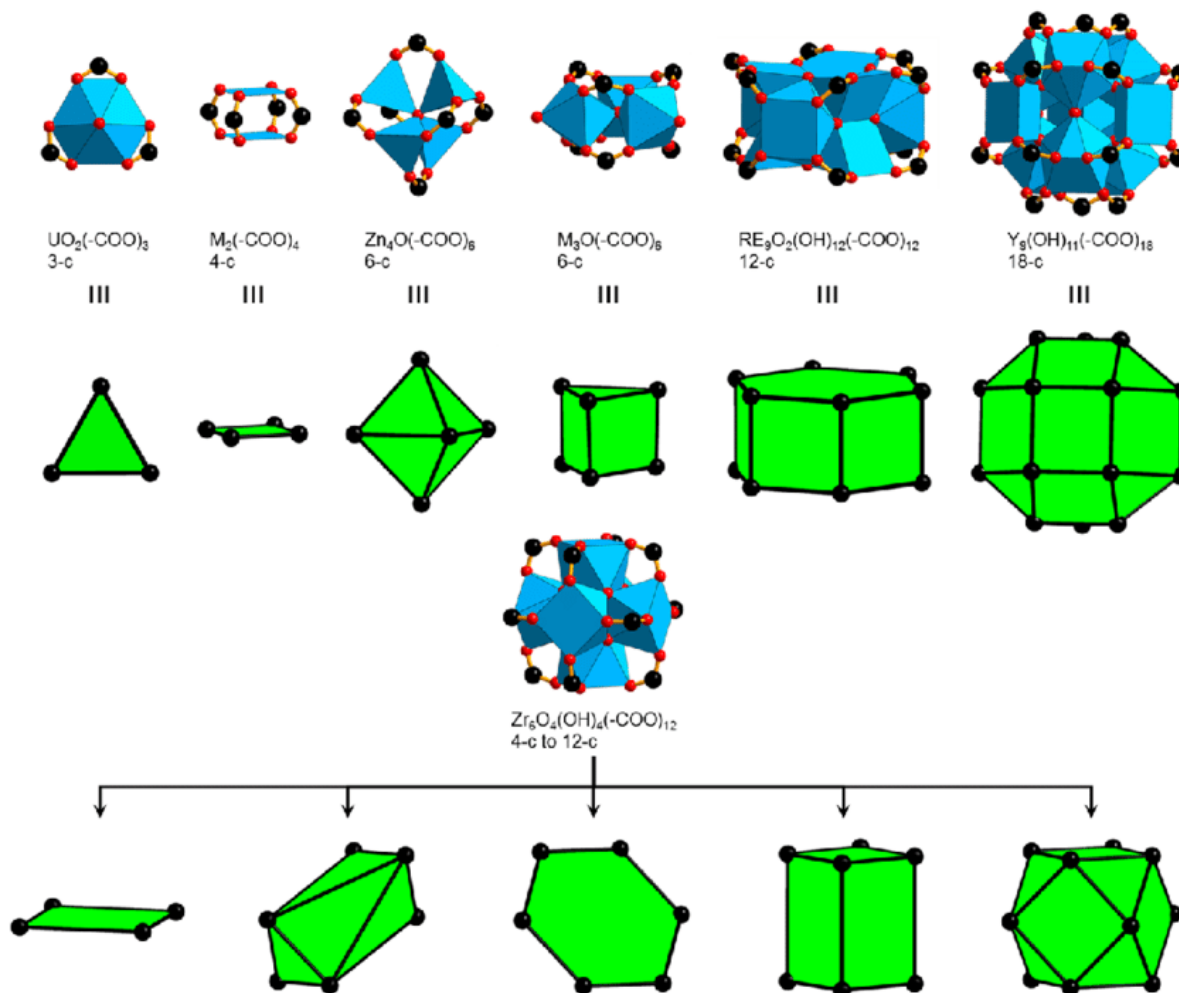


Figure 2: Common SBU geometries.⁶

Likewise, the coordination number of metals and ligands used can influence the topology of the SBU.⁷ An SBU with a coordination number of 8 may form a body-centred cubic net (bcc), whereas one with 6 may bind octahedrally with a primitive cubic net (pcu), shown in Figure 3.⁷

Building unit 1 \ Building unit 2	2-c Linear	3-c Triangle	4-c Square	4-c tet	6-c Hexagon	6-c oct
3-c Triangle	<i>srs</i>	<i>bwt, pyo, srs-b, ths-b</i>	<i>fjh, fmj, gee, iab, yac, yao</i>	<i>asn, ept, ofp</i>	<i>cys, dnf*</i>	<i>anh, ant, apo, brk, cep*, cmi, czz, eee, qom, rli, tsx, zzz</i>
4-c Square	<i>nbo, lvt, rhr</i>	<i>pto, tbo</i>	<i>cev, cdl, cdm, cdn, cds, cdz, mot, muo, qdl, qzd, ssd, sse, ssf, sst</i>	<i>pts</i>	<i>nts</i>	<i>myd, ybh</i>
4-c tet	<i>dia, lcs, qtz, sod</i>	<i>bor, ctn</i>	<i>fgl, mog, pds, pth, pli, ptr, ptt</i>	<i>bni, byl, cag, cbt, coe, crb, fel, icm, kea, lon, pcl, qtz-b, sca, tpd, ucn</i>	-	<i>alw, bix, cor, ing, spl, toc</i>
6-c Hexagon	<i>hxg</i>	<i>cys, dnf</i>	<i>she</i>	-	<i>hxg-b</i>	-
6-c oct	<i>pcu, bcs, crs, reo</i>	<i>pyr, spn</i>	<i>soc</i>	<i>gar, iac, ibd, toc</i>	-	<i>pcu-b, bcs-b</i>

Figure 3: The various SBU nets afforded by combining different building units and coordination numbers are illustrated.⁸

7.3 Organic Linkers

The properties of MOFs can be dictated by the organic linkers used in the structure i.e., the pore sizes of the framework may be adjusted by altering the length of the ligand used in synthesis.⁹ Through means of increasing the ligand length, pore volume and surface area can be increased as illustrated in Figure 4.⁹ However, interpenetration may occur upon coordination, whereby multiple networks can intertwine with one another, thus reducing the pore sizes of the MOF, this is illustrated in Figure 5.¹⁰

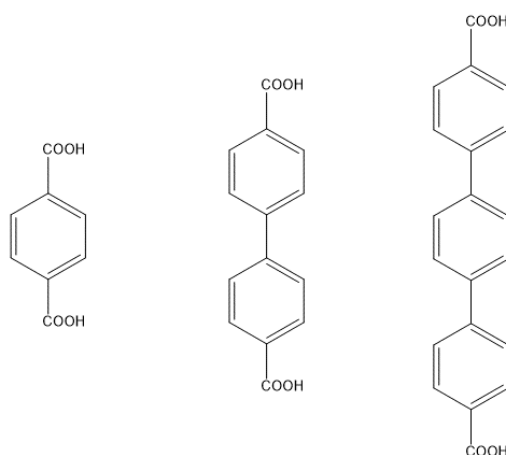


Figure 4: The bdc ligand has been extended using aromatic rings, thus increasing overall porosity of the MOF. Image made using Chemdraw.

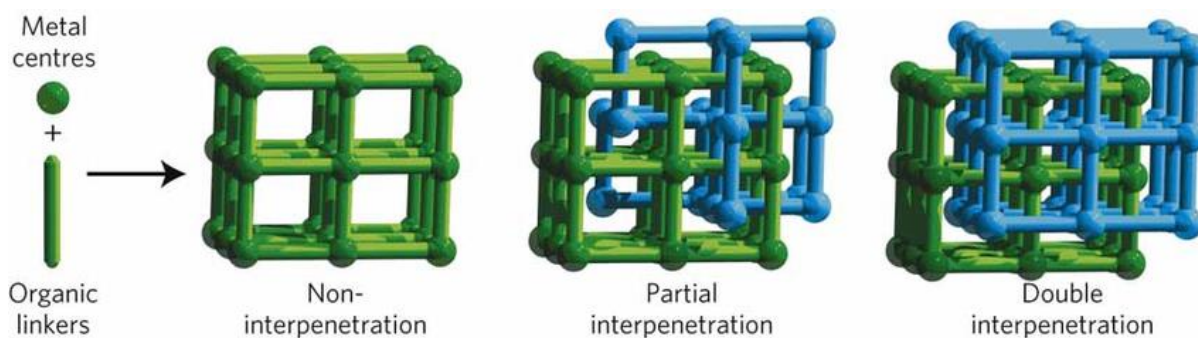


Figure 5: Interpenetration of multiple MOFs, reducing the pore sizes.¹¹

Multidentate polytopic linkers, illustrated in Figure 6, are favoured over their counterparts with lesser binding affinity. This provides a superior strength to the bonds within the framework resulting in increased stability for the overall structure⁴. Carboxylate linkers, in particular, are highly utilised in MOF synthesis for this reason⁴. These linkers were deemed superior as they are readily deprotonated, thus removing the requirement of a counter ion. Additionally, the linker inputs the chelation of metal clusters to form defined net vertices in metal-oxygen-carbon clusters¹².

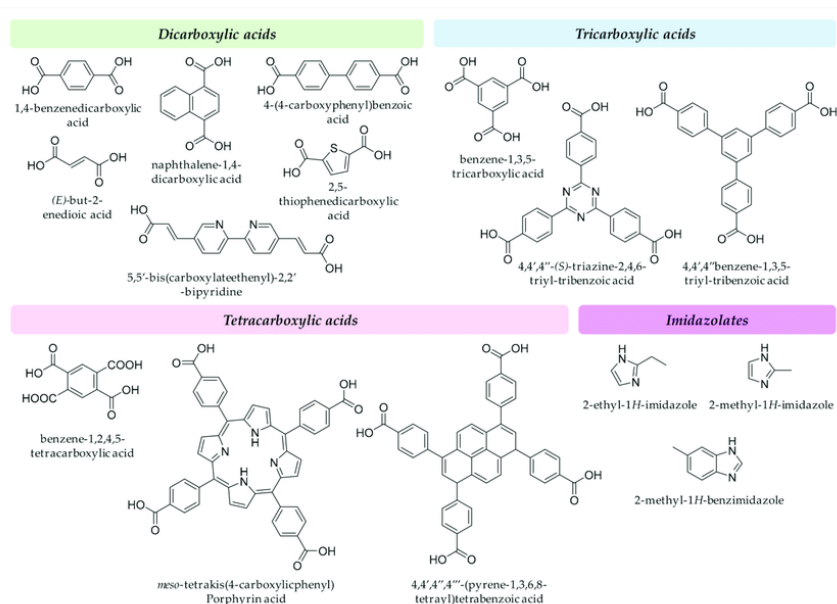


Figure 6: Multidentate ligands used in the synthesis of MOFs.¹³

Additionally, the substitution of different functional groups on the ligand can alter properties such as selectivity and stability.⁹ Neutral N-bound ligands containing functional groups such as pyridine, benzene, and nitrile have been used, with 4,4-bipyridine (BPY) being a common example. This ligand has given rise to the synthesis of a multitude of MOFs with square,

hexagonal, diamond and even bilayer nets.¹² The coordination of this linker forms structures that depend on the coordination geometry of the SBUs and the number of coordination sites that have been blocked by ligands.¹² However, this class of linker comes with downsides. Due to the ligands neutral charge, the introduction of a counter ion is essential in its coordination.¹² Alongside this, once coordinated, the frameworks thermal stability is often inadequate, with the MOF degrading upon attempted activation.¹² This is a process post synthesis where heat is used to evaporate the solvent guest molecules within the pores. The weak bonds between the N-bound ligands and metal clusters are often responsible for this lack of stability and robustness to the structure.^{7,12}

7.4 Properties

MOFs are often likened to other hybrid materials and coordination polymers such as zeolites.¹⁴ Zeolites, in both their natural and synthetic forms, are crystalline porous materials with repeating units and have been used in several applications including catalysis, drug delivery and gas storage.¹⁴ The zeolite utilizes its nano-porous structure by adsorbing and separating gas and other impurities.¹⁴ Despite these advantages, zeolites still retain an array of limitations and drawbacks, preventing the full research potential for porous materials such as these to be achieved. These include the considerably small collection of topologies, leading to a limited range of possibility and flexibility of structures. In addition, the lack of control surrounding both the synthesis of the materials, alongside their rigid, fixed nature, makes post synthetic modifications difficult.¹⁴ The introduction of MOFs to material chemistry provides a solution to many of the issues faced by materials such as synthetic zeolites.¹⁴

There are many characteristics owing to MOFs that make them largely superior to their analogous counterparts. Their highly tuneable nano-porous structure and highly populated library of potential building blocks allows for a wide variety of structures and topologies, unique to those of zeolites.¹⁴ Alongside this, it is possible to maintain control over the structure of the MOF using different synthetic approaches, those of which include post synthetic modification, solvothermal synthesis and hydrothermal synthesis.¹⁴ These desirable traits give MOFs integral structural stability, flexibility alongside a high surface area, making them ideal for applications that require such qualities, i.e., drug delivery and gas absorption.⁹

The flexible bonds attributed to MOF structure allows for structural changes under different external impulses i.e. temperature, electric field and light, allowing for it to be utilized in sensing and fluorescence.¹⁴ MOFs also outperform zeolites in their pore volume, allowing their use in catalysis of larger molecules, where the pore volumes of zeolites would have been rendered too small for this purpose.⁹

7.4.1 Porosity

MOFs are highly porous materials, with at least 50% of the total MOF volume owing to the volume of the pores.⁹ These pores are occupied by solvent guest molecules, however upon activation these are evacuated from the pores. In this activation step, the importance of the building block implementation is emphasized because if the structure is not stable enough, it may collapse. However, if the MOF is unbroken by the activation process, it gains a permanent porosity.³ This feature is characteristic of a MOF utilized for gas storage, the removal of impurities and solvent removal.³ MOFs can be described as microporous, mesoporous, or macroporous, with pore sizes falling between < 2 nm, $2\text{--}50$ nm and >50 nm respectively.¹⁰ A MOF with microporosity will be favored for gas storage due to the stability it encompasses and the interactions between gas molecules in the smaller pore areas.³

7.4.2 Surface Area

The distinct large surface area of MOFs is a defining feature in their superiority to other analogous porous structures.⁹ The surface areas of MOFs can range anywhere between $1000\text{--}10,000$ $\text{m}^2 \text{g}^{-1}$.⁹ The largest MOF surface area known to date was reported by Farha *et al.* in Northwestern University, Illinois with NU-110, having a BET surface area of 7140 $\text{m}^2 \text{g}^{-1}$, and pore volume of 4.40 $\text{cm}^3 \text{g}^{-1}$.¹⁵ The surface area of a MOF may be defined by implementing the Brunauer Emmett Teller (BET) and Langmuir methods, whereby the surface area available for gas particle adsorption is determined.^{9,16} BET surface areas are applied to nitrogen adsorption isotherms at 77 K and measure the surface in a multilayer adsorption fashion.¹⁷ Alternatively, the Langmuir methodology is based on the assumption that monolayer adsorption occurs on uniform surfaces and relies on the Langmuir binding constant.¹⁸ The BET method is preferred over Langmuir for MOF surface area measurements, however both may be used.¹⁸

7.4.3 Crystallinity

Several attractive qualities displayed by MOFs (defined geometry, predictability in topology, dimension etc.) are all owing to the integral crystallinity of the structure. Many parameters must be considered in MOF synthesis to allow for the formation of crystalline material, including temperature, pH, pressure, solvent, reaction time and concentration. These factors must be adjusted to achieve the ideal concentration gradient, thus exceeding the critical nucleation gradient and surpassing any barriers to crystallization.^{12, 14} The crystalline nature of MOFs enables their characterization using a multitude of crystallographic instrumentations i.e., single crystal X-ray diffraction (XRD) and powder X-ray diffraction (PXRD). Thus, a common goal for MOF synthesis is to achieve well defined single crystals for a detailed structural analysis.¹² Because of their crystallinity, MOFs are often stable in extremely high temperatures, the degradation of which can be measured using the destructive technique thermogravimetric analysis (TGA). Here the crystalline material is burned at decomposition temperatures ranging from 20-800 °C, and the weight loss of different components are illustrated as plateaus on the graphed data.¹²

7.5 Synthesis of Metal Organic Frameworks

Many factors must be considered in the synthesis of MOFs. Parameters including solvent, temperature, pH, pressure, metal : ligand ratio, and reaction time.¹⁴ In general, however, most synthesis methods follow a similar approach to achieve MOF crystals.¹⁴ A suitable solvent in which both ligand and metal are soluble is chosen. Common solvents for MOF synthesis include dimethylformamide (DMF), diethyl formamide (DEF), dimethylacetamide (DMA), N-Methyl-2-pyrrolidone (NMP). These solvents are favoured due to their high boiling points and their ability to dissolve many different organic linkers and metal salts.¹⁴ Solvents may also be layered in synthesis to achieve the correct concentration gradient required.¹⁴ Different solvents are used because there is evidence that adjusting solvents can alter MOFs to have more desirable structures and properties.¹⁹ Some solvents can also provide a “greener” synthetic route.²⁰ Normally, high temperatures are used, however in some instances, a MOF may even form at room temperature. Lastly, different molar ratios of metal

to ligand are investigated to find the ideal concentration for crystallization. Different metal salts are often used to repeat the same experiment as different metals have different nucleation rates.²¹

In recent years a library of MOFs using an impressive variety of ligands and metal clusters have been developed. Thus, iso-reticular synthesis has seen an increase due to the advantages of following the conditions of MOFs with similar building units to achieve the desired results. This often leads to the synthesis of a range of MOFs with similar structures and enhanced properties, known as the IRMOF family.²² The most common methodologies for MOF synthesis are as follows: Solvothermal synthesis, microwave synthesis, sonochemical synthesis, electrochemical synthesis and mechanochemical synthesis; the first two of which will be explored in more detail.¹⁴

7.5.1 Solvothermal Synthesis

Solvothermal synthesis is the most favoured method of synthesis as it generally produces high yields of a well-defined, crystalline product. The organic linker and metal salt are both added to the solvent and dissolved using sonication sequentially. The reaction may be heated above the boiling point of the solvent used as this can further promote the growth of a crystalline product. This synthesis may be carried out in sealed vials or autoclave equipment where pressure is allowed to safely build.⁹ The solvothermal process often requires many minor changes in different parameters to optimize the quality of crystals obtained, resulting in screening studies to produce the ideal conditions. As mentioned before, mixed solvents may be added or layered to tune the polarity or pH of the reaction.¹² The layering is then followed by solvent exchange whereby the MOF is soaked in a suitable solvent with a lower boiling point, after which the MOF is then activated using high temperature to evaporate the solvent guest molecules within the pores, as illustrated in Figure 7.

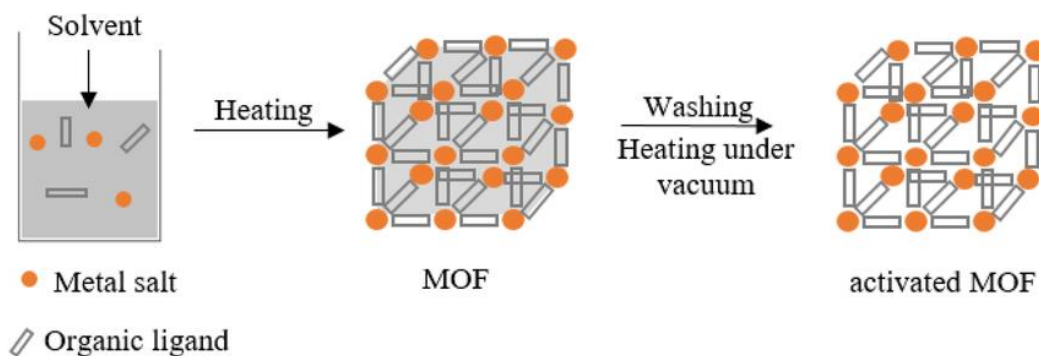


Figure 7: The synthesis of a MOF using solvothermal techniques, followed by the removal of solvent guest molecules resulting in the activated MOF.²³

7.5.2 Microwave Synthesis

Microwave synthesis follows a similar methodology to that of solvothermal synthesis. In this case, the building blocks are once again dissolved in sequential order in a chosen solvent. However, they are heated using microwave instrumentation with electromagnetic radiation, shown in Figure 8.⁹ This method heats through the electric current generated in a solution. Due to its ability to reach high temperatures rapidly, microwave synthesis often reduces reaction times, thereby making the synthesis “greener”. This also results in higher yields as this system is highly reactive⁹.

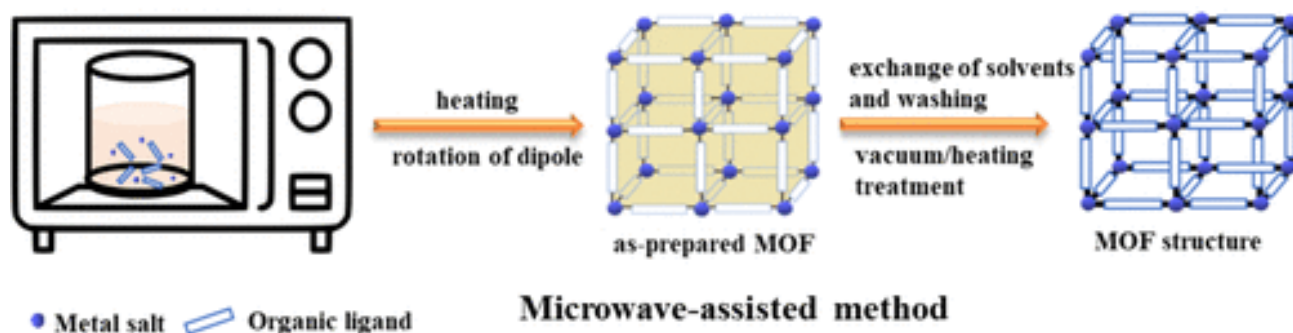


Figure 8: Microwave assisted MOF synthesis.²⁴

7.6 Stilbene ligands in MOF synthesis

Stilbenes are ligands well known for their luminescent properties.²⁵ This occurs as the *trans-cis* isomerization of stilbene derived ligands can be triggered using light as an external

stimulus, i.e., photoisomerization.²⁶ This isomerization is shown in Figure 9. Stilbenes have been commonly implemented as building blocks in MOF synthesis as the ligands photoluminescence can give rise to sensing applications.²⁵ Alongside this, the structure of the stilbene ligands, particularly in their *trans* state can give rise to highly porous, non-interpenetrating frameworks which can pertain to high loading capacities.²⁵ The luminescent properties, and quantum yields of these ligands can be greatly reduced when undergoing constant isomerization. However, this can be suppressed through the incorporation of a functional group on the central ethylene bond of the stilbene, whereby the *trans* isomer of the stilbene is effectively “locked” in place.²⁵ Alongside this, the *trans* isomer is given further rigidity upon coordination of stilbene based ligands with metal clusters in a MOF structure.³ This locking effect is particularly advantageous as it can increase the emission lifetimes of these photoluminescent stilbene ligands coordinated in the framework compared to ligand in solution.³ Because of these properties, stilbenes are widely used in sensory applications.²⁵

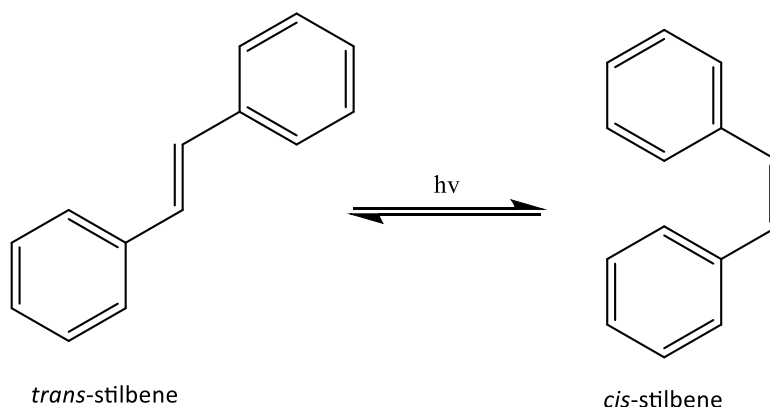


Figure 9: *Trans-cis* isomerisation of stilbene ligand.

7.7 Mixed Metal MOFs

Mixed metal MOFs (MM-MOFs) are MOFs that encompass multiple different metals within their structure.²⁷ MM-MOFs are highly advantageous due to the synergistic effects gained when combined metal sources are used in the framework. They often demonstrate improved functionality compared to their homometallic counterparts in applications, of which include biomedical, gas storage and catalysis.^{27,28} Alongside this, the presence of more than one metal source can improve the stability and the bio relevance of the structure.²⁷ MM-MOFs have

been known to produce original topologies with an improved metal node density, while also forming a tiered channel that encourages the interaction forces of molecules in the framework.²⁹

The synthesis of MM-MOFs follows the same routes of methodology as that for single-metal MOFs, with the main difference being the multiple metal sources added sequentially.²⁷ One-pot solvothermal and microwave methods are often the most implemented for MM-MOF synthesis.²⁷ This is shown in Figure 10. These methods are favoured due to their simple procedures and minimal steps required. However, an issue that presents itself when following this method is the inconstant metal distribution and coordination in the structure.²⁷ This can be overcome by carefully choosing compatible metal ions for synthesis as well as including suitable parameters.²⁷ Another synthesis method is trans metalation whereby a single-metal MOF includes another metal into its structure post synthesis through post-synthetic modification (PSM).^{27,30}

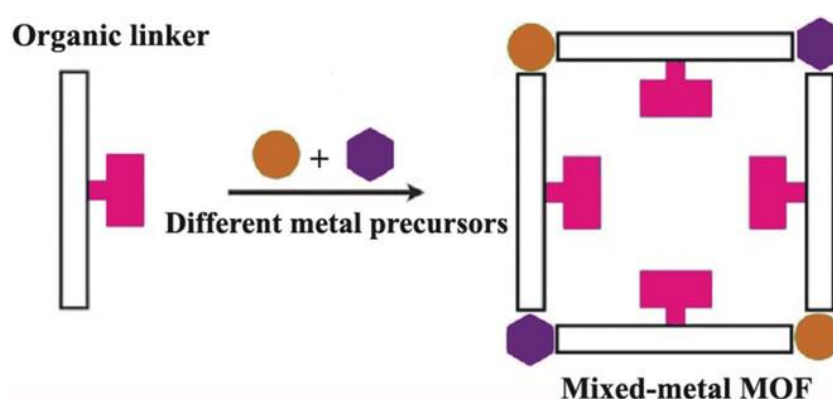


Figure 10: The synthesis of a Mixed Metal MOF using different metal precursors, resulting in the formation of a heterometallic, synergistic MOF.²⁷

Metal ions are often known for their roles in biological processes i.e. wound repair, metabolism and antioxidation.²⁸ Many metals also exhibit significant antimicrobial properties.³¹ The incorporation of multiple metals in a MOF could thus result in a synergistic effect whereby the combined properties of two different metals provide substantially more antibacterial activity than that of a homometallic MOF containing either metal alone.³¹ By using biorelevant metals in the framework, the biocompatibility of the MOF will also be maintained.^{28,32} Metal ions such as copper, iron, magnesium and zinc are all known for their

important roles in cellular functions.³³ Zinc holds a significant relevance in biological systems, in particular the immune system where it is utilized by cells to kill bacteria.³² On the other hand, copper has a key role in the body's immune and inflammatory system responses.^{28,32} Zinc in particular is accredited for its biocompatibility, as very high concentrations can be administered with no toxic effects.³³ The average composition of zinc in the human body is ~2.3 g, and ~0.072 g for the less abundant copper.³³ Although some metals may prove to be toxic at high doses i.e. copper, with controlled release and synergistic effects from other more non-toxic metals, the biocompatibility of the approach may be sustained.^{28,34}

7.8 Biomedical Applications of Metal Organic Frameworks

MOFs have been utilised in many different areas, ranging from the uptake of environmentally harmful dyes to gas absorption and separation.³ However, arguably its largest potential lies in its biomedical applications. These applications may include anything from bioactive MOFs used as drug delivery systems to fluorescent MOFs used as biosensors and bioimaging agents.^{33,35}

Although modern medicine has made significant and innovative progress in the development of new drugs, there are still integral flaws in relation to pharmacokinetics and pharmacodynamics when it comes to the delivery of these medications to patients. Drug resistance is becoming an increasingly concerning problem globally as antibiotic resistance and multi-drug resistant bacterial strains are on the rise at a much faster rate than the development of alternative treatments.³⁶ In 2014, the World Health Organisation (WHO) stated that if the required actions are not taken, by 2050 antibiotic resistant bacterial infections will overtake cancer as the leading cause of human death.³⁶ The current implementation of regular high drug doses and subsequent high clearance rates also leads to further problems of adverse drug reactions in patients. Thus, the need for an alternate method of delivering drugs using a safe, targeted, and effective approach, surpassing these issues is necessary for the prevention of drug resistance becoming a much larger issue¹.

Drug delivery systems (DDS) have been developed to resolve these issues. Therapeutic nanocarriers such as liposomes, micelles, dendrimers and mesoporous silica, as shown in Figure 11, are the most commonly implemented DDS.³⁷ These nanocarriers have exhibited

success in delivering therapeutics while maintaining a drug loading capacity and controlled release ³⁷. Despite these promising features, current DDS are still lacking in certain areas. Liposomes have been reported to display leakage of the loaded drug as well as lower loading capacities and high cost. On the other hand, micelles are limited due to their instability, low drug loading and lack of chemical adaptability. Lastly, dendrimers, despite their advantageous polymeric character, also have drawbacks of which include high production costs.^{38,39} Thus, the development of polymeric DDS capable of facilitating controlled, targeted, and biorelevant drug release sparked interest in their potential for overcoming these issues.³

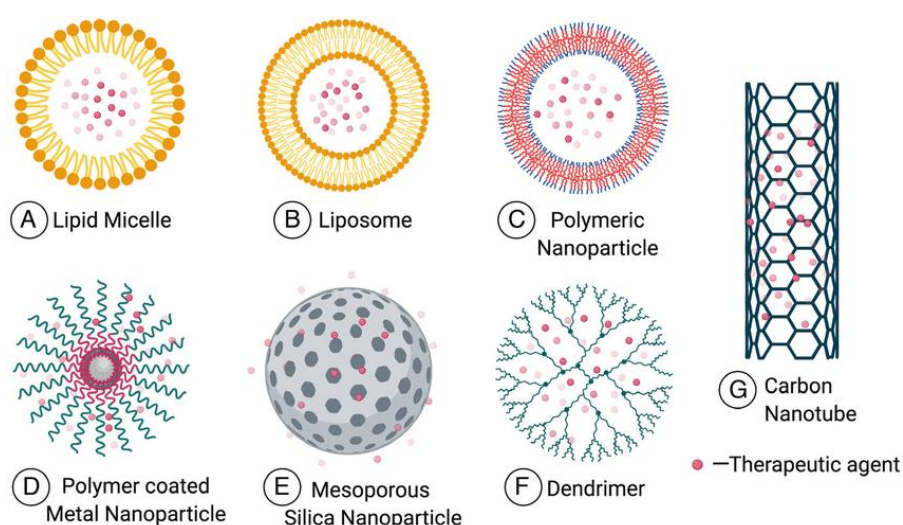


Figure 11: Some of the most commonly used DDS, including micelles, liposomes, dendrimers and mesoporous silica.⁴⁰

The viability of MOFs for use as drug carriers was first investigated by Férey and coworkers in Institute Lavoisier using the MIL MOF family. MIL MOFs were synthesised from trivalent metal centres and carboxylate linkers and held pore volumes of 25-34 Å, as well as BET surface areas of 3100-5900 m² g⁻¹.³ MIL-101 and MIL-100 were the main focus of studies on ibuprofen loading, with drug release studies lasting for six and three days respectively.¹ MIL-100 successfully encapsulated 0.35 g of ibuprofen per gram of dehydrated MIL-100, while MIL-101 was capable of encapsulating an impressive 1.4 g of ibuprofen per gram of dehydrated MIL-100.³ This research led the way for the subsequent studies of MOFs in biomedicine.

MOFs provide an opportune route for controlled drug delivery that would provide a biocompatible, biodegradable and targeted treatment resulting in minimized adverse drug

reactions.³ Alongside this, they are capable of high drug loading and controlled release which will consequently increase the re-administration intervals for patients.³⁹ MOF's can undergo PSM to further improve all of these factors.⁴¹ MOF's hold some of the highest reported surface areas and pore sizes of any delivery systems, being able to load considerably higher amounts than the average drug carrier, as illustrated in Figure 12, whereby the parameters measuring the suitability of each drug carrier favours MOF's over mesoporous silica for insulin loading.⁴¹

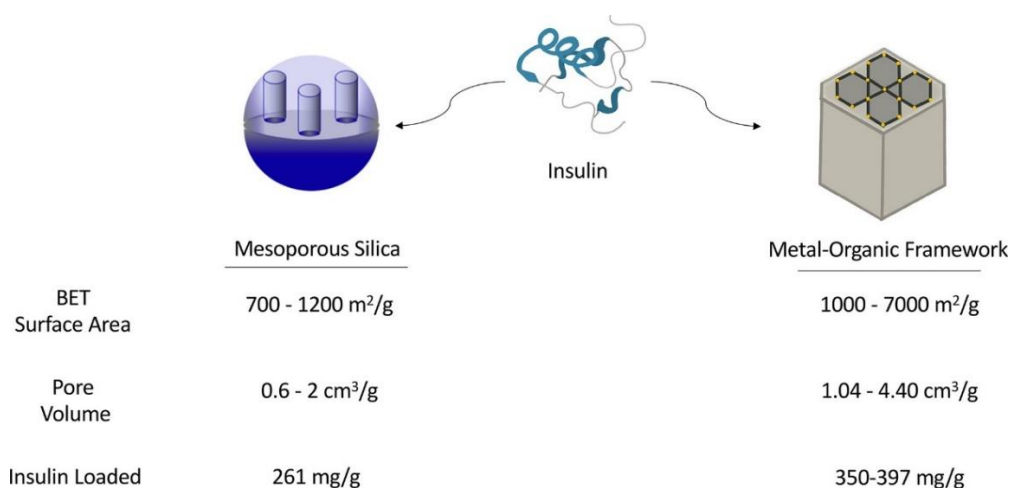


Figure 12: The larger BET surface area and pore volumes attributed to MOF's enables a far superior insulin loading in comparison to that of mesoporous silica.⁴¹

In the development of MOFs for biomedical applications, the biocompatibility of the building blocks used must be taken into consideration. Metals such as chromium are toxic to cells and should be avoided in synthesis, whereas some are already present in the body, with iron and zinc having a concentration of 22 μ M in blood plasma and 180 μ M in tissue respectively.¹ Alongside this, these building blocks can be chosen to produce synergistic effects paired with the active pharmaceutical ingredient (API) encompassed within. For example, many metals have antimicrobial effects, and combined with the correct antibiotic, can strengthen the efficacy of the drug. Furthermore, by using biorelevant materials, i.e. iron and zinc, any biocompatibility issues that may arise are surpassed.⁴¹ The rate of release may also be controlled and altered by interchanging ligands in synthesis as different functional groups can render different structural changes in the MOF. Furthermore, different stimuli may be utilised to activate drug release in MOFs.⁴¹ For example, MOF's can be sensitive to different pH environments. Normal human cells have a pH of \sim 7.2-7.4, however tumour cells are often

lower (pH of ~6.1-6.9). Thus, the drug release of a pH sensitive MOF can be targeted to the site of infection.⁴²

7.9 Multi Drug Resistant Tuberculosis

Multi-drug resistant bacterial strains are on the rise due to the over-administration and misuse of antibiotics. An example of this is multidrug-resistant tuberculosis (MDR TB), which is effectively a strain of *Mycobacterium tuberculosis* which has built resistance against the first line drugs to treat TB, namely isoniazid and rifampicin.^{43,44} Alongside this, there is also growing resistance against most fluoroquinolones i.e., ciprofloxacin, and second line treatments in a further developed stage of MDR TB, named Extensively drug resistant TB (XDR TB). Tuberculosis itself is a disease effecting mainly the respiratory system, with the main symptoms including coughing, chest pain, weakness, fever, weight loss and coughing up blood. However, the disease may also spread to other body parts including the brain or spine, leading to further severity of symptoms.⁴⁴ TB holds its place as the second highest cause of death by infectious disease, behind Covid-19, and is responsible for the death of 1.5 million people every year.⁴⁵

With the rapid rise of MDR TB, there is a high chance that the mortality rate of the disease will increase. In 2018, it was reported that from approximately 500,000 new cases of MDR TB, around 15% of these led to patient death.⁴³ As mentioned previously, MDR TB can be caused by the mismanagement of TB drugs in patients. This mismanagement can include a lack of patient compliance in completing their full course of antibiotics, the incorrect dose or treatment prescribed to a patient or the lack of access or supply to good quality antibiotics. It may also occur in TB patients who have had the disease previously and have built up resistance to the treatment they used prior.⁴⁴ Current treatments include combined antibiotic therapies over the course of 6-9 months up to 2 years in some cases, which as a result may further increase drug resistance as the MDR TB strain continues to strengthen.^{43,45} The traditional TB therapy course includes daily doses of multiple drugs taken orally. This further increases the issue of patient compliance as adverse reactions can occur after undergoing treatment for a prolonged time.⁴⁵

It is evident that an alternative approach must be developed to combat the rise of MDR TB. As the conventional treatment for TB involves oral administration it is also important to investigate other superior administration routes. The oral route presents problems as it is often difficult for a sufficient concentration of drug to reach the site of action after the first pass metabolism.⁴⁵ Pulmonary administration offers an appropriate method of drug delivery for a number of reasons. Firstly it is suitable for both large and small molecules, with the ideal diameter of particles ranging between 1–5 microns.⁴⁵ As the therapeutic is directly delivered to the respiratory system it ensures a targeted delivery with increased therapeutic concentration at the site of action, thus reducing dose concentration and increasing re-administration intervals.⁴⁵

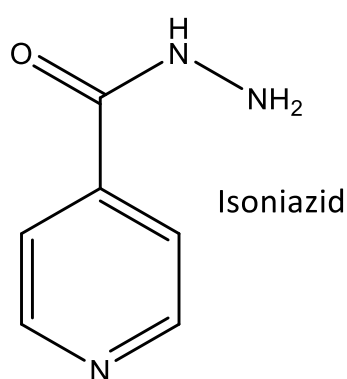


Figure 13: Structure of Isoniazid. Made using Chemdraw.

Isoniazid, shown in Figure 13, is a first line treatment effective against *Mycobacterium tuberculosis*.⁴⁶ Isoniazid itself is a prodrug and is activated by a bacterial catalase.⁴⁷ Once in its active form, isoniazid functions as an inhibitor at the bacterial cell wall to prevent the synthesis of mycolic cells resulting in bacterial cell death.⁴⁸ However, isoniazid resistance is becoming more prevalent with the emerging MDR TB obstacle. Many isoniazid resistant TB strains appear as a precursor to MDR TB.⁴⁷ There are also often toxicity risks associated with the administration of the drug, as it is hepatotoxic.⁴⁷

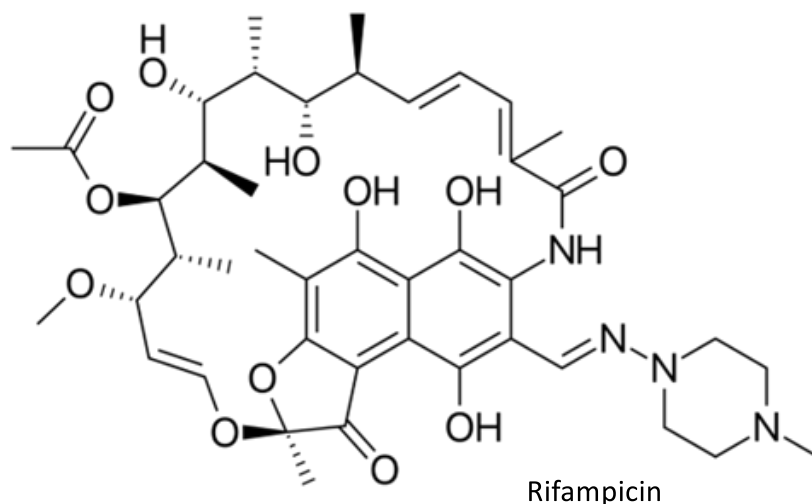


Figure 14: Structure of Rifampicin. Made using Chemdraw.

Rifampicin, shown in Figure 14, is another first line drug used against *Mycobacterium tuberculosis*. Rifampicin's mechanism of action follows the inhibition of bacterial RNA polymerase, thus suppressing bacterial RNA synthesis leading to cellular death.⁴⁹ Bacterial resistance to rifampicin is also on the rise, as well as cross resistance when paired with other treatments with addition to the poor solubility and adverse side effects entailed by the drug.⁴⁹

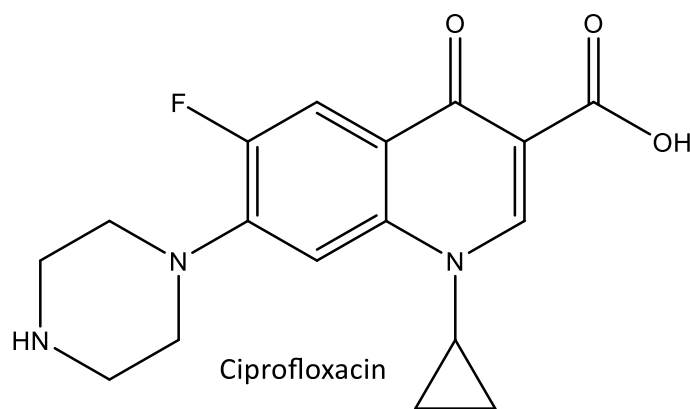


Figure 15: Structure of Ciprofloxacin. Made using Chemdraw.

Ciprofloxacin, shown in Figure 15, is a fluoroquinolone which can be used in the prevention and treatment of TB and is often combined with other therapies.⁵⁰ Ciprofloxacin's mechanism of action is to inhibit DNA replication by targeting the alpha subunits of DNA gyrase on topoisomerase II and topoisomerase IV.⁵¹ However, ciprofloxacin also encounters solubility issues, side effects and has developed multiple mechanisms of resistance by means of drug target mutations, mutations preventing drug acclimation and bacterial cell shielding plasmids.⁵¹

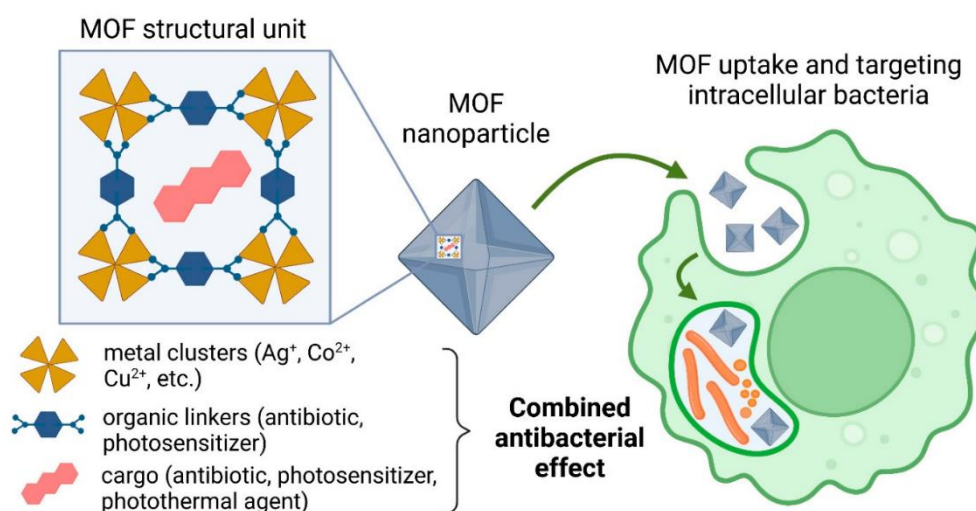


Figure 16: Combined delivery system; MOF made up of three different APIs with antimicrobial properties.⁵²

MOFs as a DDS have the potential to be effective in overcoming the issue of drug resistance because of their targeted delivery, alongside the high uptake and controlled release of drug.⁴¹ Additionally, as MOFs can be synthesised at a range of sizes matching that required of pulmonary delivery, they present themselves as an ideal DDS to deliver first line TB drugs using this alternative pulmonary administration route.⁴⁵ MOFs can also provide a combined therapy to treat disease when using antimicrobial metal centres, as a synergistic effect can be achieved when coupled with an antibiotic.⁴⁵ Ligands that double as prodrugs can also be implemented in the structure of the MOF.⁴¹ This proposed strategy would encompass 3 different APIs; the loaded drug, an antimicrobial metal and a prodrug ligand, to treat MDR TB, as shown in Figure 16.³³ This combinatorial strategy would act as an optimised treatment regimen and improve patient compliance as it would decrease administration frequency and adverse effects.³⁹

7.10 Multimodal MOFs

7.10.1 Combined MOF therapeutic delivery

There are many disadvantages to the current conventional therapies available to treat TB, the most alarming of which is the rise of drug resistance.³⁴ This research considers an alternative approach to combat this using MOFs as a system to combine multiple APIs while controlling their release.³⁴ A multifunctional and bioactive MOF that provides both drug delivery and a therapeutic effect of its own would be a promising new route to overcoming barriers to

effective treatment. It is important to ensure all MOF components are non-toxic, thus choosing building blocks that double as biocompatible APIs to simultaneously boost the efficacy and safety of the MOF.³⁴

The co-delivery of multiple drugs simultaneously can be achieved using MOFs as the foundation of treatment. By employing a ligand that gives therapeutic effect, both the encapsulated drug molecules, and the prodrug ligand can be delivered to the site of infection.³³ Olsalazine is a drug that has been applied to the treatment of multiple different diseases as it is a prodrug for the well know anti-inflammatory, para-aminosalicylic acid (PAS).^{53,54} The metabolism of olsalazine to PAS is illustrated in Figure 17.

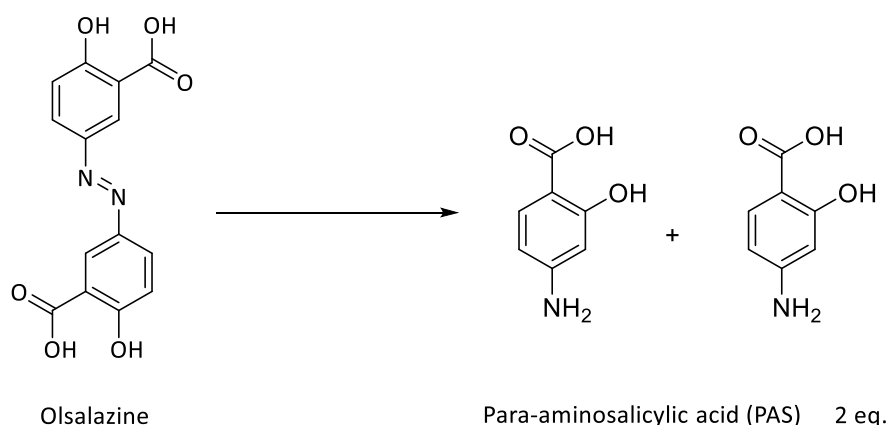


Figure 17: Scheme of the metabolism of olsalazine to PAS. Made using Chemdraw.

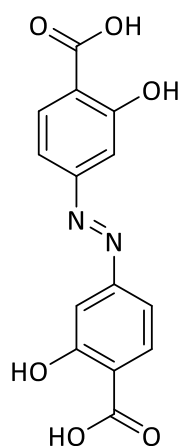
PAS, although primarily used in the treatment of ulcerative colitis, is an antitubercular agent that is often administered to patients alongside the first-line therapies.⁵⁵ The drug takes bacteriostatic action against tuberculosis meaning it prevents the rapid multiplication of *Mycobacterium tuberculosis*. Additionally, this bacterial growth prevention helps to reduce the risk of drug resistance.^{54,55} Therefore, by incorporating a ligand that can be metabolised to an antitubercular drug, a very successful dual treatment may be developed. Furthermore, a MOF synthesised using both antimicrobial metals and a prodrug ligand may act as a multimodal MOF for TB drug delivery.

8 Aims and Objectives

This research project centres upon two main sections: the synthesis of a MOF capable of encompassing 3 different APIs to provide an alternate treatment route for MDR TB, and the synthesis of stilbene derived ligands with fluorescent properties for MOF synthesis.

The first section centres on encapsulating TB therapeutics within a MOF composed of a prodrug ligand and antimicrobial metal. The objectives of the research undertaken includes the synthesis of MOFs using components with antibacterial properties, the encapsulation of antitubercular therapeutics within the MOF, and the future evaluation of these compounds' antibacterial activity by undertaking bacterial assays. The importance of the multimodal potential for MOFs used in drug delivery is rapidly increasing as the rise of drug resistant bacterial strains has necessitated the development of alternate treatment routes. The isomer of prodrug olsalazine, azodisalcyclic acid (AZA), shown in Figure 18, has been implemented as a ligand in the synthesis of MOFs for drug delivery. This paired with the use of antimicrobial metals in the MOF synthesis has enabled the synthesis of a MOF that has the potential to encompass 3 different APIs in the treatment of TB.

The desired outcome of combining these three APIs in the framework is a synergistic effect. Hereby, the combined therapeutic potential of each component is optimised, and a more effective treatment and efficient delivery may be developed. This project aims to utilise these MOFs in the loading of first line TB drugs; isoniazid and rifampicin, as well as second line fluoroquinolone antibiotic ciprofloxacin, for their use in antibacterial assays against *Staphylococcus aureus*, *Escherichia coli* and *Pseudomonas aeruginosa*. Alongside this, the synergistic effects of synthesizing a mixed metal MOF using this ligand will be explored.



Azodisalicylic acid (AZA)

Figure 18: Structure of Azodisalicylic acid. Made using Chemdraw.

Another objective of this research project is to implement stilbene derived ligands with fluorescent properties in MOF synthesis. The synthesis of a luminescent MOF could give rise to new potential biosensors, as well as MOFs used for bioimaging. This may be further manipulated as the prospective MOF could give rise to a multimodal system using both fluorescent ligands and metals, all while acting as a controlled drug delivery system. The main aim of this section of the project includes the synthesis and characterization of a MOF or otherwise porous material using a stilbene derived ligand, cyanostilbene dicarboxylic acid and an array of various metal sources. Alongside this, the hydrolysis of the ligand to improve its suitability for MOF synthesis is explored.

9 Results and Discussion

9.1 Cyanostilbene dicarboxylic acid synthesis

The cyanostilbene dicarboxylic acid ligand was synthesised following a two-step reaction, reported by Bell *et al.*, involving a condensation and hydrolysis step respectively.⁵⁶ This ligand is made up of a stilbene with a carboxylic acid on each terminus and a central nitrile group, and was chosen due to its multimodal potential. Being a stilbene ligand, it can hold luminescent properties, via UV induced *trans-cis* stilbene isomerization giving possible sensory applications.⁵⁷ Alongside this, the presence of two carboxylic acid moieties increases the coordination potential of the ligand to metal which in turn may increase the porosity of a MOF using the polytopic ligand.¹⁰ A highly porous MOF is desirable in drug delivery for its high drug loading capacity.¹⁰ The presence of a nitrile group can give rise to an increased structural flexibility of a MOF because of the increased coordination between the nitrile group and metal.⁵⁸

The reactants 4-formylbenzonitrile and 4-cyanophenylacetonitrile were heated until molten 130°C and stirred to encourage the formation of a homogenous mixture. Following this mixing, piperidine was added, thus forming a solid tricyanostilbene linker which was washed thrice using EtOH to remove unreacted 4-formylbenzonitrile and other reactants. This synthesis is illustrated in Figure 19. The ¹H NMR and IR of the product are available in the appendix at Figure 54 and Figure 55 respectively.

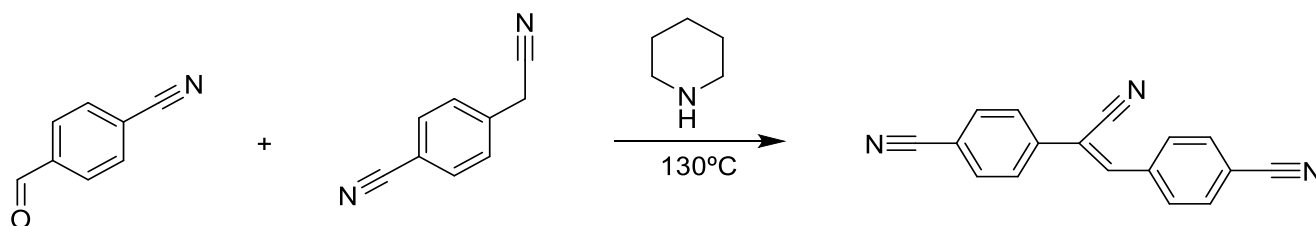


Figure 19: The synthesis of tricyanostilbene. This condensation reaction of 4-formyl benzonitrile and 4-cyanophenylacetonitrile at 130°C, with the addition of piperidine to precipitate the tricyanostilbene ligand.

The tricyanostilbene acted as a precursor to the desired ligand and underwent a hydrolysis reaction in acetic acid under reflux at (135 °C), with added sulfuric acid for catalysis (Figure

20). After 8 hours, cyanostilbene dicarboxylic acid was precipitated as a white powder from the reaction as reported in the literature and was washed thoroughly in EtOH once more to ensure removal of remaining acetic acid and other reactants. It was then dried for 24 hours at 80 °C, and ground into a fine powder using a pestle and mortar.⁵⁶ The final product was then analysed using IR (Figure 21) and ¹H NMR (Figure 22). The IR spectrum exhibited a clear nitrile peak at 2226 cm⁻¹, as well as carbonyl stretches present at 1650 cm⁻¹ and 1398 cm⁻¹. The ¹H NMR exhibited 9 different signals between 7-9 ppm that account for the protons present however also indicate there is still unreacted material present.

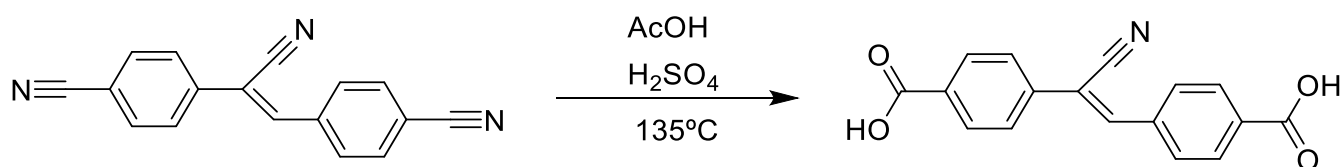


Figure 20: The synthesis of cyanostilbene dicarboxylic acid. The hydrolysis of the precursor tricyanostilbene at 130°C, with the addition of acetic acid in excess and a catalytic amount of sulfuric acid to precipitate the cyanostilbene dicarboxylic acid ligand.

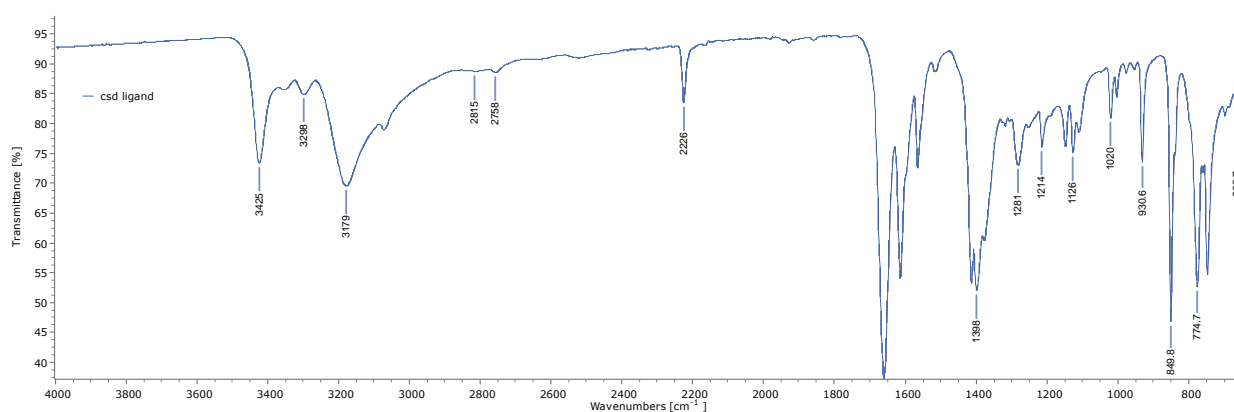


Figure 21: IR spectrum of cyanostilbene dicarboxylic acid ligand.

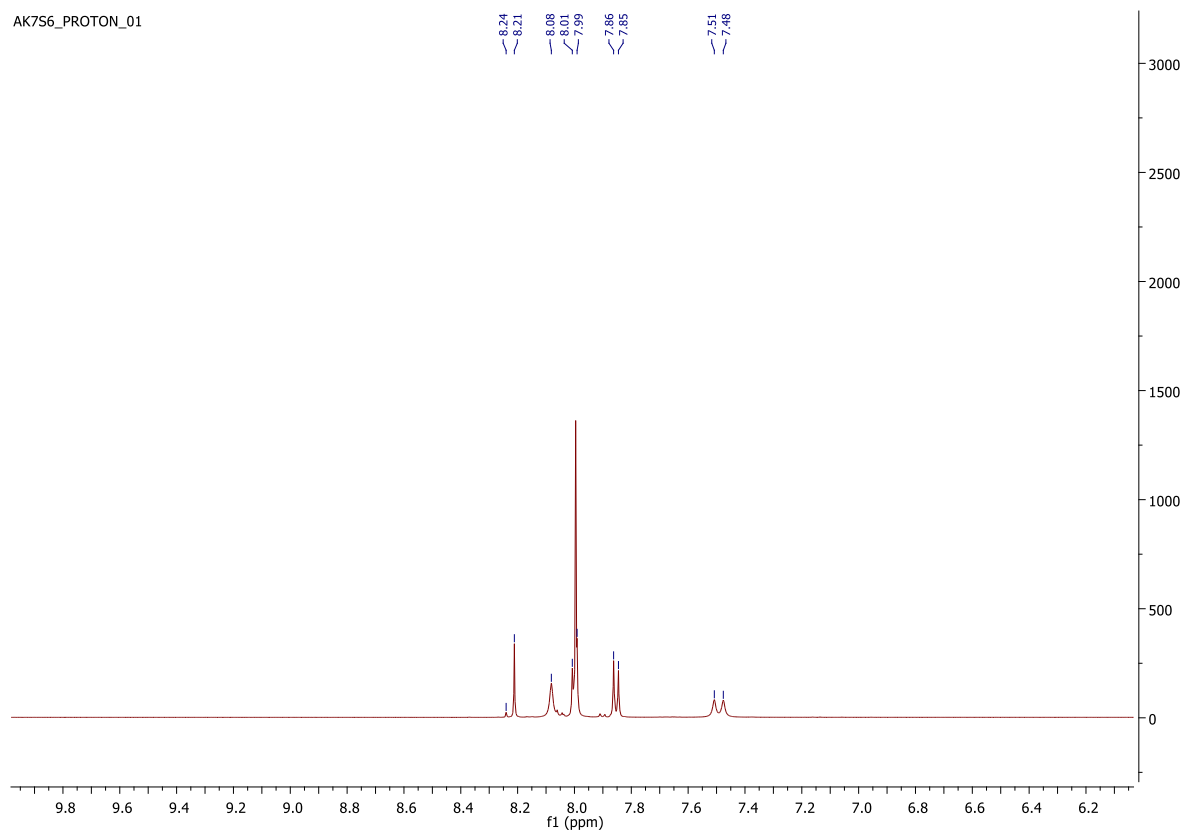


Figure 22: The ^1H NMR obtained from the synthesis of cyanostilbene dicarboxylic acid, with DMSO- d_6 used as a solvent.

Upon attempting MOF synthesis using this ligand, a large range of metal-ligand molar ratios were used ranging from 1–7.5 equivalents of each in different combinations (see Table 1). Different solvents and solvent combinations were implemented, and different parameters including temperature, reaction time and concentrations were all trialled. The metals used in synthesis include nitrate and acetate salts of zinc, copper, cobalt, magnesium, and gadolinium. No crystalline material was formed however, gel material was obtained. It is possible that this lack of crystalline product is because the nitrile group centred in the ligand was too electron withdrawing, thus preventing coordination. Thus, further synthesis was carried out to hydrolyse this nitrile group to a carboxylic acid (see section 8.3).

Table 1: Parameters and synthesis conditions trialled during attempted MOF synthesis using cyanostilbene dicarboxylic acid.

Metal Salt	Molar ratio (M:L)	Temperature (°C)	Solvents	Reaction Time (h)
Zn ^{II} nitrate	1:1,2:1....6:1 1:2,1:3....1:6 2:2, 1:1.5, 1.5:1 1:7.5, 7.5:1	60, 70, 90, 100, 120	DMF, DEF, DMSO, DMA, H ₂ O, EtOH, MeOH, NaOH, TEA	6-12, 24, 48, 72
Cu ^{II} nitrate	1:1,2:1....6:1 1:2,1:3....1:6 2:2, 1:1.5, 1.5:1 1:7.5, 7.5:1	60, 80, 90, 100, 120	DMF, DEF, DMSO, DMA, H ₂ O, EtOH, MeOH, NaOH	3-12, 24, 48, 72
Co ^{II} nitrate	1:1,2:1....6:1 1:2,1:3....1:6 2:2, 1:1.5, 1.5:1	60, 90, 100, 120	DMF, DEF, DMSO, DMA, H ₂ O, EtOH, NaOH	24, 48
Mg ^{II} nitrate	1:1,2:1....6:1 1:2,1:3....1:6	90, 100, 120	DMF, DEF, H ₂ O	24, 48
Gd ^{III} nitrate	1:1,2:1....6:1 1:2,1:3....1:6	100, 120	DMF, H ₂ O	24, 48, 72
Zn ^{II} acetate	1:1,2:1....5:1 1:2,1:3....1:5 2:2	70, 100, 120	DMF, DEF, H ₂ O, MeOH, EtOH	24, 48

9.2 Compound A

Compound A was synthesised using cyanostilbene dicarboxylic acid and copper nitrate. This gel material was obtained by using similar parameters as those outlined by Li *et al.* in their paper.⁵⁹ A molar ratio of 1.5:1 of metal to ligand was used to achieve the gel product. Two solvents, DMF (7 ml) and H₂O (5 ml) were first added to the vial and stirred. The cyanostilbene dicarboxylic acid ligand and copper nitrate salt were added and dissolved by sonication sequentially. The reaction was heated solvothermally in an oven at 90°C for 24 hours. A pale blue gel began to form after 3 hours. However, upon cooling the gel exhibited instability as its colour faded and some of the gel degraded. The gel was analysed before and after cooling to investigate whether a MOF was forming before or after the cooling.

The gel was removed and dried at 60°C in an oven for 24 hours, with one sample pre-cooling and the other post-cooling. These samples were then analysed using IR spectroscopy, as seen in Figure 23 and Figure 24. Both samples displayed a distinct shift in the IR peaks compared to the as-synthesised ligand indicating the presence of both metal and ligand in the material.

The peak for the nitrile of the ligand at 2226 cm^{-1} has shifted to 2219 cm^{-1} in the gel. The carboxylate peaks also have shifted from 1660 cm^{-1} to 1659 cm^{-1} . The shift of carboxylate peaks indicates metal-carboxylate binding; however, with a gel product a coordination polymer or MOF formation may only be confirmed by TGA and PXRD analysis.

Upon IR analysis of the gel material post-cooling, there appeared to be some degradation of material as some peaks present pre-cooling had disappeared. The peak shifts present pre-cooling appeared remain in most cases as ligand peak indicating a nitrile group, 2220 cm^{-1} , is present. However, peaks at 1419 cm^{-1} and 693 cm^{-1} in the gel pre-cooling had disappeared in the spectrum. Although there is good indication that both metal and ligand had coordinated in the gel pre-cooling, it is important to analyse this degradation of material in future studies using PXRD.

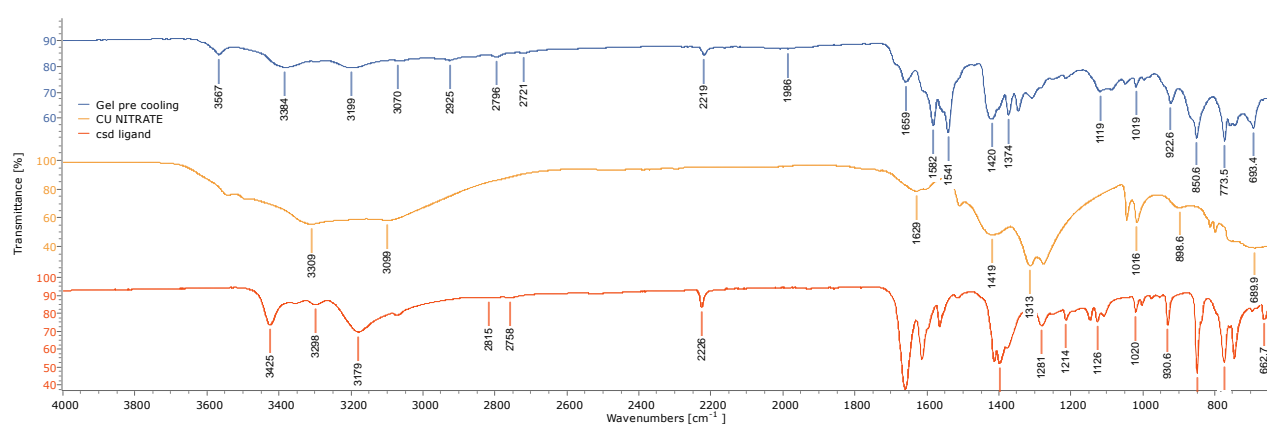


Figure 23: IR of Compound A pre-cooling.

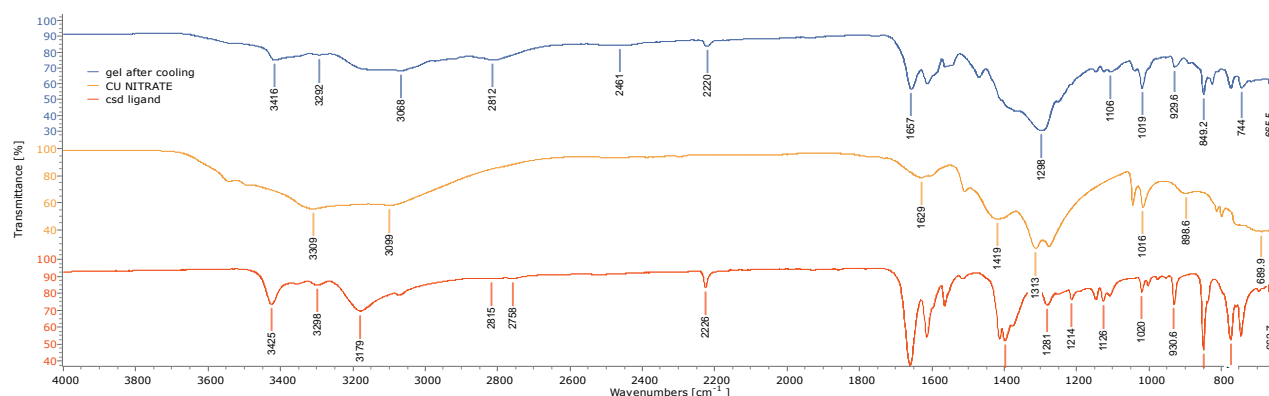


Figure 24: IR of Compound A post-cooling.

9.3 Stilbene tricarboxylic acid synthesis

Stilbene tricarboxylic acid was synthesised using cyanostilbene dicarboxylic acid as a precursor, following the methods outlined by Bell *et al.*⁵⁶ By hydrolysing the lone nitrile to a carboxylic acid, the ligand has a central group that is much less electron withdrawing. The three carboxylic acid groups extending from the structure of this ligand make it a promising ligand for MOF synthesis. The cyanostilbene dicarboxylic acid was heated for 5 hours at 150°C in a 10% solution of KOH in ethylene glycol, shown in Figure 25. A viscous brown liquid was obtained, which was then crystallised in a 1:1 dilution of acetic acid and H₂O. The product is shown in Figure 26.

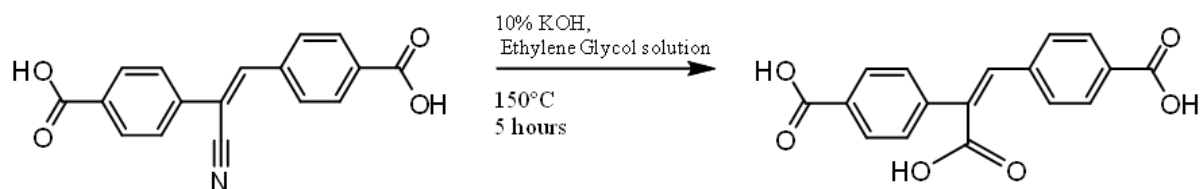


Figure 25: Scheme of the hydrolysis of the nitrile group in cyanostilbene dicarboxylic acid to form the ligand stilbene tricarboxylic acid.

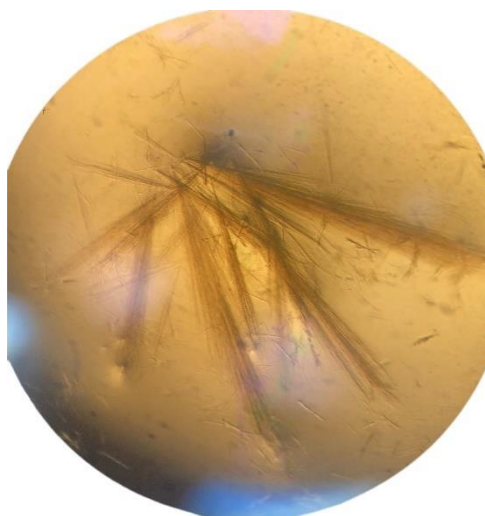


Figure 26: Needle crystals of stilbene tricarboxylic acid under the microscope (x 10 magnification)

The product obtained was analysed using IR spectroscopy (Figure 27). When comparing the IR spectra of this product to that of its precursor, the peak indicating the presence of a nitrile at 2226 cm^{-1} in the precursor is no longer present in the product. Peaks present at 1681 cm^{-1} , 1587 cm^{-1} , 1536 cm^{-1} and 1378 cm^{-1} are all indicative of the carboxylic acid groups present in both stilbene tricarboxylic acid and its precursor. The broadening of the carboxylate peaks in the product obtained could suggest the additional carboxylate.

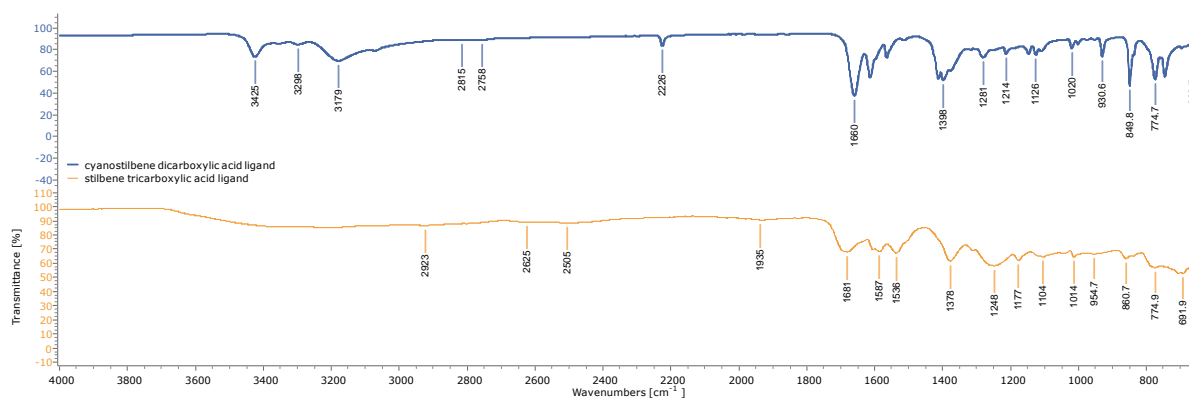


Figure 27: The IR spectrum of stilbene tricarboxylic acid compared to cyanostilbene dicarboxylic acid.

When attempting to analyse the product with NMR, the DMSO- d_6 , DCl and $d\text{-CDCl}_3$ were used as the deuterated solvents. However, there were solubility issues for the ligand in all the above deuterated solvents. In future work, an NMR may be achieved by using acetone- d_6 or ethanol- d_6 as solvent. This analysis was not completed in this research because the solvents were not received in the time frame required. Due to time restraints, MOF synthesis was not attempted using this linker. However, in future research following the methods of MOFs synthesised with linker 4,4-stilbene dicarboxylate, or other tricarboxylic acid linkers would potentially be a successful strategy.

9.4 Azodisalicylic Acid MOFs

9.4.1 Azodisalicylic Acid Linker

The AZA linker chosen for this project is a prodrug for PAS because it is metabolised in the body by an enzyme called azoreductase.⁶⁰ It also is not commercially available, and has not been reported to be used in MOF synthesis previously. The synthesis of this ligand was developed by using a similar procedure in literature reported by D.S. Bhate, and was developed and characterized by Dr. Ahmed Ahmed, a previous member of Galway Porous

Materials.⁶¹ There is a 2:1 molar ratio on the equivalents of PAS obtained from the degradation of AZA as the central N-N bond is reduced thus breaking the structure into 2 identical units of PAS. As PAS has been proved to have therapeutic effect against TB, if this ligand is incorporated into the structure of the MOF, upon administration and reduction via azoreductase, the 2 molecules of PAS would be released.^{55,60} In this way, the linker of the MOF itself would act as a prodrug, as seen in Figure 28.

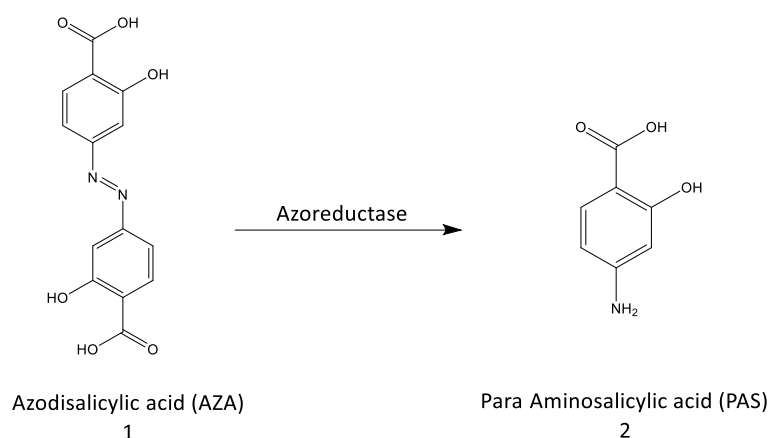


Figure 28 Metabolic degradation pathway of Azodisalicylic acid via Azoreductase to the prodrug PAS

Reactant 4-nitrosalicylic acid is used in the ligand synthesis, whereby, with the addition of 5M NaOH, D-glucose is introduced to the reaction and acts as an oxidising agent.⁶⁰ This solution is heated (50 °C) and stirred before being removed from the heat and allowed to stir for 48 hours at room temperature. This allows for the precipitation of a dark brown material which is then acidified using HCl and filtered, collecting the crude product. After being dried overnight, the crude product is dissolved in H₂O with added Na₂CO₃ under heating (80 °C). The resulting solution is then filtered and allowed to recrystallize overnight. The solution is then filtered, and an orange material is obtained. After drying overnight, this material is re-dissolved in H₂O. The solution is then acidified to pH 1 using concentrated HCl. This results in the formation of an orange precipitate which is collected via filtration and washed with excess H₂O before being dried overnight. The purified product is collected via Buchner filtration. The final ligand was analysed using IR (Figure 29) and ¹H NMR (Figure 56).

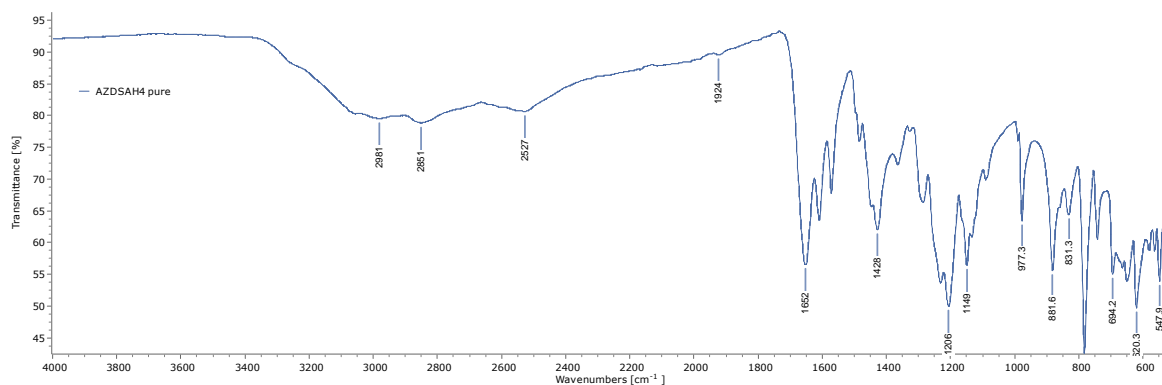


Figure 29: IR spectrum of AZA linker.

9.4.2 Azodisalicylic Acid MOFs

Upon MOF synthesis with the AZA linker, solvothermal synthesis was decided to be the best synthetic procedure. Solvothermal synthesis is the most commonly used synthetic method in literature and so it was used as first protocol. MOFs were synthesised using the nitrate salts of zinc, copper, cobalt and magnesium because these metals have antimicrobial activity, thus resulting in the synthesis of $Zn_2(AZA)$, $Cu_2(AZA)$, $Co_2(AZA)$ and $Mg_2(AZA)$. Each MOF had a different synthetic procedure with varied parameters and solvents. Previous research by Dr Ahmed Ahmed of the Galway Porous Materials group analysed these MOFs using PXRD methods, from which unit cell parameters and the computational model of the MOF with a hexagonal crystal system and 25 Å pore sizes were solved, shown in Figure 30, and Figure 31 respectively.⁶²

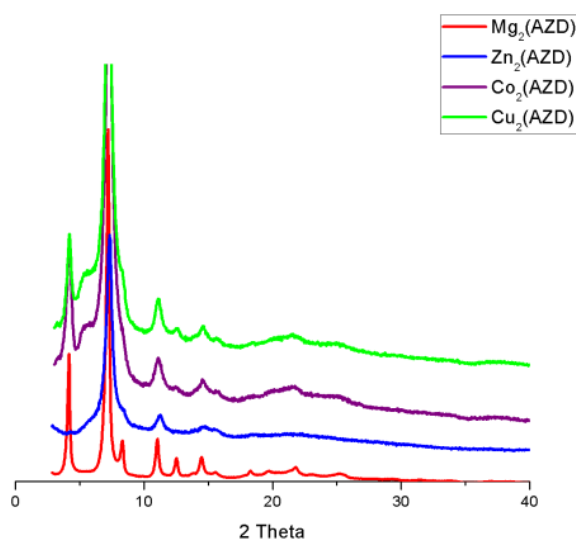


Figure 30: PXRD patterns of $Mg_2(AZA)$, $Zn_2(AZA)$, $Co_2(AZA)$ and $Cu_2(AZA)$.⁶²

Table 2: Unit cell parameters of AZA MOFs.⁶²

<i>Parameter</i>	Zn₂(AZA)	Mg₂(AZA)	Cu₂(AZA)	Co₂(AZA)
<i>Space group</i>	P6	P6	P6	P6
<i>a/ Å</i>	24.61(3)	24.32(2)	24.45(3)	24.39(5)
<i>b/ Å</i>	24.61(3)	24.32(2)	24.45(3)	24.39(5)
<i>c/ Å</i>	5.894(7)	5.84(14)	5.81(4)	5.85(3)
<i>alpha/ °</i>	90	90	90	90
<i>beta/ °</i>	90	90	90	90
<i>gamma/ °</i>	120	120	120	120
<i>Volume/ Å³</i>	3091(5)	2972(8)	2974(18)	3011(14)

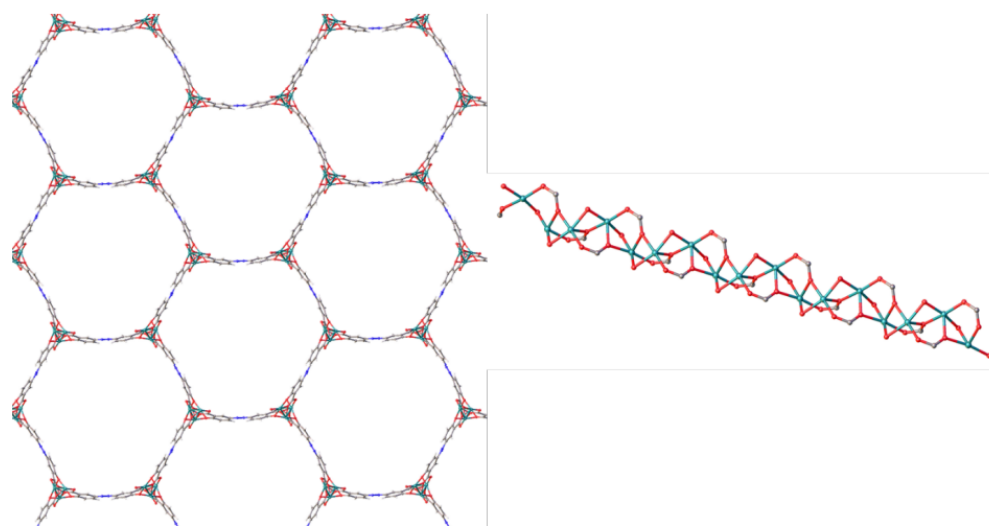


Figure 31: The crystal structure of Mg₂(AZA) along 001 crystallographic axis, and its rod SBU on the right.⁶²

The IR spectra (Figure 32), exhibits a shift in the carbonyl group belonging to the linker AZA at 1653 cm⁻¹. These shifts were seen at peaks 1656 cm⁻¹, 1594 cm⁻¹, 1598 cm⁻¹ and 1566 cm⁻¹ in Mg₂(AZA), Zn₂(AZA), Cu₂(AZA) and Co₂(AZA) respectively. This peak shift is indicative of metal carboxylate coordination in the materials. These MOFs contain the prodrug AZA linker and various antimicrobial metals. The prime focus of this project was to encapsulate the first line therapies for MDR TB, which are isoniazid and rifampicin, alongside antibiotic ciprofloxacin, was of prime focus for this project. Each MOF synthesised retained different unique physical characteristics depending on the metal source present, i.e., a distinct colour was observed in

each MOF, with $Zn_2(AZA)$ forming a fine dark red-orange material, $Cu_2(AZA)$ forming green-blue spheroid material etc.

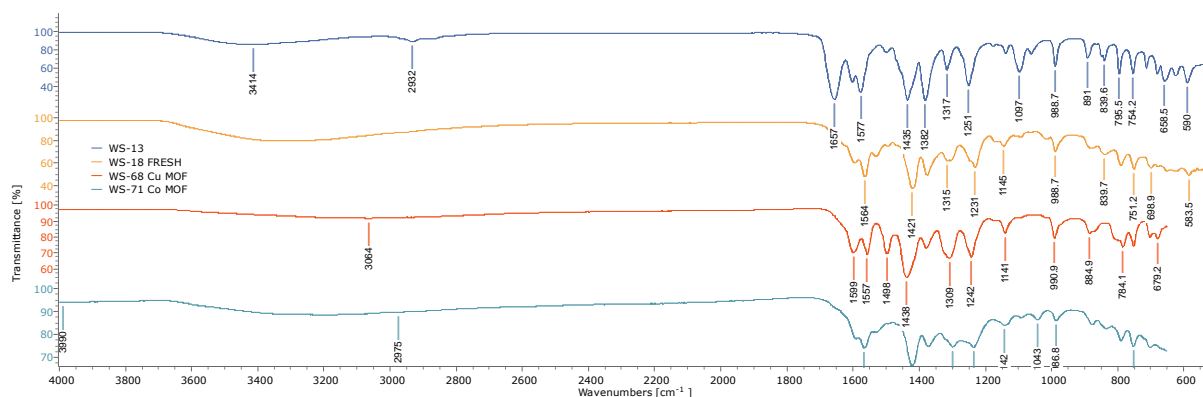


Figure 32: IR spectra of $Mg_2(AZA)$, $Zn_2(AZA)$, $Cu_2(AZA)$ and $Co_2(AZA)$ respectively.

Dissolution studies were previously carried out by Dr. Ahmed Ahmed of Galway Porous Materials to investigate the stability and controlled release of each MOF, illustrated in Figure 33. It was found that $Cu_2(AZA)$ exhibited high stability and controlled prodrug (ligand) release. In comparison, its $Zn_2(AZA)$ analogue exhibited a poor controlled prodrug release mechanism, with 30% of AZA being released in the first hour water dissolution, and over 55% released in phosphate buffer solution (PBS) in the same timeframe. Alongside this, after 24 hours the prodrug had been fully released in both water and PBS. In comparison, $Cu_2(AZA)$ exhibited much improved stability, with controlled prodrug release continuing steadily for 72 hours. Additionally, in the first 5 hours, under 17% and 23% of prodrug had been released in both water and PBS respectively, with a maximum of 40% in PBS after 72 hours and 20% in water after 48 hours. The slow release exhibited by $Cu_2(AZA)$ is ideal for pulmonary delivery as the re-administration rate would be significantly decreased with a slow release of the MOF in vivo.⁶²

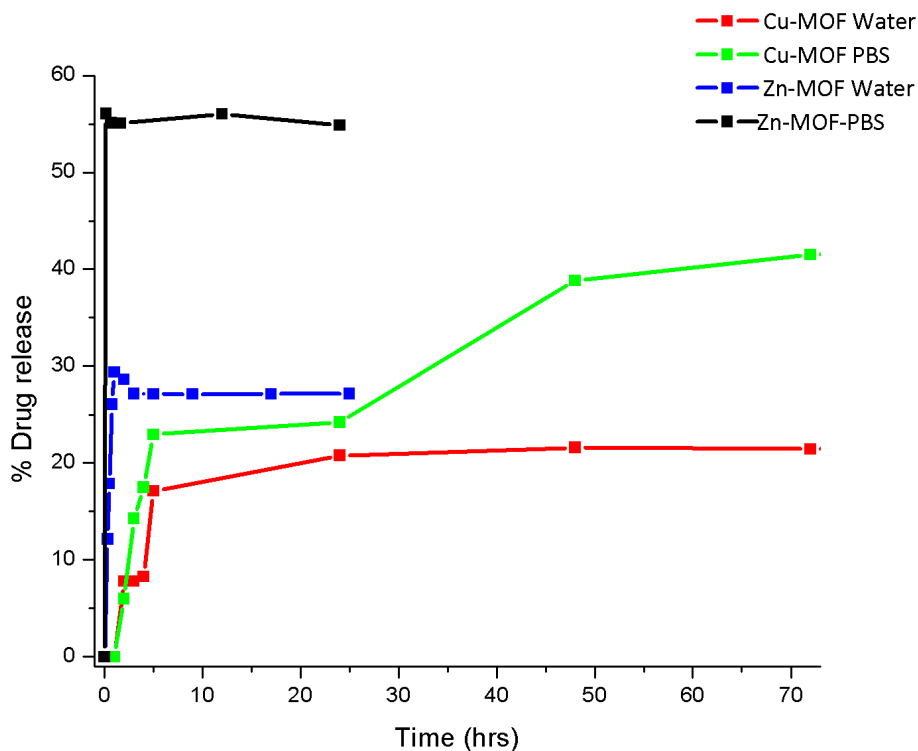


Figure 33: Graph indicating the % prodrug release of Zn₂(AZA) and Cu₂(AZA) in both water and PBS over 72 hours.⁶²

9.4.3 Copper-Zinc Mixed Metal MOF

From these prodrug dissolution studies it is evident that copper gave rise to heightened stability in the MOF. In this project, Cu₂(AZA) is the MOF which displays the most promising controlled drug delivery capacity thus far. However, using copper in biomedical applications can come with drawbacks due to its heightened toxicity in large concentrations.³² Copper is a biorelevant metal, however it is much less populous compared to the likes of zinc or magnesium due to its toxicity levels. On top of this, zinc is a highly efficacious anti-microbial agent and has previously been proved effective against *Mycobacterium tuberculosis*.³² Thus, the potential for a mixed metal MOF that would encapsulate both the improved stability and drug release of Cu₂(AZA), while maintaining the biocompatibility and anti-microbial effects of Zn₂(AZA) is clear.

Metal salts copper nitrate and zinc nitrate, alongside the AZA linker were used in the mixed metal MOF solvothermal synthesis. First, the molar ratio 3:1:1 of copper, zinc and AZA respectively, was synthesised at 100°C for 6 hours, using DMF as a solvent. The temperature and solvent choice were chosen to mimic the previous synthesis of Cu₂(AZA) and Zn₂(AZA).

However, this ratio proved unsuccessful as after EDX analysis and elemental mapping, there was no zinc present in the structure. From here molar ratios of 2:2:1 and 1:3:1 of copper, zinc and AZA respectively were synthesised under the same conditions, with the latter proving successful as both metals were present after EDX/SEM and IR analysis. The average ratio of each metal present in the sample was 7.6:1 of copper and zinc respectively, with overall copper content lying between 34.9% and 25.2% and overall zinc content lying between 4.99% and 2.9%, (Figure 34). This was repeated with the molar ratios 4:1:1, 5:1:1 and 6:1:1 of zinc to copper, this time repeating the synthesis in both pure DMF and mixed solvents (EtOH, MeOH) to try improve the size and shape of the material obtained.¹⁹ The most uniform material was formed when using a mix of DMF (3 ml) and EtOH (2 ml) as solvent and so this was used for EDX analysis. The EDX results exhibited polydispersity of the metals in the material, with different metal to metal ratios throughout. In particular, the 4:1 zinc to copper material exhibited the least uniform dispersion, with zinc abundance varying from 18.98% to 32.59% and copper abundance varying from 10.26% to 34.72%. Alongside this the metal to metal ratios varied from 1.98:1 to 1:1.57 of zinc to copper respectively.

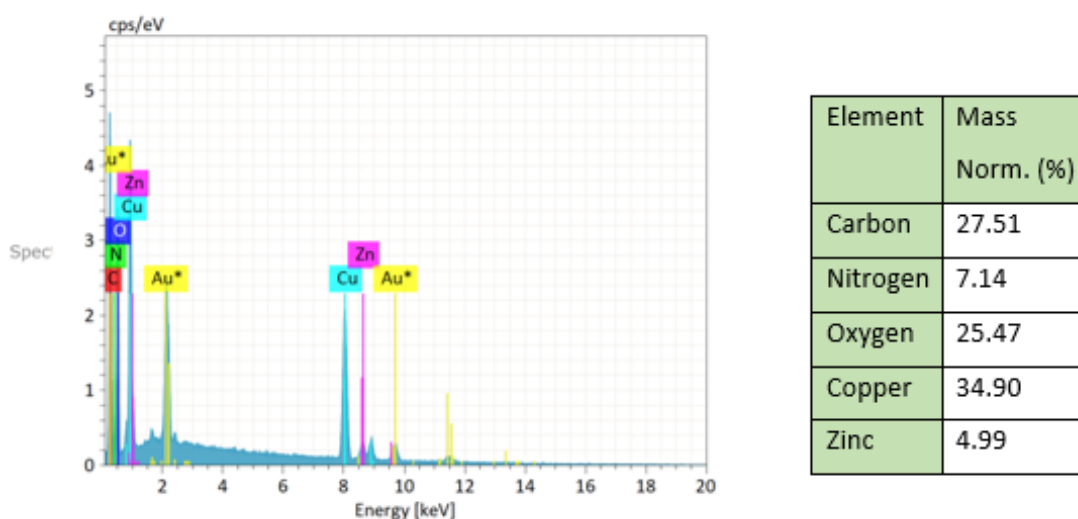


Figure 34: The EDX spectrum and data for solvothermally synthesised Zn:Cu 3:1.

The main issue presented was the lack of uniform metal dispersion when carrying out EDX analysis on each sample. Due to this, a different approach was taken to the synthesis of the MOF. By synthesizing the MOF under reflux with constant stirring and heat applied, it is

possible to improve the uniformity and dispersion of coordinated metals in the framework.⁶³ Thus the synthesis was carried out under reflux using a round bottom flask, heated using an oil bath. The reactants were heated to 100°C for 20 hours, using DMF and EtOH as solvents to improve the uniformity of the material. Molar ratios of zinc, copper and AZA respectively used were as follows: 1:3:1, 2:2:1, 3:1:1, 4:1:1, 5:1:1, and 6:1:1. The uniform dispersion of metals coordinated was greatly improved compared to the previous conventional solvothermal synthesis. In particular, ratios 3:1:1 and 4:1:1 provided the most uniform distribution, as shown in Figure 35 and Figure 36. In 3:1:1, the abundance of copper present ranges from 17.97% to 20.21% and the abundance of zinc ranges from 26.05% to 33.91%. Alongside this the metal to metal ratios for zinc to copper through different samples taken from the material are as follows: 1.45:1, 1.68:1, 1.75:1. In 4:1:1, the abundance of copper present ranges from 6.92% to 15.01% and the abundance of zinc ranges from 21.32% to 29.53%. Alongside this the metal-to-metal ratios for zinc to copper through different samples taken from the material are as follows: 1.97:1, 3.395:1, 3.08:1. This, paired with elemental mapping was used to analyse the dispersion of the metals coordinated in the sample. The elemental mapping for 3:1:1 and 4:1:1 is shown in Table 3, where the presence of zinc and copper is seen to be scattered evenly.

Table 3: The % abundance of zinc and copper present in each refluxed mixed metal sample.

Zn:Cu ratio	Sample	Sample	Sample	Sample	Sample	Sample
	1 Zn%	1 Cu %	2 Zn%	2 Cu %	3 Zn%	3 Cu %
3:1	26.05	17.97	33.91	20.21	31.92	18.25
4:1	29.53	15.01	28.08	8.27	21.32	6.92
5:1	55.05	10.78	46.15	8.44	54.25	5.26
6:1	27.77	6.95	33.69	5.10		

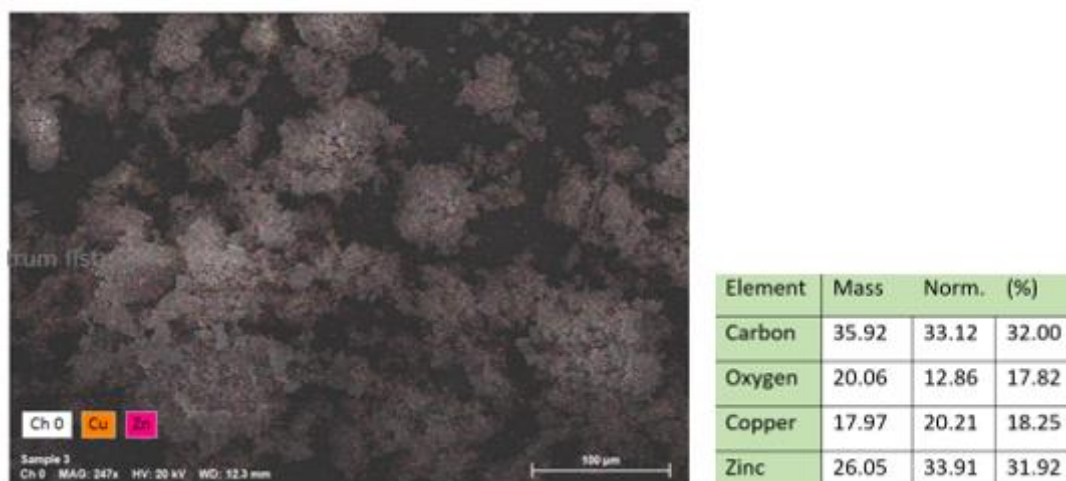


Figure 35: Elemental mapping and EDX data for refluxed Zn:Cu 3:1.

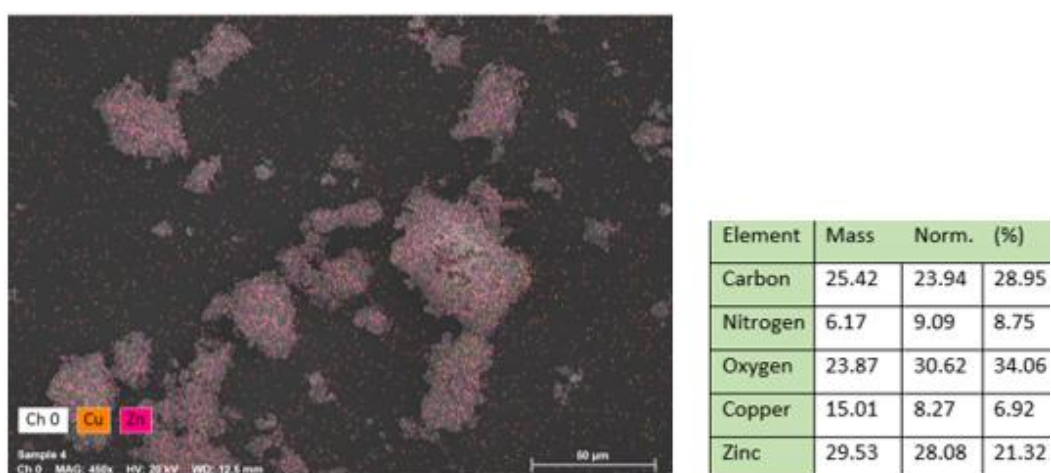


Figure 36: Elemental mapping and EDX data for refluxed Zn:Cu 4:1.

This was further investigated by repeating the methodology using microwave synthesis. Microwave synthesis was chosen as it can perform synthesis under stirring at higher temperatures for shorter times. This may allow it to achieve similar results as the synthesis under reflux, but with much shorter reaction times, making the process greener. The same molar ratio of zinc to copper and AZA respectively; 3:1:1, was used. The reaction time was increased in 30 minute intervals for each sample. The microwave synthesis was done at 150W and 2.5 GHz at 120°C under constant stirring from 30 minutes to 2 hours at constant pressure. DMF and EtOH were used as solvents once more. The dark brown powder material obtained

was once again analysed using EDX and elemental mapping. This method proved an increase in metal coordination and uniform distribution directly proportional to an increase in reaction time. After 1 hour reaction time, the zinc abundance varied from 30.17% to 14.43% and the copper abundance varied from 5.33% to 4.98%. After 1.5-hour reaction time, the zinc abundance varied from 30.76% to 26.05% and the copper abundance varied from 2.76% to 7.92%. After 2 hours reaction time, the zinc abundance varied from 49.2% to 52.5% and the copper abundance varied from 10.98% to 11.64%. The uniform dispersion of metal in the 2 hour reaction was confirmed by the elemental map which indicated better dispersion of the metals throughout the product, as no metal was localised in one spot and can be observed throughout. It was also important to ensure that one homogenous material was being synthesised and not a mixture of two products. The elemental mapping played a key role in this as it was possible to analyse if any material present had coordinated to only one metal instead of two uniformly. Any cluster of one metal without the presence of the other on the map would have been an indication of this, however this was not present in any of the samples synthesised as a single mixed metal product was achieved.

The microwave synthesis with 2 hour reaction time was also analysed using solid state UV/Vis. All samples were analysed using EDX, SEM and IR. TGA analysis could be applied to this to further exclude the possibility of a mixture of products. Overall, it is evident that both the reflux and microwave methods increased experimental control in metal dispersion and coordination. Therefore, by finding the optimal ratio to find both balance in metal coordination and thus their synergistic dynamics, it is possible to synthesise a mixed metal MOF that will both encapsulate the therapeutic effect of the anti-bacterial agents, while also controlling their combined bioavailability and lastly, their controlled drug release.

9.4.4 Dissolution Studies

Dissolution studies were completed on the mixed metal $Zn_2Cu_2(AZA)$ MOF synthesised via reflux. The 3:1:1 and 4:1:1 zinc to copper to ligand ratios were focused on due to their even metal dispersion and high metal co-ordinations according to EDX data. Dissolution studies were done in H_2O (Figure 37 and Figure 38) and PBS (Figure 39 and Figure 40) at $37^\circ C$ over the course of 1 hour, with intervals of the following: 5 min, 10 min, 15 min, 30 min, 1 hour.

The dissolutions carried out in H₂O exhibited a gradual breakdown of the MOF, with an increased release after every reading. In future studies, a hydrophobic coating may be applied to the MOF to improve its controlled release.

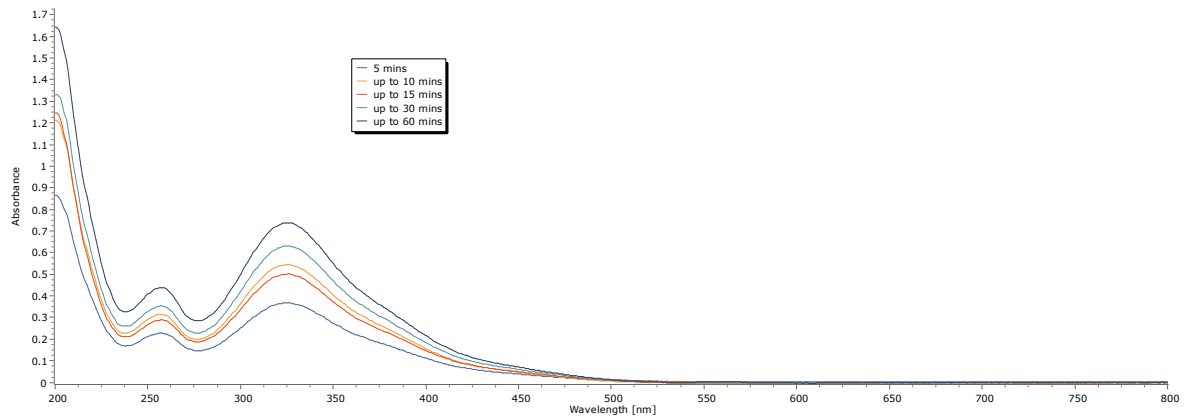


Figure 37: Dissolution of 3:1:1 zinc and copper sample in water over 1 hour.

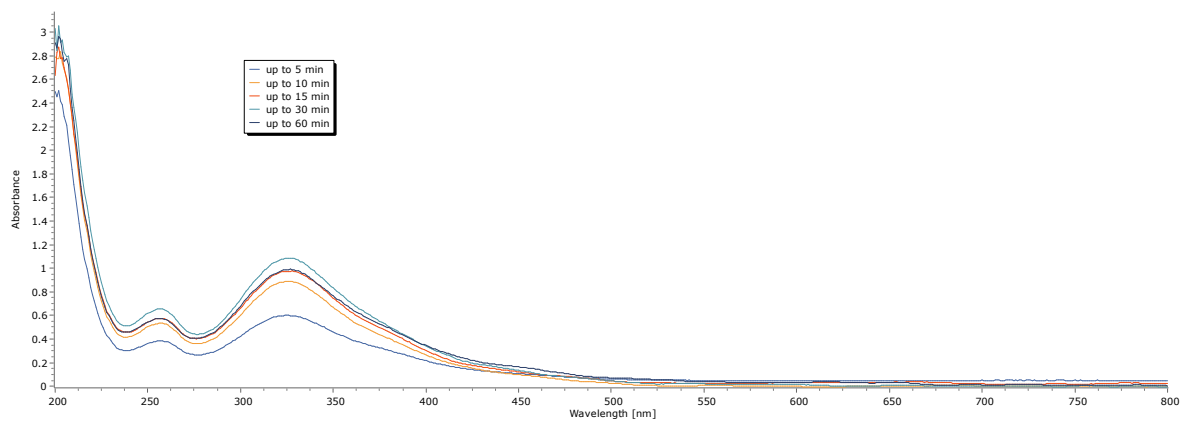


Figure 38: Dissolution of 4:1:1 zinc and copper sample in water over 1 hour.

In comparison, the studies carried out in PBS at pH 7.4 exhibited a much more rapid and extreme breakdown from the initial readings, with almost instant release of both metals in both samples. This breakdown can be explained as the phosphate ions may have coordinated to the metal centres leading to the quick release of copper nitrate and zinc nitrate.

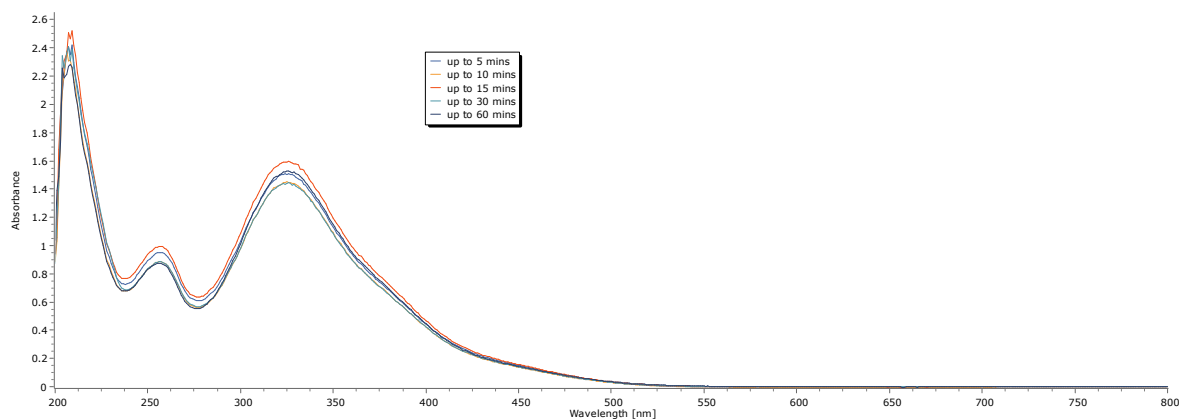


Figure 39: Dissolution of 3:1:1 zinc and copper sample in PBS over 1 hour.

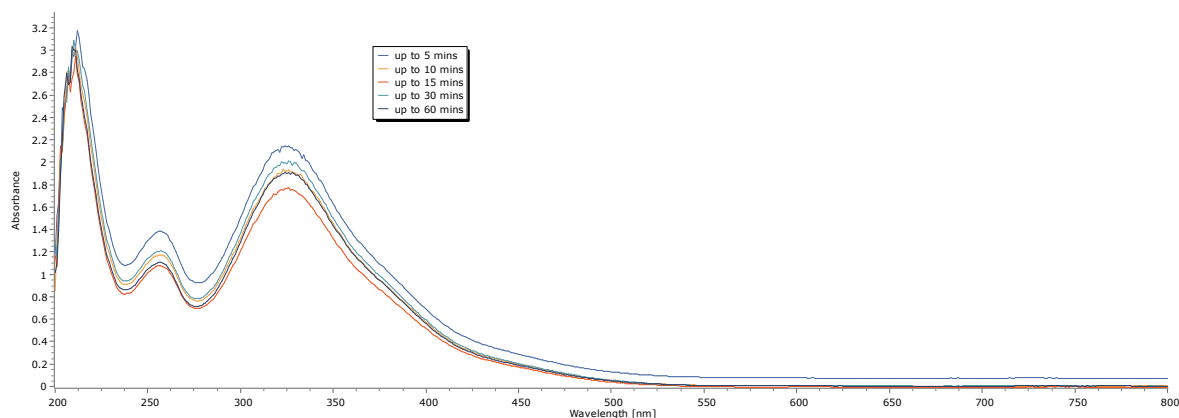


Figure 40: Dissolution of 4:1:1 zinc and copper sample in PBS over 1 hour.

9.4.5 MOF Activation

As the MOFs synthesised in this research all presented as hygroscopic, it was important to complete both their activation and drug loading in an anhydrous atmosphere. The activation process was preceded by solvent exchange whereby the sample was washed with fresh DMF every 24 hours for 3 days, followed by fresh MeOH every 24 hours for 3 days. The solvent was then removed, and the sample was dried at 80°C before being added quickly to a stoppered round bottom flask for activation, thus minimizing water absorption. The activation was done at 170°C under vacuum in a stoppered round bottom flask for 7 hours. The vacuum was incorporated to ensure an anhydrous atmosphere. The activation of these samples will be analysed using TGA in due course. The activated MOF was analysed using IR spectroscopy, (see Figure 32), to determine the absence of a solvent peak. To ensure that activation has

indeed occurred, TGA could be used to analyse this. However, as this material is hygroscopic, once removed from its anhydrous atmosphere it will once again absorb moisture and this will appear as a solvent peak. TGA would be useful to check if DMF was gone through absence of the DMF peak around 154 °C, however a solvent peak for water would still show up.

9.4.6 Antibiotic Encapsulation

Isoniazid loading was successfully completed in anhydrous EtOH under nitrogen using a balloon system to minimize further water absorption. A solution of isoniazid (50 mg) in the anhydrous EtOH (15 ml) was prepared and added to the activated MOF after allowing 5 minutes for it to cool down. This was then left unstirred under nitrogen for 72 hours, after which the MOF was washed using anhydrous EtOH and dried for 24 hours at 80°C. Isoniazid loading had previously been achieved on $Zn_2(AZA)$ and $Mg_2(AZA)$ by Dr. Ahmed Ahmed of the Galway Porous Materials group. In this project, isoniazid loading, see Figure 41, was completed on $Zn_2(AZA)$, $Mg_2(AZA)$ and $Co_2(AZA)$, shown in Figure 42, Figure 43, and Figure 44 respectively. Each sample was analysed using 1H NMR and IR. The proton signal for AZA is present at 7.99 ppm for all samples. The isoniazid signal in 1H NMR appears at 9.13 ppm, which can be seen in both $Zn_2(AZA)$ and $Mg_2(AZA)$, with the $Zn_2(AZA)$ signal being significantly weaker due to poor loading. In $Co_2(AZA)$ it is unclear as to whether isoniazid loading was achieved as there is no signal present.

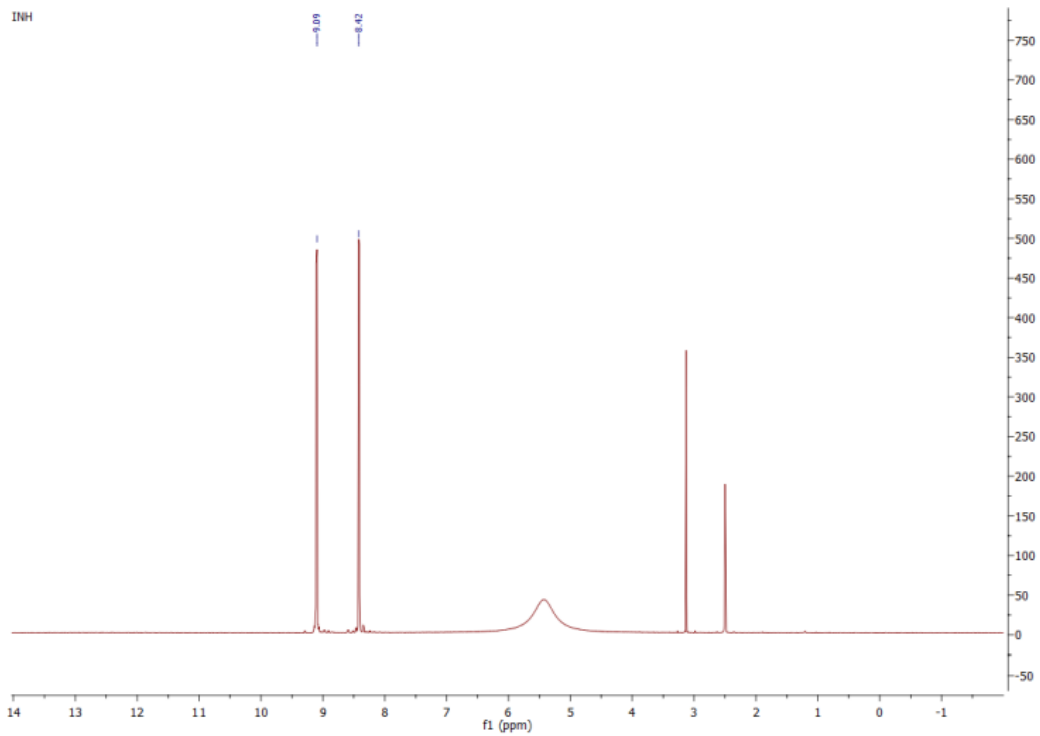


Figure 41: ^1H NMR of isoniazid in DMSO-d_6 and DCl .

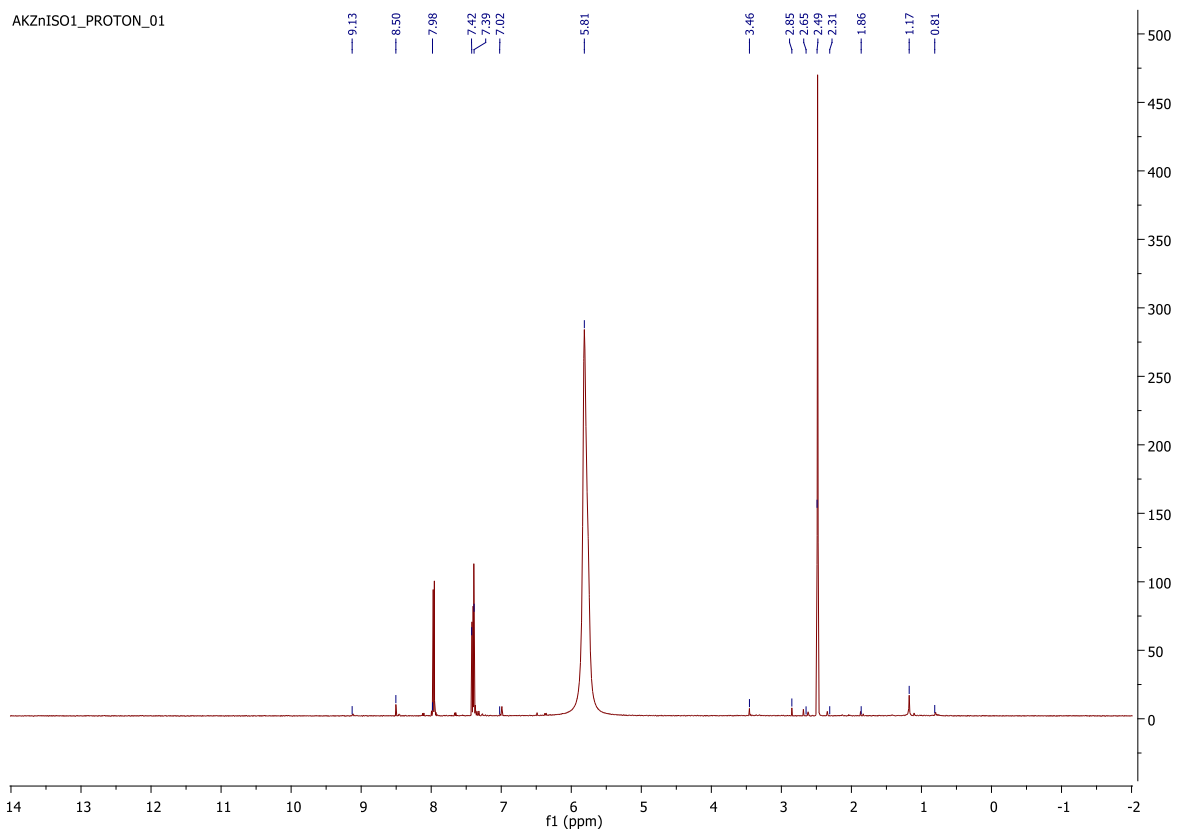


Figure 42: ^1H NMR of $\text{Zn}_2(\text{AZA})$ loaded with isoniazid, solvents used were DMSO-d_6 and DCl .

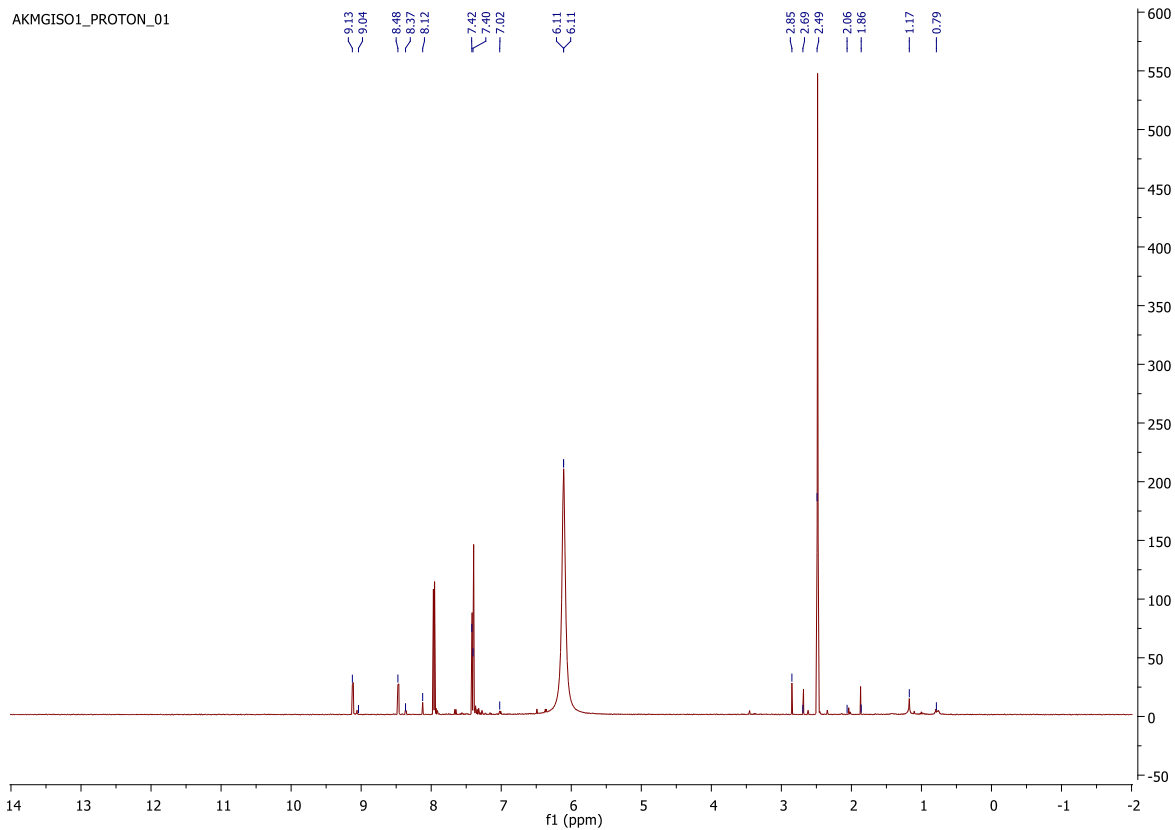


Figure 43: ^1H NMR of $\text{Mg}_2(\text{AZA})$ loaded with isoniazid, solvents used were DMSO-d_6 and DCl .

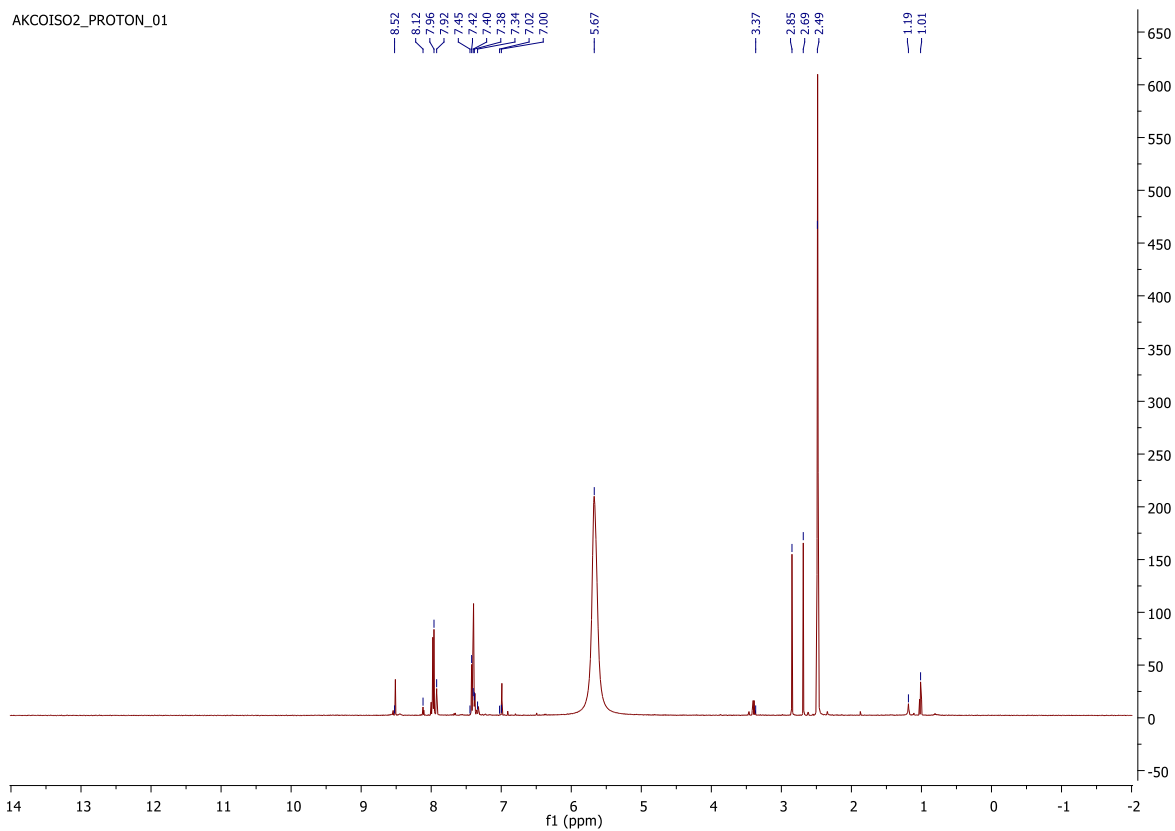


Figure 44: ^1H NMR of $\text{Co}_2(\text{AZA})$ after undergoing isoniazid loading, solvents used were DMSO-d_6 and DCl

Rifampicin loading was attempted under the same anhydrous conditions under nitrogen. A solution of rifampicin (50 mg) in anhydrous MeOH (15 ml) was prepared and added to the activated MOF with the same methodology as isoniazid. Rifampicin loading was attempted on $Zn_2(AZA)$, $Mg_2(AZA)$ and $Co_2(AZA)$. Again, each sample was analysed using H^1 NMR. An in-situ $Zn_2(AZA)$ rifampicin encapsulation was also undertaken, due to its low loading capacity exhibited in the loading of isoniazid. Here, the drug is incorporated into the initial synthesis of the framework, thus allowing the MOF building blocks to assemble around the drug guest molecules. This followed the same method for the synthesis of $Zn_2(AZA)$, but after adding the AZA linker and zinc nitrate to DMF sequentially, rifampicin is added and dissolved with the linker and metal salt in solution, giving a molar ratio of 1:4:2 of AZA linker, zinc nitrate and rifampicin, respectively. The reaction is heated at $100^\circ C$ for 24 hours before being washed with DMF and dried at $80^\circ C$. The obtained crystalline material was then analysed using IR spectroscopy and H^1 NMR. The rifampicin proton signals are present from 12-0 ppm, including 12.52 ppm, 8.8 ppm, 8.06 ppm, 3.33 ppm. Due to the high population of rifampicin peaks present by those of the solvent (DMSO- d_6), the peaks mentioned were used as a reference for analysing drug loading. Through this analysis it is unclear whether drug loading was successful due to the majority of rifampicin signals in H^1 NMR appearing next to that of the solvent signals for each sample (DMSO- d_6 & DCl), as the main reference signal, 12.52 ppm was not present in any sample. The H^1 NMR of $Zn_2(AZA)$, $Zn_2(AZA)$ in situ, $Mg_2(AZA)$ and $Co_2(AZA)$ respectively, (see Figure 46, Figure 47, Figure 48 and Figure 49) all have the characteristic proton signal for AZA at 7.99 ppm. Failure to achieve loading may be due to the size of the rifampicin drug molecule, as it is larger than both isoniazid and ciprofloxacin and may need altered drug loading conditions to enable encapsulation by the MOF.

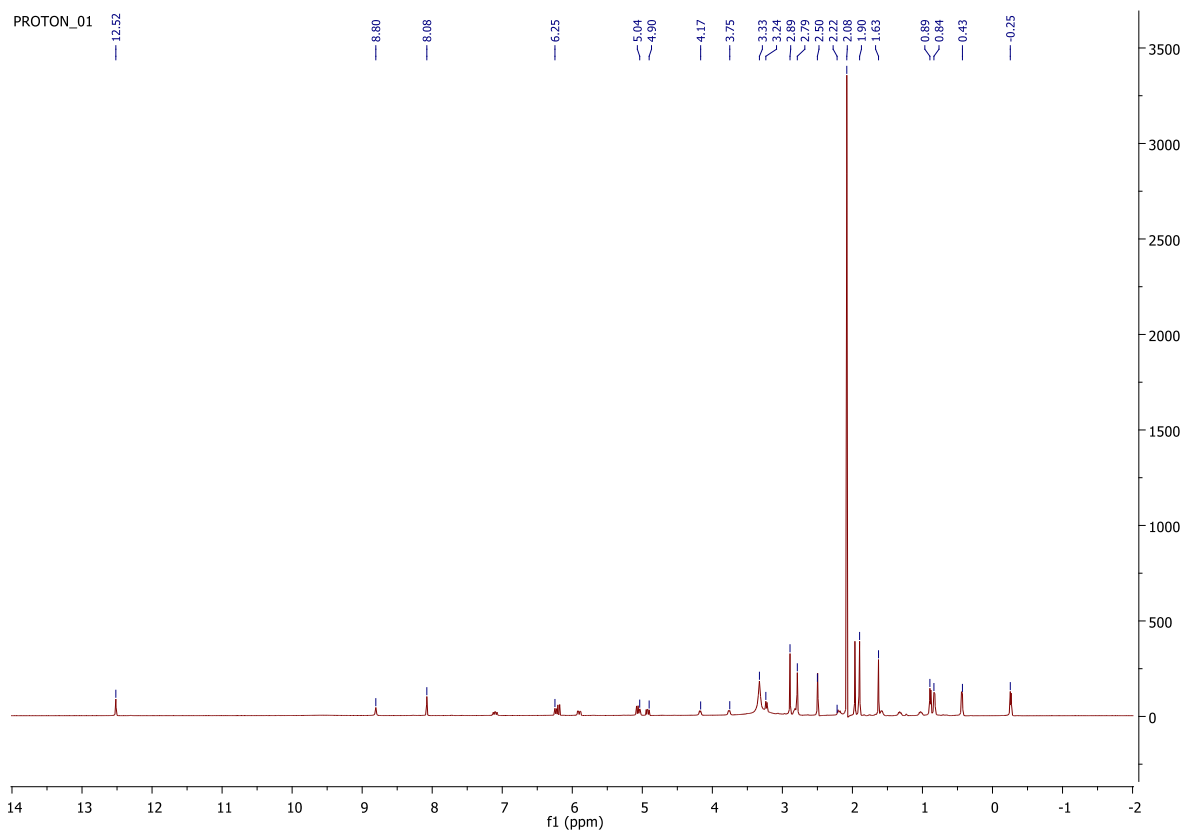


Figure 45: ^1H NMR of rifampicin in DMSO-d_6 .

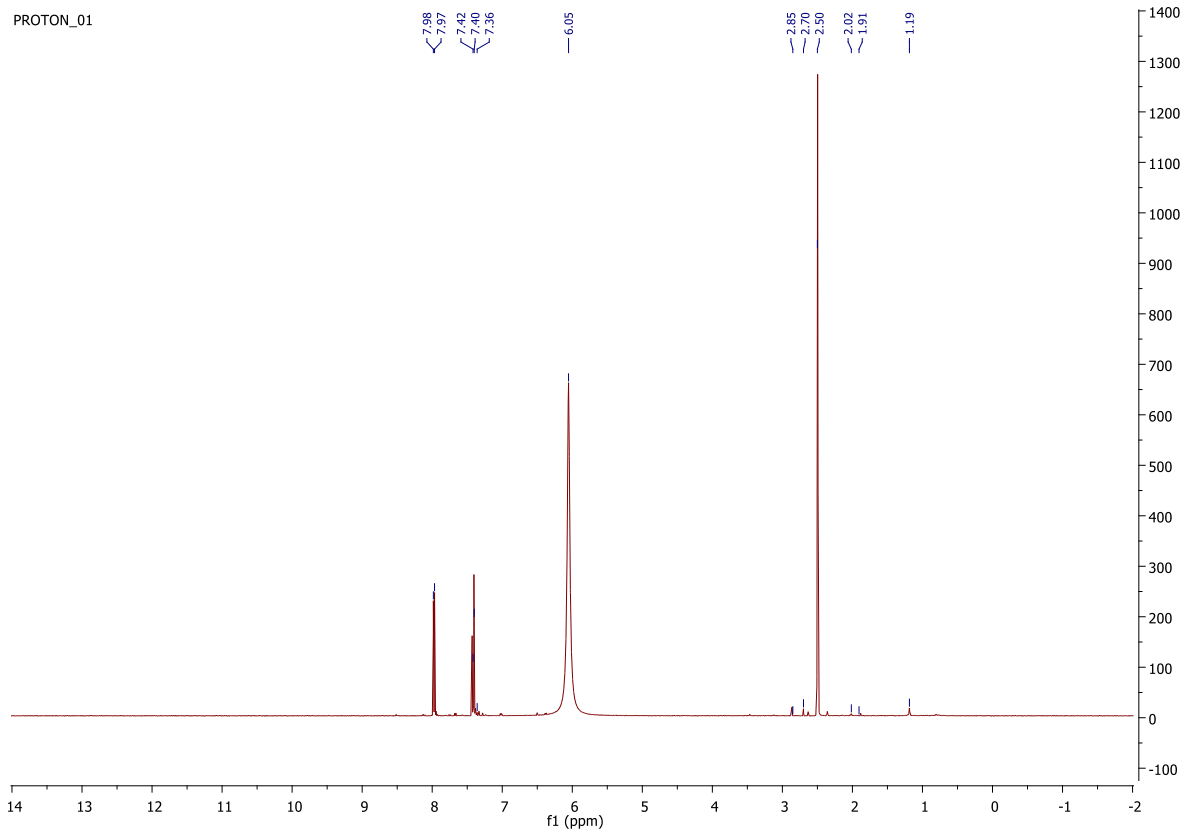


Figure 46: ^1H NMR of $\text{Zn}_2(\text{AZA})$ rifampicin loading, solvents used were DMSO-d_6 and DCI .

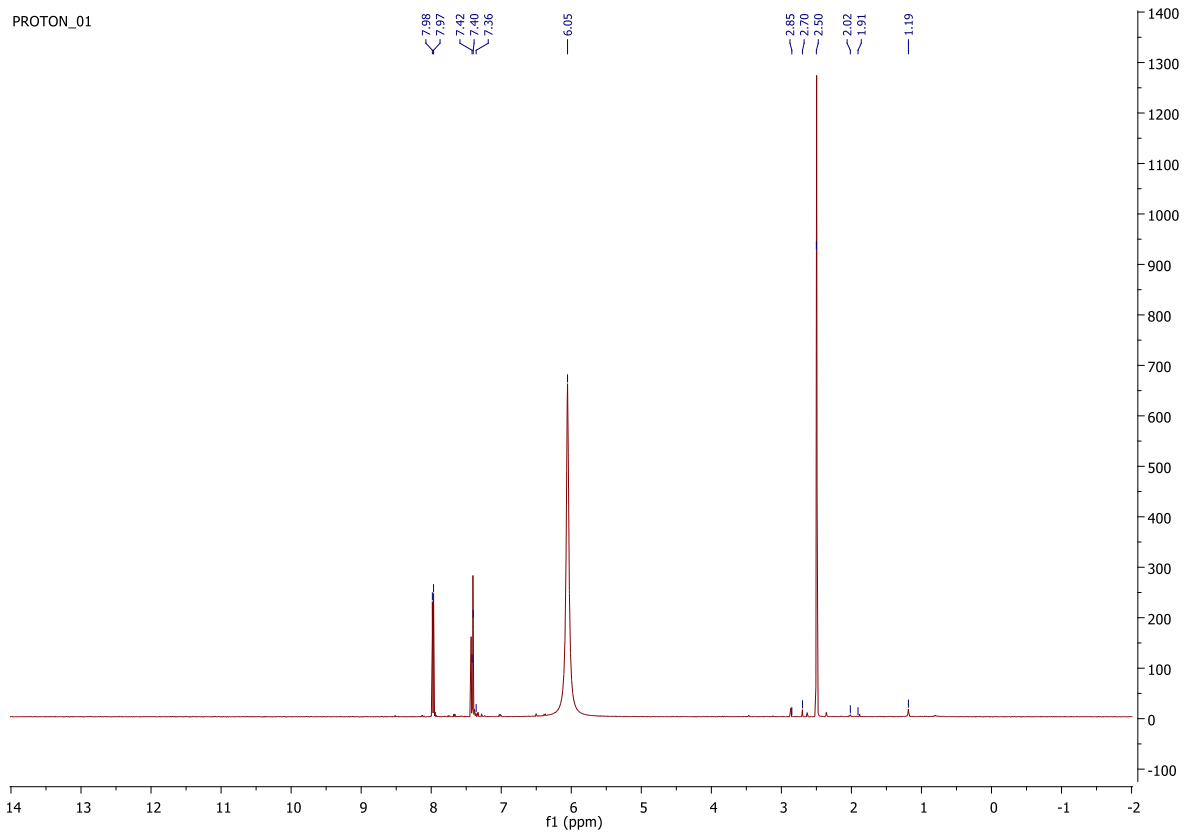


Figure 47: ^1H NMR of $\text{Zn}_2(\text{AZA})$ in situ rifampicin loading, solvents used were DMSO-d_6 and DCI.

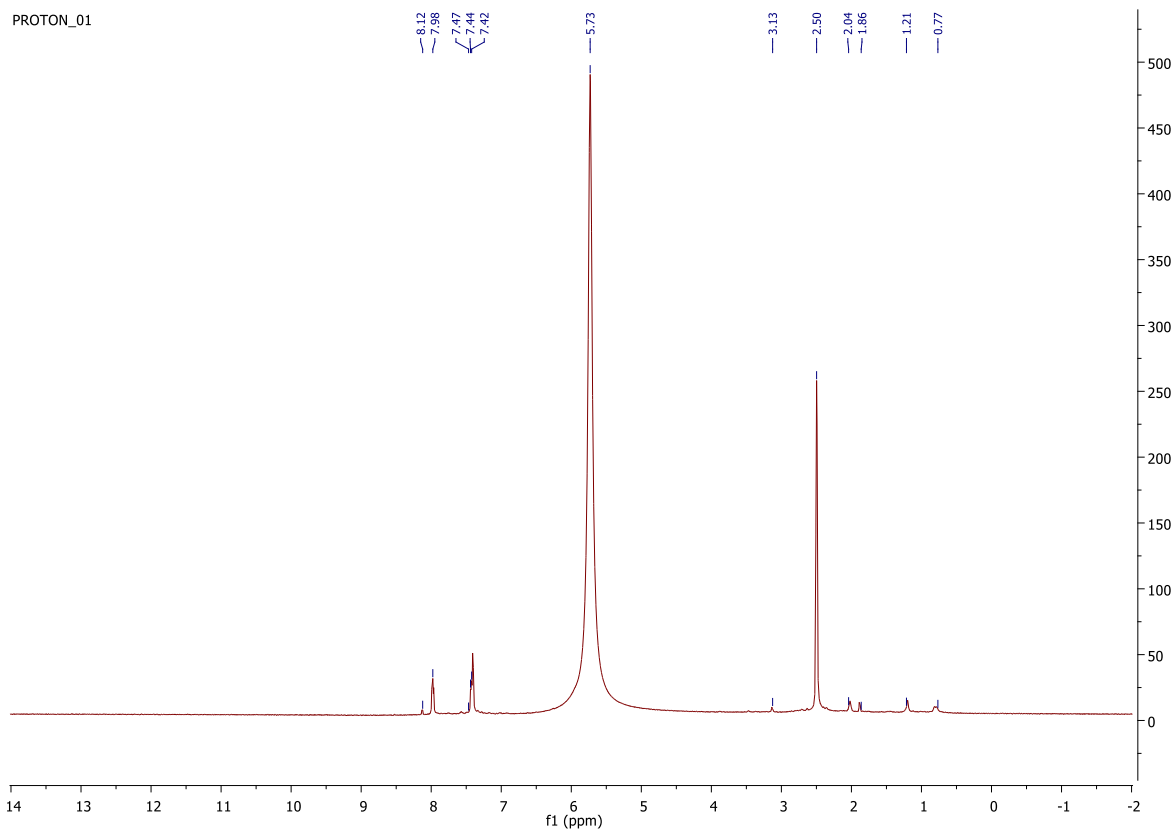


Figure 48: ^1H NMR of $\text{Mg}_2(\text{AZA})$ rifampicin loading, solvents used were DMSO-d_6 and DCI.

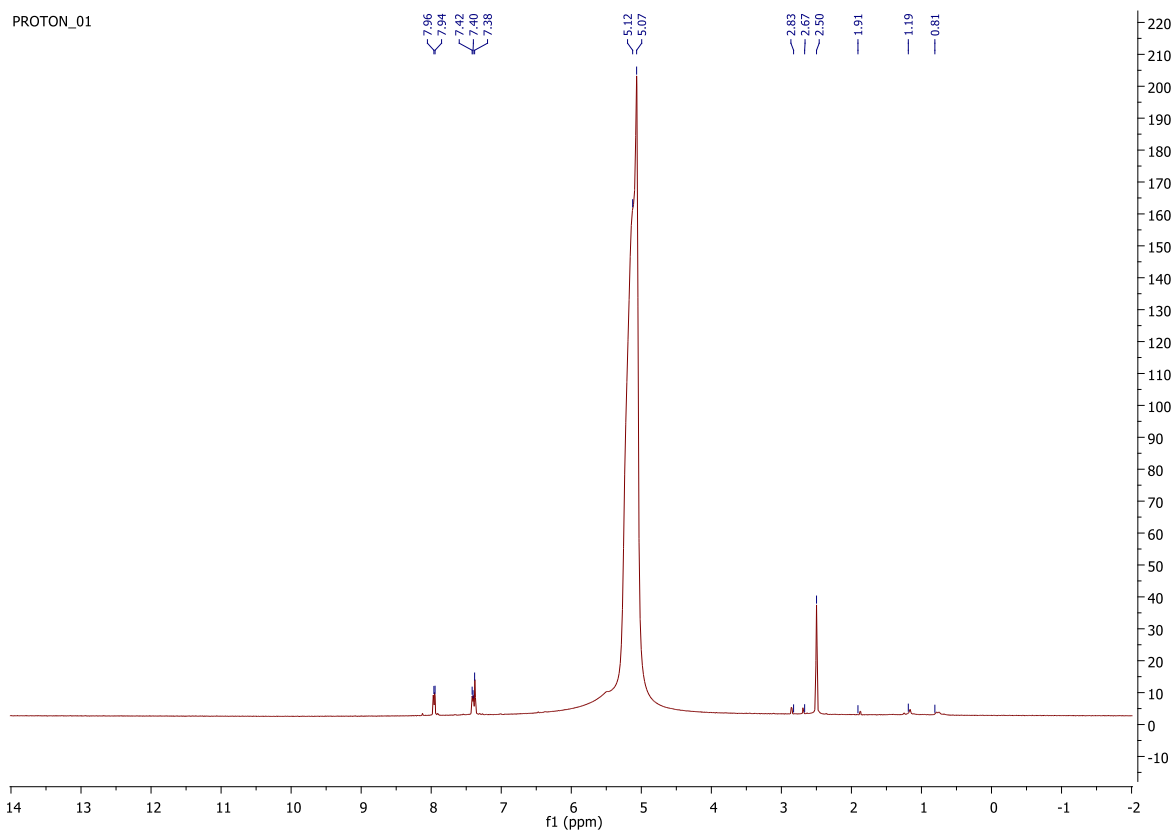


Figure 49: ^1H NMR of $\text{Co}_2(\text{AZA})$ rifampicin loading, solvents used were DMSO-d_6 and DCI .

Ciprofloxacin was chosen as a final antibiotic for drug loading for several reasons. Alongside its use in the treatment and prevention of TB as a fluoroquinolone, both gram-positive and gram-negative bacteria are susceptible to this antibiotic, making it ideal for antibacterial assays. It is also relatively inexpensive and easily sourced. The same method for both rifampicin and isoniazid encapsulation was followed for ciprofloxacin. Solubility issues were prevalent when finding a suitable anhydrous solvent for ciprofloxacin loading. However, it was found that the addition of a negligible amount of glacial acetic acid (2 ml) could be added to anhydrous EtOH (13 ml) to dissolve ciprofloxacin for drug encapsulation. Minimal acetic acid was used as it was able to dissolve the drug without causing any degradation of the MOF during loading. Once again, the activated MOF was left unstirred in solution for 72 hours under nitrogen and washed with anhydrous EtOH before drying. The loaded MOF was analysed using both IR spectroscopy and ^1H NMR. Ciprofloxacin exhibited the most impressive drug loading from the three. As seen in Figure 50, there is a distinct proton signal at 8.63 ppm for ciprofloxacin. This signal is used as a reference point and is present in all 3 ciprofloxacin loadings, $\text{Zn}_2(\text{AZA})$, $\text{Mg}_2(\text{AZA})$ and $\text{Co}_2(\text{AZA})$, (Figure 51, Figure 52 and Figure 53 respectively).

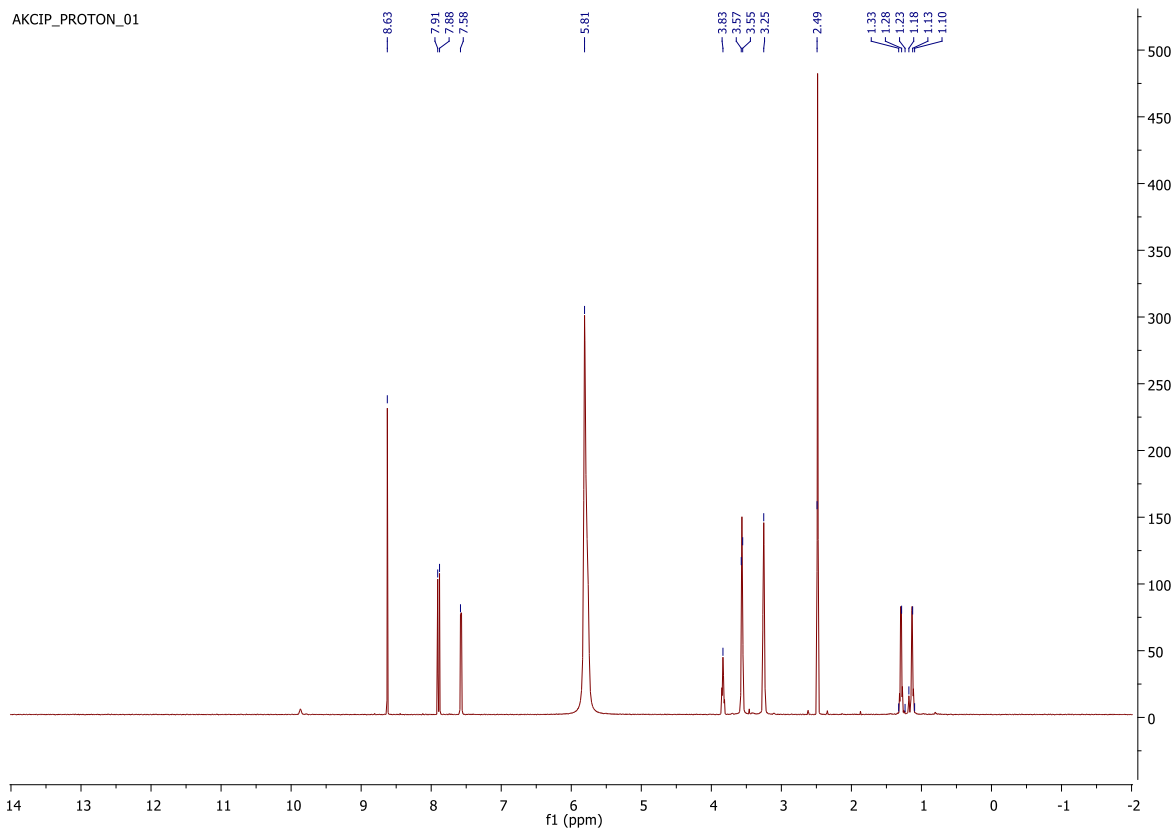


Figure 50: ^1H NMR of ciprofloxacin, solvents used were DMSO-d_6 and DCl .

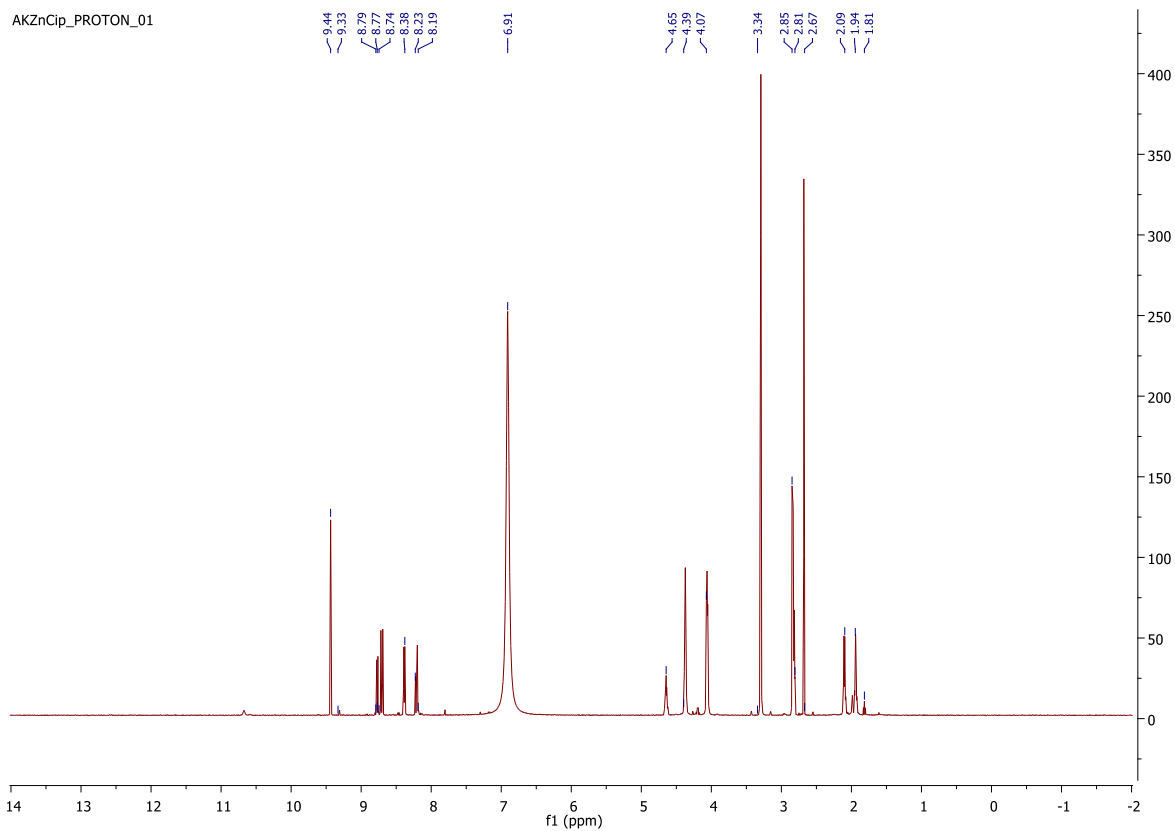


Figure 51: ^1H NMR of $\text{Zn}_2(\text{AZA})$ ciprofloxacin loading, solvents used were DMSO-d_6 and DCl .

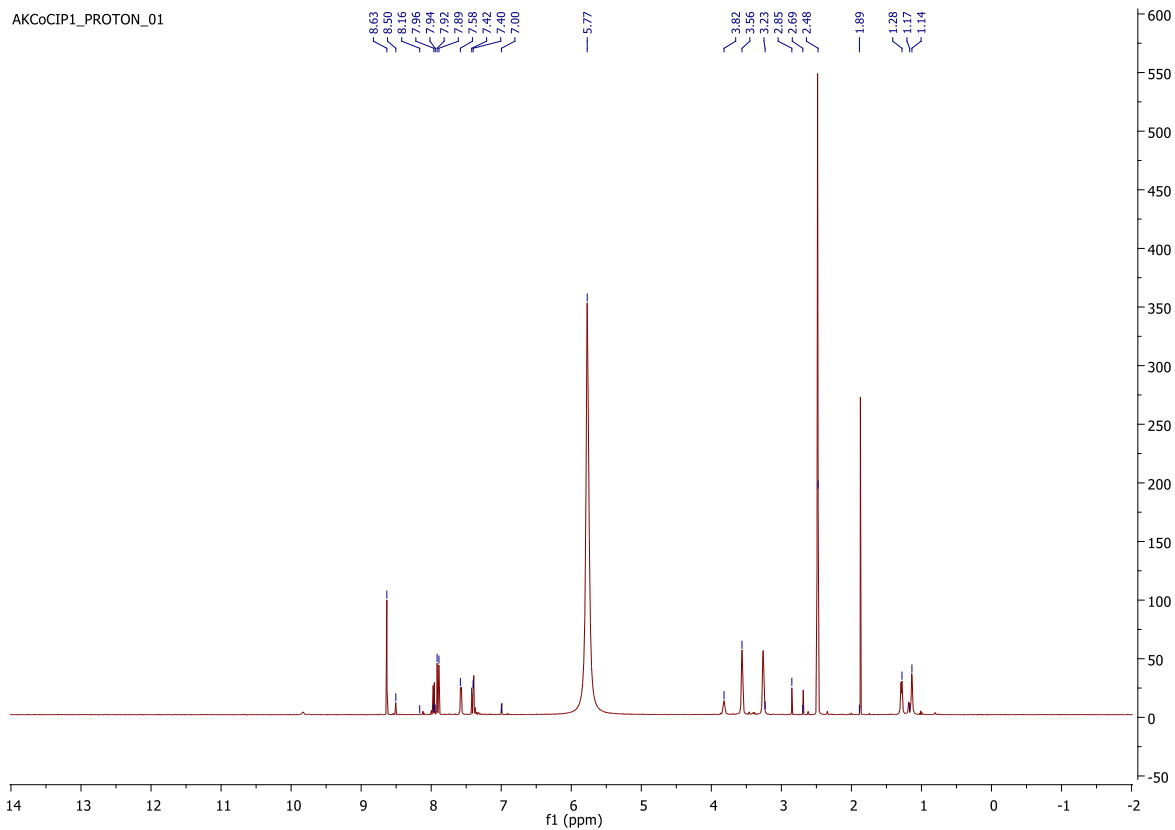


Figure 52: ^1H NMR of $\text{Mg}_2(\text{AZA})$ ciprofloxacin loading, solvents used were DMSO-d_6 and DCI .

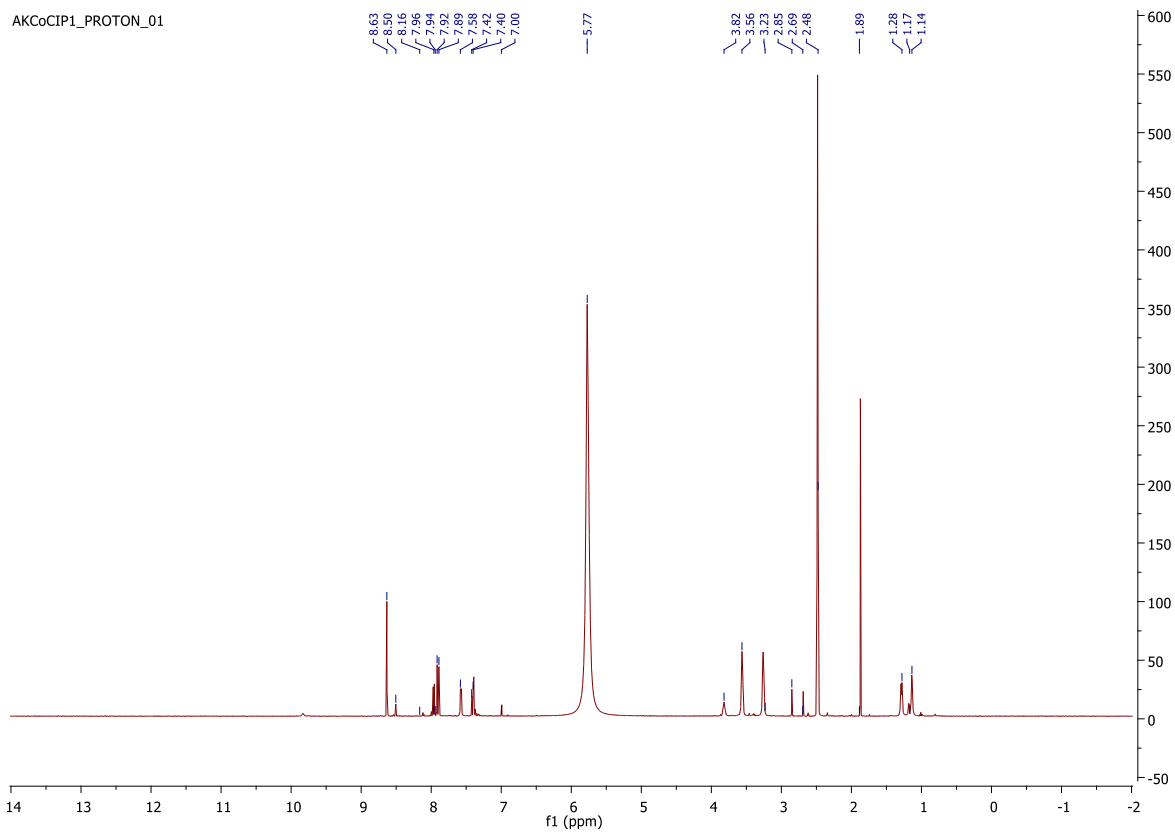


Figure 53: ^1H NMR of $\text{Co}_2(\text{AZA})$ ciprofloxacin loading, solvents used were DMSO-d_6 and DCI .

9.4.7 Antibacterial Assays

Antibacterial assays were carried out on bacteria *Staphylococcus aureus* and *Pseudomonas aeruginosa*, whereby a 1 mg / 100 µl concentration of each sample was prepared. However, these assays produced data that presented very little antibacterial evidence of each sample (Table 4). The lack of bacterial inhibition may be due to insufficient concentration of each antimicrobial moiety in the sample administered.⁶²

Table 4: The growth of *P. aeruginosa* and *S. aureus* after 18 hours of exposure to each sample.⁶²

Material	<i>P. aeruginosa</i> % inhibition	<i>S. aureus</i> % inhibition
<i>Isoniazid</i>	1.88	-35.96
AZA	-7.60	7.52
Mg ₂ (AZA)	-40.12	-59.28
Zn ₂ (AZA)	-150.45	-11.09
Cu ₂ (AZA)	-20.27	-7.50
Co ₂ (AZA)	2.71	18.28
Mg ₂ (AZA) isoniazid	-41.385	-11.80
Zn ₂ (AZA) isoniazid	-19.13	15.60

Therefore, it was clear a need for higher sample concentration was required to achieve more accurate results. Samples containing 10 mg/ 100 µl of the following were prepared for assays; activated Zn₂(AZA), activated Mg₂(AZA), activated Co₂(AZA), isoniazid encapsulating Zn₂(AZA), isoniazid encapsulating Mg₂(AZA), isoniazid encapsulating Co₂(AZA), ciprofloxacin encapsulating Zn₂(AZA), ciprofloxacin encapsulating Mg₂(AZA), ciprofloxacin encapsulating Co₂(AZA), ultrasonicated Zn₂(AZA), ultrasonicated Mg₂(AZA), ultrasonicated Co₂(AZA), AZA ligand, Zn II nitrate, Mg II nitrate and Co II nitrate. This antibacterial assay is currently being carried out.

10 Conclusion & Future work

In this project the multimodal MOFs, $[Zn_2(AZA)]$, $[Mg_2(AZA)]$ and $[Co_2(AZA)]$, were synthesised. These MOFs combined the prodrug organic linker azodisalicyclic acid (AZA) as the organic component of the MOF and the antimicrobial metals Zn^{2+} , Mg^{2+} , Co^{2+} & Cu^{2+} . Drug encapsulation studies of the APIs isoniazid, rifampicin, and ciprofloxacin indicate encapsulation of isoniazid and ciprofloxacin. These MOF is an extremely promising route of treatment for MDR TB as the proposed treatment route may be able to overcome the problems of drug resistance for isoniazid, rifampicin and ciprofloxacin, which are all drugs used in its treatment. Alongside this, the combined delivery of therapeutic, prodrug and antimicrobial metal will allow for a more effective line of therapy overall. In future work, designing a successful activation technique for $[Cu_2(AZA)]$ will be important to incorporate the copper MOF of the series in antibiotic encapsulation studies and any antibiotic assays therefore after.

The future antibacterial assay is an important factor in investigating the efficacy of the loaded AZA MOFs compared to the first line drugs alone. In particular, the MOFs loaded with ciprofloxacin will be a key indicator to the antibacterial properties of the MOFs, as the drug is effective against both bacterial strains. The results of such assay would give rise to the possibility of future assays of the MOF on Mycobacterium tuberculosis. Furthermore, it may be beneficial to undertake the encapsulation of doxorubicin in the MOF, to compare its uptake to the likes of NUIG4, which had one of the highest reported uptakes of the drug, at 1955 mg DOX/g NUIG4.³⁹

The mixed metal MOF, $Zn_2Cu_2(AZA)$, was successfully synthesised therefore creating a MOF capable of encompassing the synergistic properties of the two different metals to further improve the antimicrobial effects and stability of the MOF. After undertaking different metal ratios and reaction times, and using various synthesis methods, an optimised metal ratio of 1:1.45, 1:1.68 and 1:1.75, (Zn to Cu respectively), was reached when using a 3:1:1 (Zn, Cu, AZA) metal to linker ratio. The loading of isoniazid would be the next step for this mixed metal MOF to compare the drug loading properties with the single metal MOF and investigate if the mixed metal MOF is capable of a synergistic effect in drug loading. An insufficient concentration of MOF was utilised during the antibacterial assay studies therefore to investigate whether the mixed metal MOF exhibits improved antibacterial properties, further

antibacterial assays with the concentration of 10 mg MOF / 100 µl DMSO need to be carried out.

The cyanostilbene dicarboxylic acid ligand was synthesised. MOF synthesis attempts were unsuccessful in forming a crystalline material however, the gel product, Compound A, was achieved. Analysis of using IR indicated possible MOF or polymer formation. PXRD and TGA analysis is necessary to determine if MOF/polymer formation has indeed occurred. However, these forms of analysis were not available at the time of this project. . This analysis would also be important to compare the obtained material with that reported by Li *et al.* when working with a similar cyano-substituted ligand, 4-(6-(4-cyanophenyl)-[2,3'-bipyridin]-4-yl)benzoic acid, under the same conditions whereby crystals of USTC-2 were synthesized.⁵⁹ Additionally, the synthesis of a stilbene tricarboxylic acid was attempted with preliminary studies using IR indicated possible ligand formation. Further work including NMR spectroscopy and Mass Spectroscopy is required for fully characterisation and determination of ligand synthesis. With this further characterisation, this ligand has the potential to create a highly porous MOF capable of luminescence and drug encapsulation.

11 Experimental

11.1 General Synthesis

Solvents: Dimethylformamide, Water, Ethanol, Methanol, Acetone, Dimethyl sulfoxide, Deuterated chloride, Acetic acid, Sulphuric acid, Ethylene glycol.

Metal Salts: Zinc (II) nitrate, Copper (II) nitrate, Cobalt (II) nitrate, Magnesium (II) nitrate.

Antibiotics: Ciprofloxacin, Isoniazid, Rifampicin.

Other materials: 4-formyl benzonitrile, 4-cyanophenylacetonitrile, Piperidine, Potassium hydroxide, Sodium hydroxide, D (+) Glucose, 2-hydroxyl-4-nitrobenzoic acid, Sodium carbonate.

Table 5 Instrument Information

Analysis	Instrument Details
<i>SEM/EDX</i>	All samples were then gold-coated prior to imaging and elemental composition analyses in the Hitachi S-4700 SEM .
<i>IR</i>	A Perkin Elmer spectrum one FT-IR was used for IR spectra measurements.
<i>NMR</i>	¹ H NMR analysis was carried out on the Varian VNMRS 500 MHz 54 mm AR spectrometer using CDCl ₃ , DMSO-d ₆ and DCl as solvents with TMS as an internal standard.
<i>UV-Vis</i>	Cary 5000 UV-Vis-NIR spectrometer (200–2500 nm range) with a deuterium UV lamp light source. Solid state UV-vis measurements used a diffuse reflectance accessory (DRA), with powder samples dried thoroughly before use, and pure MgO used as a blank reference.

11.2 Tricyanostilbene synthesis

4-Formyl benzonitrile (1.05 g, 8 mmol) and 4-cyanophenylacetonitrile (1.09 g, 7.7 mmol) were added to a round bottom flask under a fumehood and heated in an oil bath under reflux at 130°C. Once the mixture turned molten, it was swirled to encourage mixing. Next it was taken

off the heat and 2 drops of piperidine were added, turning the solution to a white solid. The yellow/white solid is washed with EtOH 3 times before being dried in an oven at 80 °C for 24 hours. The solid obtained was crushed to a fine powder using a pestle and mortar. A yield of 1.83 g was obtained. Tricyanostilbene material obtained is soluble in chloroform. Data from ¹HNMR and IR analysis is available in appendix (see Figure 54 and Figure 55).

11.3 Cyanostilbene dicarboxylic acid synthesis

Tricyanostilbene obtained from prior step was used as a precursor in this synthesis. Tricyanostilbene (1.83 g, 7.2 mmol) was added to a round bottom flask under a fume hood. Acetic acid (25 ml) was added in excess to the round bottom flask along with a catalytic amount of sulfuric acid (<0.5 ml). The contents of the flask were then heated under reflux and constant stirring at 135°C for 8 hours using an oil bath. The white solid which formed was then washed 3 times using EtOH and dried in an oven at 80 °C for 24 hours. The solid was then crushed to a fine powder using pestle and mortar. A yield of 1.56 g was obtained. The powder obtained was found to be soluble in DMSO. Data was obtained from ¹HNMR and IR analysis.

¹H NMR (500 MHz, DMSO-d₆) δ: 7.86 (d), 7.99 (m), 8.21 (s)

11.4 Stilbene tricarboxylate synthesis

KOH (1.00 g, 17.8 mmol) was added to a round bottom flask containing Ethylene glycol (10 ml) and stirred under fumehood until dissolved. Cyanostilbene dicarboxylic acid (1.5 g, 5.11 mmol) was then added to the flask. The contents of the flask were then heated under reflux and constant stirring at 160°C using an oil bath. After 5 hours, a viscous brown liquid had formed. This was added to a large flask containing a 1:1 solution of acetic acid and H₂O (8 ml) and left unstirred for a week to crystallise. The crystalline product obtained was found to have a lot of solubility issues, thus preventing NMR analysis because of precipitation of the solid.

11.5 Compound A synthesis

Cyanostilbene dicarboxylate (0.038 g, 0.1 mmol) was added to a 20 ml scintillation vial containing DMF (7 ml) and H₂O (5 ml) and sonicated for three minutes until dissolved. Copper nitrate (44 mg, 0.15 mmol) was then added to the vial and sonicated for a further three minutes. The vial was then sealed and placed in an oven at 90°C for 24 hours. A pale blue gel formed and was immediately extracted from the vial using a glass pipette before cooling. The gel formed was dried at 80 °C overnight. A yield of 14 mg was obtained.

11.6 Azodisalicylic acid ligand synthesis

4-Nitrosalicylic acid (1.5 g, 8.2 mmol) was added to a solution of 5M aqueous NaOH (22.5 ml) in a conical flask. This produced a dark red solution. This was stirred under heat at 50°C while exposed to air. Separately, D (+) glucose (10 g, 55 mmol) was added to H₂O (10 ml) and dissolved under heat at 50°C. The solution of D (+) glucose was added slowly to the flask containing 4-Nitrosalicylic acid in NaOH over the course of 1 hour, resulting in the formation of a black solution. This solution was then stirred under heating at 50°C for 15 minutes. After this the solution was allowed to cool and left under constant stirring for 48 hours, while open to the air. A dark brown precipitate was obtained at the end of this time. Concentrated HCl was added dropwise to the solution until it was acidified to pH 1. This solution was then filtered using a Buchner flask to obtain the dark brown precipitate. This was washed with excess H₂O and allowed to dry for 24 hours in an oven at 60°C. This crude product was then used in the recrystallization process for purification. The crude product was added to a conical flask containing H₂O (200 ml) and was heated to 80°C until solid suspended. Na₂CO₃ was then added bit by bit until the crude product was dissolved and a clear red/black solution was obtained. This was taken off heat and gravity filtered before being allowed to cool. The solution was then left to recrystallise for 24 hours. The pure AZA ligand was collected via Buchner filtration and dried for 24 hours at 60°C. This product was then redissolved in minimal H₂O and acidified to pH 1 by adding concentrated HCl dropwise. This resulted in the formation of an orange precipitate which was collected via Buchner filtration, washed with excess H₂O and dried for 24 hours at 60°C. A yield of 1.02 g was obtained.

¹H NMR (500 MHz, DMSO-d₆) δ: 7.422 (dd), δ 7.99 (d)

11.7 Zn₂(AZA) synthesis

When synthesizing Zn₂(AZA), a 4:1 molar ratio of zinc nitrate to linker respectively was used. AZA (0.030 g, 0.1 mmol) was added to a 20 ml scintillation vial containing DMF (5 ml) and was sonicated for three minutes until dissolved. Zinc nitrate (0.119 g, 0.4 mmol) was then added to the vial and sonicated for a further three minutes. The vial was then sealed and placed in an oven at 100°C for 7 hours. The crystalline product obtained was washed with DMF (10 ml) 3 times. A yield of 18 mg was achieved.

11.8 Co₂(AZA) synthesis

When synthesizing Co₂(AZA), a 1:1 ratio of cobalt nitrate to linker respectively was used. AZA (0.030 g, 0.1 mmol) was added to a 20 ml scintillation vial containing DMF (5 ml) and was sonicated for three minutes until dissolved. Cobalt nitrate (0.029 g, 0.1 mmol) was then added to the vial and sonicated for a further three minutes. The vial was then sealed and placed in an oven at 100°C for 24 hours. The crystalline product obtained was washed with DMF (10 ml) 3 times. A yield of 22 mg was achieved.

11.9 Mg₂(AZA) synthesis

When synthesizing Mg₂(AZA), a 3:1 ratio of magnesium nitrate to linker respectively was used. AZA (0.030 g, 0.1 mmol) was added to a 20 ml scintillation vial containing DMF (4 ml), EtOH (1 ml) and H₂O (1 ml) and was sonicated for three minutes until dissolved. Magnesium nitrate (0.077 g, 0.3 mmol) was then added to the vial and sonicated for a further three minutes. The vial was then sealed and placed in an oven at 100°C for 24 hours. The crystalline product obtained was washed with DMF (10 ml) 3 times. A yield of 16 mg was achieved.

11.10 Mixed Metal Zn₂Cu₂ (AZA) synthesis

11.10.1 Solvothermal Synthesis

When synthesizing Zn₂Co₂(AZA), a 3:1:1 ratio of zinc nitrate to copper nitrate to linker respectively was used. AZA (0.030 g, 0.1 mmol) was added to a 20 ml scintillation vial containing DMF (4 ml), EtOH (2 ml) and was sonicated for three minutes until dissolved. Zinc nitrate (0.089 g, 0.3 mmol) was then added to the vial and sonicated for three minutes.

Copper nitrate (0.023 g, 0.1 mmol) was then added to the vial and sonicated for a further three minutes. The vial was then sealed and placed in an oven at 100°C for 6 hours. The powder product obtained was washed and centrifuged with DMF (10 ml) 3 times at 3500 rpm for 5 minutes. A yield of 20 mg was achieved.

11.10.2 Reflux Heated Synthesis

When synthesizing a 3:1:1 molar ratio of zinc nitrate to copper nitrate to linker of $Zn_2Co_2(AZA)$ under reflux, the following procedure was followed. AZA (0.030 g, 0.1 mmol) was added to a round bottom flask containing DMF (6 ml), EtOH (4 ml) and was sonicated for three minutes until dissolved. Zinc nitrate (0.089 g, 0.3 mmol) was then added to the flask and sonicated for three minutes. Copper nitrate (0.023 g, 0.1 mmol) was then added to the flask and sonicated for a further three minutes. The flask was stoppered and heated using an oil bath under reflux and constant stirring at 100°C for 20 hours. The powder product obtained was washed and centrifuged with DMF (10 ml) 3 times at 3500 rpm for 5 minutes. A yield of 29 mg was obtained.

When synthesizing a 4:1:1 ratio of zinc nitrate to copper nitrate to linker of $Zn_2Co_2(AZA)$ under reflux, the following procedure was followed. AZA (0.030 g, 0.1 mmol) was added to a round bottom flask containing DMF (4 ml), EtOH (2 ml) and was sonicated for three minutes until dissolved. Zinc nitrate (0.119 g, 0.3 mmol) was then added to the flask and sonicated for three minutes. Copper nitrate (0.023 g, 0.1 mmol) was then added to the flask and sonicated for a further three minutes. The flask was stoppered and heated using an oil bath under reflux and constant stirring at 100°C for 20 hours. The powder product obtained was washed and centrifuged with DMF (10 ml) 3 times at 3500 rpm for 5 minutes. A yield of 31 mg was obtained.

11.11 Microwave Synthesis

When synthesizing a 3:1:1 molar ratio of zinc nitrate to copper nitrate to linker of $Zn_2Co_2(AZA)$ using microwave synthesis, the following procedure was followed. AZA (0.030 g, 0.1 mmol) was added to a glass microwave tube containing DMF (4 ml), EtOH (2 ml) and was sonicated for three minutes until dissolved. Zinc nitrate (0.089 g, 0.3 mmol) was then added to the tube

and sonicated for three minutes. Copper nitrate (0.023 g, 0.1 mmol) was then added to the tube and sonicated for a further three minutes. The glass microwave tube was inserted to the microwave and heated to 120°C with constant stirring at high setting and a pressure of 17.2 kPa. The reaction was repeated with the following reaction times: 30 mins, 1 hour, 1.5 hours, 2 hours. The powder product obtained was washed and centrifuged with DMF (10 ml) 3 times at 3500 rpm for 5 minutes. A yield of ~35 mg was obtained.

11.12 MOF Activation

The Zn₂(AZA), Mg₂(AZA) and Co₂(AZA) MOFs were activated under specific conditions due to their hygroscopic nature. First the MOF underwent solvent exchange as they were washed in fresh DMF every 24 hours for 72 hours, followed by fresh MeOH every 24 hours for 72 hours. Following this process, the MOF was then dried at 80°C for 24 hours. The round bottom flask being used in activation was also put into an oven at 80°C for 1-2 hours before activation to remove moisture from glassware. The MOF (20 mg) was weighed and placed inside the empty round bottom flask, which was then stoppered and attached to a vacuum system. This flask was then heated to 180°C using an oil bath under vacuum for 7 hours. After MOF activation, the round bottom flask was removed from heat and allowed to cool for 5 min.

11.13 Isoniazid Encapsulation

A solution of isoniazid (0.050 g) in anhydrous EtOH (15 ml) was made in a stoppered round bottom flask under nitrogen to minimize moisture absorption. This solution was sonicated for 3 min until fully dissolved and then was added to the cooled activated MOF, which had been removed from vacuum and sealed. This was placed under nitrogen and left unstirred for 72 hours, after which it is washed 3 times using anhydrous EtOH and dried at 80°C for 24 hours. The loaded MOF was then analysed using IR and NMR.

11.14 Rifampicin Encapsulation

A solution of rifampicin (0.050 g) in anhydrous MeOH (15 ml) was made in a stoppered round bottom flask under nitrogen to minimize moisture absorption. This solution was sonicated for 3 min until fully dissolved and then was added to the cooled activated MOF, which had been removed from vacuum and sealed. This was placed under nitrogen and left unstirred for 72

hours, after which it is washed 3 times using anhydrous MeOH and dried at 80°C for 24 hours. The loaded MOF was then analysed using IR and NMR.

11.15 Ciprofloxacin Encapsulation

A solution of ciprofloxacin (0.050 g) in anhydrous EtOH (13 ml) and glacial acetic acid (2 ml) was made in a stoppered round bottom flask under nitrogen to minimize moisture absorption. This solution was sonicated for 3 min until fully dissolved and then was added to the cooled activated MOF, which had been removed from vacuum and sealed. This was placed under nitrogen and left unstirred for 72 hours, after which it is washed 3 times using anhydrous EtOH and dried at 80°C for 24 hours. The loaded MOF was then analysed using IR and NMR.

11.16 In-situ Zn₂(AZA) rifampicin loading

When synthesizing Zn₂(AZA) with in situ rifampicin loading, a 4:1 ratio of zinc nitrate to linker respectively was used. AZA (0.030 g, 0.1 mmol) was added to a 20 ml scintillation vial containing DMF (5 ml) and was sonicated for 3 min until dissolved. Zinc nitrate (0.119 g, 0.4 mmol) was then added to the vial and sonicated for 3 min. Rifampicin (0.050 g) was then added to the vial and sonicated for a further 3 min. The vial was then sealed and placed in an oven at 100°C for 24 hours. The crystalline product obtained was washed with DMF 3 times.

11.17 Dissolution studies

Water dissolution studies were carried out over 24 hours. First enough dissolution vials for the number of samples are prepared, each with H₂O (4.5 ml). The MOF sample (0.015 g) is added to a centrifuge tube containing 15 ml H₂O. A sample is taken at 0 min before the dissolution studies begin. The tube is added to a water bath at 37 °C and stirred. At each time interval, a sample (500 µl) is taken from the dissolution tube and added to a dissolution vial. H₂O (500 µl) is then added back to the dissolution tube. The following intervals were followed for taking samples: 5 min, 10 min, 15 min, 30 min, 1 hour. All samples were analysed using a Varian Cary 50 UV-Vis scan spectrophotometer.

PBS dissolution studies were carried out over 24 hours. First enough dissolution vials for the amount of samples are prepared, each with H₂O (4.5 ml). The MOF sample (0.015 g) is added to a centrifuge tube containing 15 ml PBS. A sample is taken at 0 min before the dissolution studies begin. The tube is added to a water bath at 37 °C and stirred. At each time interval, a sample (500 µl) is taken from the dissolution tube and added to a dissolution vial. PBS (500 µl) is then added back to the dissolution tube. The following intervals were followed for taking samples: 5 min, 10 min, 15 min, 30 min, 1 hour. All samples were analysed using a Varian Cary 50 UV-Vis scan spectrophotometer.

12 Bibliography

- 1 R. C. Huxford, J. Della Rocca and W. Lin, *Curr. Opin. Chem. Biol.*, 2010, **14**, 262–268.
- 2 H. Li, M. Eddaoudi, M. O’Keeffe and O. M. Yaghi, *Nature*, 1999, **402**, 276–279.
- 3 R. J. Kuppler, D. J. Timmons, Q. R. Fang, J. R. Li, T. A. Makal, M. D. Young, D. Yuan, D. Zhao, W. Zhuang and H. C. Zhou, *Coord. Chem. Rev.*, 2009, **253**, 3042–3066.
- 4 M. Eddaoudi, D. B. Moler, H. Li, B. Chen, T. M. Reineke, M. O’Keeffe and O. M. Yaghi, *Acc. Chem. Res.*, 2001, **34**, 319–330.
- 5 V. Bhatt and S. Ram, *Chem Sci Rev Lett*, 2015, **4**, 414–428.
- 6 A. Schoedel and S. Rajeh, 2020, pp. 1–55.
- 7 M. Eddaoudi, D. B. Moler, H. Li, B. Chen, T. M. Reineke, M. O’keeffe and O. M. Yaghi, *Ann Acc. Chem. Res*, 1995, **34**, 19.
- 8 M. J. Kalmutzki, N. Hanikel and O. M. Yaghi, *Sci. Adv.*, ,
DOI:10.1126/SCIADV.AAT9180/ASSET/B6C0FDB7-F181-4CF2-95C2-
C3407FF1F51E/ASSETS/GRAPHIC/AAT9180-F6.JPEG.
- 9 V. V Butova, M. A. Soldatov, A. A. Guda, K. A. Lomachenko and C. Lamberti, *Russ. Chem. Rev.*, 2016, **85**, 280–307.
- 10 A. Ahmed, D. McHugh and C. Papatriantafyllopoulou, *Molecules*, 2022, **27**, 6585.
- 11 S. Yang, X. Lin, W. Lewis, M. Suyetin, E. Bichoutskaia, J. E. Parker, C. C. Tang, D. R. Allan, P. J. Rizkallah, P. Hubberstey, N. R. Champness, K. Mark Thomas, A. J. Blake and M. Schröder, *Nat. Mater.*, 2012, **11**, 710–716.
- 12 J. L. C. Rowsell and O. M. Yaghi, *Microporous Mesoporous Mater.*, 2004, **73**, 3–14.
- 13 P. Rocío-Bautista, I. Taima-Mancera, J. Pasán and V. Pino, *Separations*, 2019, **6**, 33.
- 14 R. K. Motkuri, J. Liu, C. A. . Fernandez, S. K. . Nune, P. Thallapally and B. . P. McGrail, in *Industrial Catalysis and Separations*, eds. K. . V. . Raghavan and B. . M. . Reddy, Apple Academic Press, 2014, pp. 61–103.
- 15 O. K. Farha, I. Eryazici, N. C. Jeong, B. G. Hauser, C. E. Wilmer, A. A. Sarjeant, R. Q. Snurr, S. T. Nguyen, A. Ö. Yazaydin and J. T. Hupp, *J. Am. Chem. Soc.*, 2012, **134**, 15016–15021.
- 16 M. Naderi, , DOI:10.1016/B978-0-12-384746-1.00014-8.
- 17 K. S. Walton and R. Q. Snurr, *J. Am. Chem. Soc.*, 2007, **129**, 8552–8556.
- 18 S. Shimizu and N. Matubayasi, *Langmuir*, 2022, **38**, 7989–8002.

- 19 B. Zhang, J. Zhang, C. Liu, X. Sang, L. Peng, X. Ma, T. Wu, B. Han and G. Yang, , DOI:10.1039/c5ra02440d.
- 20 E.-S. M. El-Sayed and D. Yuan, , DOI:10.1039/d0gc00353k.
- 21 M. A. Abdelkareem, Q. Abbas, M. Mouselly, H. Alawadhi and A. G. Olabi, *J. Sci. Adv. Mater. Devices*, 2022, **7**, 100465.
- 22 H. Furukawa, K. E. Cordova, M. O’Keeffe and O. M. Yaghi, *Science*, , DOI:10.1126/SCIENCE.1230444.
- 23 Solvothermal synthesis of a MOF material | Download Scientific Diagram, https://www.researchgate.net/figure/Solvothermal-synthesis-of-a-MOF-material_fig1_327870658, (accessed 11 August 2023).
- 24 V. F. Yusuf, N. I. Malek and S. K. Kailasa, *ACS Omega*, 2022, **7**, 44507–44531.
- 25 S. T. Golafale, C. W. Ingram, J. Bacsa, A. Steiner and K. M. Solntsev, *Inorganica Chim. Acta*, 2018, **478**, 243–249.
- 26 H. Xu, Y. Tan, Z. Hou, C. Fu and L.-R. Lin, 2021, **7**, 947–958.
- 27 M. Y. Masoomi, A. Morsali, A. Dhakshinamoorthy and H. Garcia, *Angew. Chemie Int. Ed.*, 2019, **58**, 15188–15205.
- 28 T. Abdelkareem, M. Amer, S. Palanisamy, P. B. So, P. Vijayaraghavan, S.-C. Tzou, T.-T. Lu, C.-H. Lin and Y.-M. Wang, , DOI:10.1021/acs.bioconjchem.3c00325.
- 29 J. Liu and Y. Pan, *Met. Fram. Biomed. Appl.*, 2020, 45–68.
- 30 S. Abednatanzi, P. Gohari Derakhshandeh, H. Depauw, F.-X. Coudert, H. Vrielinck, P. Van Der Voort and K. Leus, *Chem. Soc. Rev.*, 2019, **48**, 2535–2565.
- 31 X. Zhang, F. Peng and D. Wang, *J. Funct. Biomater.*, 2022, **13**, 215.
- 32 Z. Sepehri, N. Mirzaei, A. Sargazi, A. Sargazi, A. Panahi Mishkar, Z. Kiani, H. O. Oskoe, D. Arefi and S. Ghavami, *J. Clin. Tuberc. Other Mycobact. Dis.*, 2017, **6**, 8–13.
- 33 S. Rojas, T. Devic and P. Horcajada, *J. Mater. Chem. B*, 2017, **5**, 2560–2573.
- 34 S. Rojas, A. Arenas-Vivo and P. Horcajada, *Coord. Chem. Rev.*, 2019, **388**, 202–226.
- 35 H.-S. Wang, , DOI:10.1016/j.ccr.2017.08.015.
- 36 Y. Liu, Y. Li and L. Shi, *J. Control. Release*, 2021, **329**, 1102–1116.
- 37 D. Chen, X. Liu, X. Lu and J. Tian, *Front. Pharmacol.*, , DOI:10.3389/fphar.2023.1111991.
- 38 Q. Y. Wei, Y. M. Xu and A. T. Y. Lau, *Cancers (Basel)*, 2020, **12**, 1–37.
- 39 A. Ahmed, C. G. Efthymiou, R. Sanii, E. Patyk-Kazmierczak, A. M. Alsharabasy, M.

- Winterlich, N. Kumar, D. Sensharma, W. Tong, S. Guerin, P. Farras, S. Hudson, D. Thompson, M. J. Zaworotko, A. J. Tasiopoulos and C. Papatriantafyllopoulou, *J. Mater. Chem. B*, 2022, **10**, 1378–1385.
- 40 G. Muthiah and A. Jaiswal, *Adv. NanoBiomed Res.*, 2022, **2**, 2100074.
- 41 H. D. Lawson, S. P. Walton and C. Chan, *ACS Appl. Mater. Interfaces*, 2021, **13**, 7004–7020.
- 42 H. Yang, J. Chen, Y. Liang, Y. Zhang, W. Yin, Y. Xu, S.-Y. Liu, Z. Dai and X. Zou, *ACS Appl. Mater. Interfaces*, 2021, **13**, 45291–45299.
- 43 World Health Organization, *WHO consolidated guidelines on tuberculosis.*, 2022.
- 44 Centers for disease control and prevention (CDC), *Centers Dis. Control Prev.*, 2012, 1–2.
- 45 C. Fernández-Paz, E. Fernández-Paz, P. Salcedo-Abraira, S. Rojas, S. Barrios-Esteban, N. Csaba, P. Horcajada and C. Remuñán-López, *Molecules*, 2021, **26**, 6408.
- 46 In *Meyler's Side Effects of Drugs*, Elsevier, 2016, pp. 341–350.
- 47 C. O'Connor and M. F. Brady, *Isoniazid*, 2023.
- 48 S. R. Khan, Y. Manialawy and A. G. Siraki, *Br. J. Pharmacol.*, 2019, **176**, 4599–4608.
- 49 W. Wehrli, *Clin. Infect. Dis.*, 1983, **5**, S407–S411.
- 50 F. A. SIRGEL, F. J. BOTHA, D. P. PARKIN, B. W. VAN de WAL, R. SCHALL, P. R. DONALD and D. A. MITCHISON, *Am. J. Respir. Crit. Care Med.*, 1997, **156**, 901–905.
- 51 A. Shariati, M. Arshadi, M. A. Khosrojerdi, M. Abedinzadeh, M. Ganjalishahi, A. Maleki, M. Heidary and S. Khoshnood, *Front. Public Heal.*, , DOI:10.3389/fpubh.2022.1025633.
- 52 X. Qi, N. Shen, A. Al Othman, A. Mezentsev, A. Permyakova, Z. Yu, M. Lepoitevin, C. Serre and M. Durymanov, *Pharmaceutics*, 2023, **15**, 1521.
- 53 D. J. Levine, T. Runčevski, M. T. Kapelewski, B. K. Keitz, J. Oktawiec, D. A. Reed, J. A. Mason, H. Z. H. Jiang, K. A. Colwell, C. M. Legendre, S. A. Fitzgerald and J. R. Long, *J. Am. Chem. Soc.*, 2016, **138**, 10143–10150.
- 54 Y. Minato, J. M. Thiede, S. L. Kordus, E. J. McKlveen, B. J. Turman and A. D. Baughn, *Antimicrob. Agents Chemother.*, 2015, **59**, 5097–5106.
- 55 Aminosalicylic acid: Uses, Interactions, Mechanism of Action | DrugBank Online, <https://go.drugbank.com/drugs/DB00233>, (accessed 18 August 2023).
- 56 F. Bell and D. H. Waring, *J. Chem. Soc.*, 1948, 1024–1026.

- 57 S. R. Mathis II, S. T. Golafale, J. Bacsa, A. Steiner, C. W. Ingram, F. P. Doty, E. Auden and K. Hattar, *Dalt. Trans.*, 2017, **46**, 491–500.
- 58 C. Das and S. Horike, , DOI:10.1039/d0fd00003e.
- 59 B. Li, Q. Q. Yan, Z. Q. Xu, Y. B. Xu and G. P. Yong, *CrystEngComm*, 2020, **22**, 506–514.
- 60 D. Suneela, V. Gaurav and S. Samuel, *Inflamm. Allergy - Drug Targets*, 2013, **12**, 419–432.
- 61 D. S. Bhate, T. B. Panse and K. Venkataraman, *Proc. Indian Acad. Sci. - Sect. A*, 1949, **29**, 196–202.
- 62 A. Ahmed, Design and synthesis of biocompatible metal-organic frameworks for anti-cancer, anti-tubercular and MRI application, University of Galway, 2023, 1–262.
- 63 Y. Liang, H. Huang, L. Kou, F. Li, J. Lü and H. Cao, *Cryst. Growth Des.*, 2018, **18**, 6609–6616.

13 Appendix

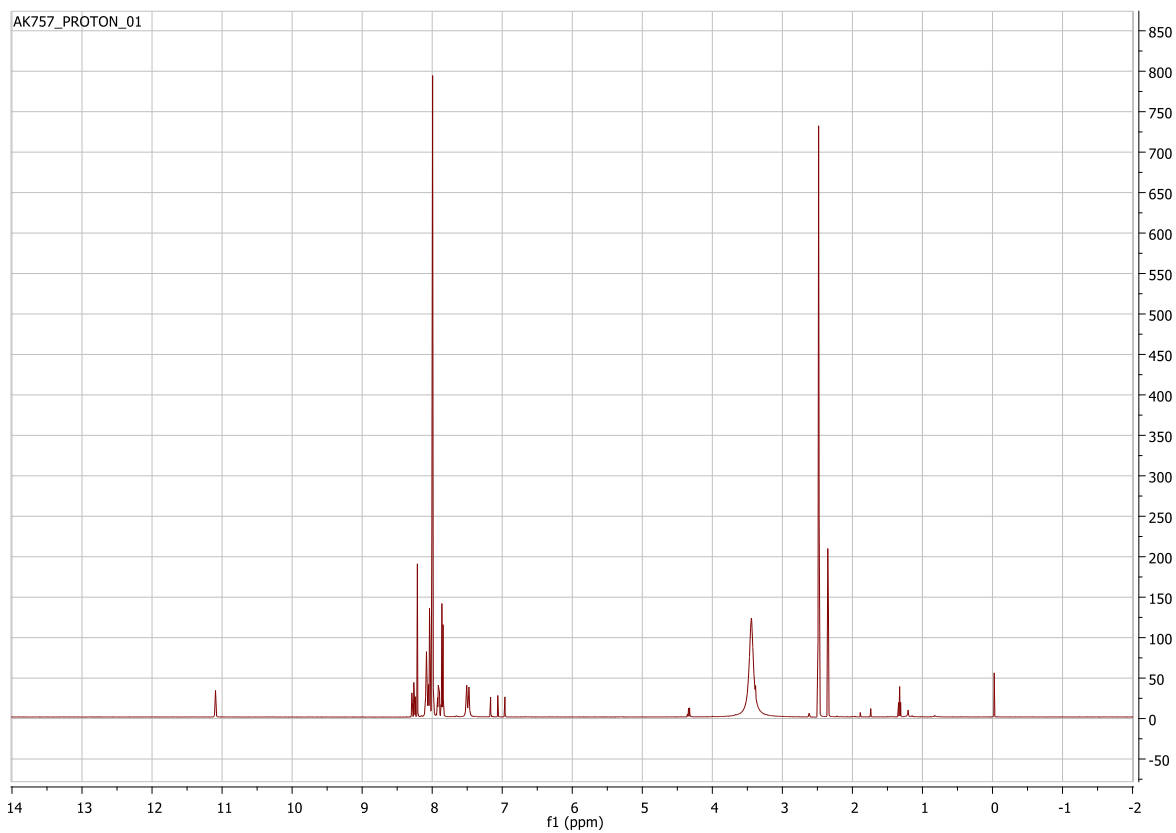


Figure 54: ^1H NMR on tricyanostilbene in d-CDCl_3

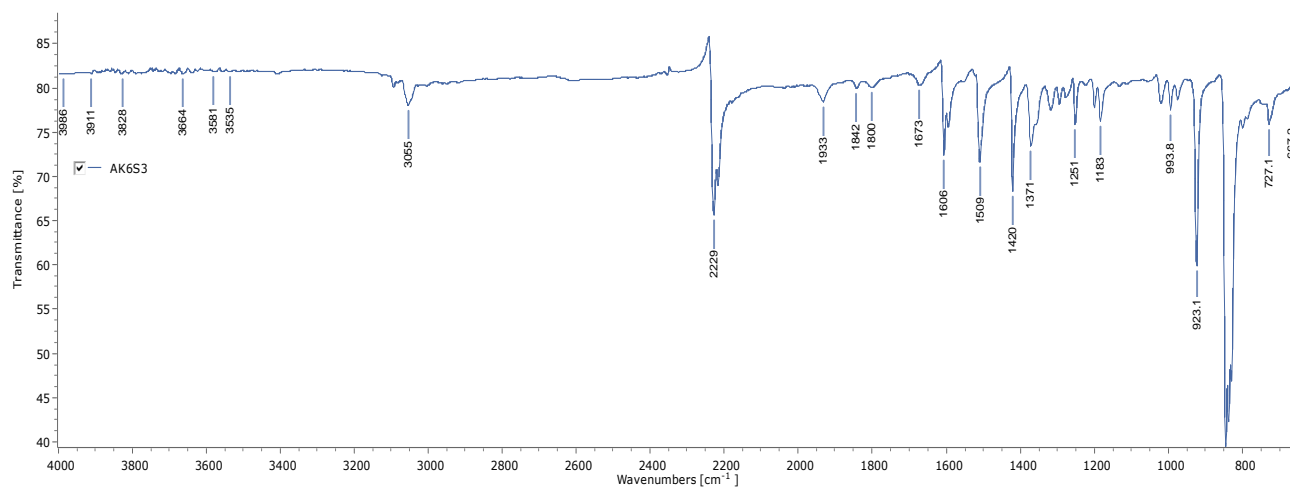


Figure 55: IR spectra of tricyanostilbene ligand.

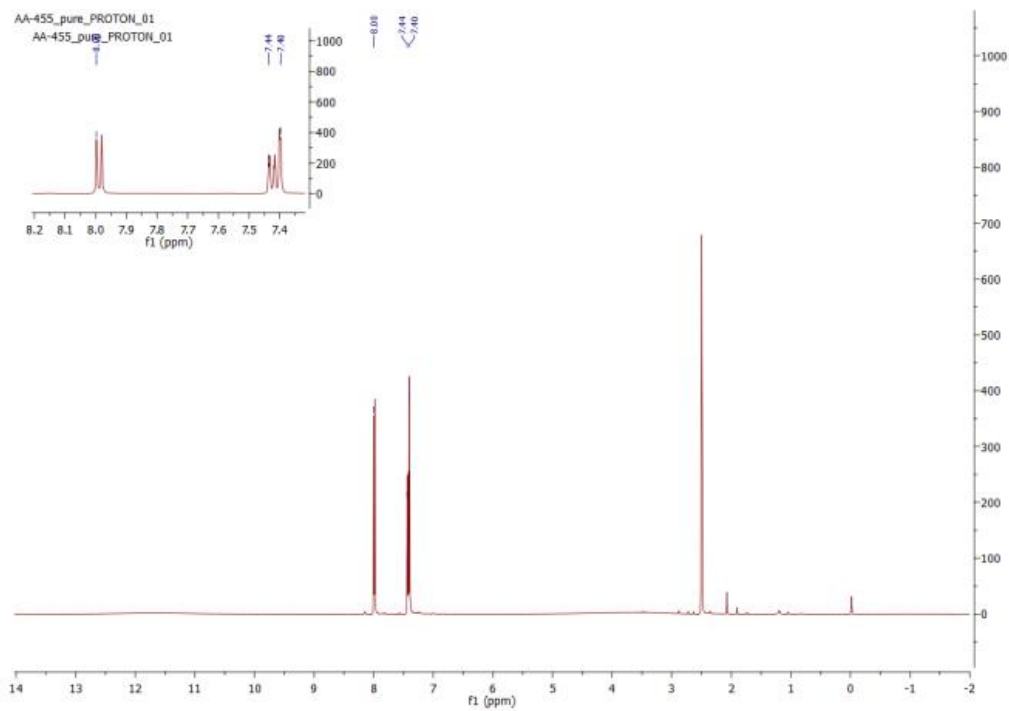


Figure 56: ^1H NMR of AZA linker, using DMSO- d_6 as solvent.⁶²

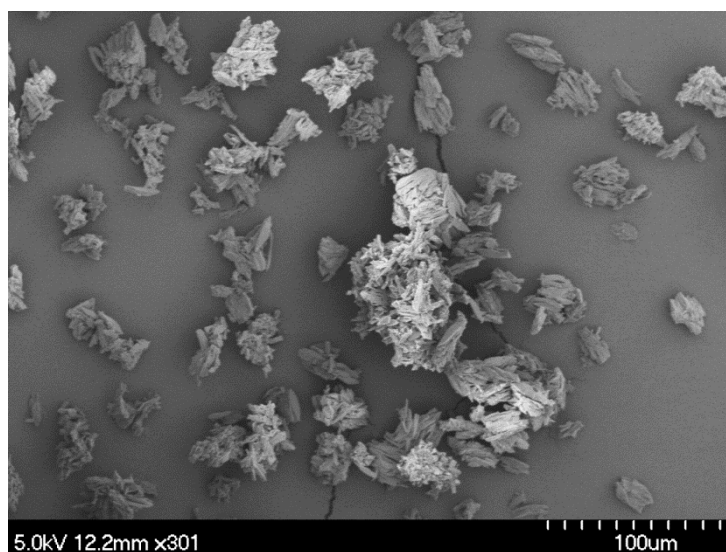


Figure 57: SEM image of solvothermally synthesised 3:1:1 zinc to copper to AZA.

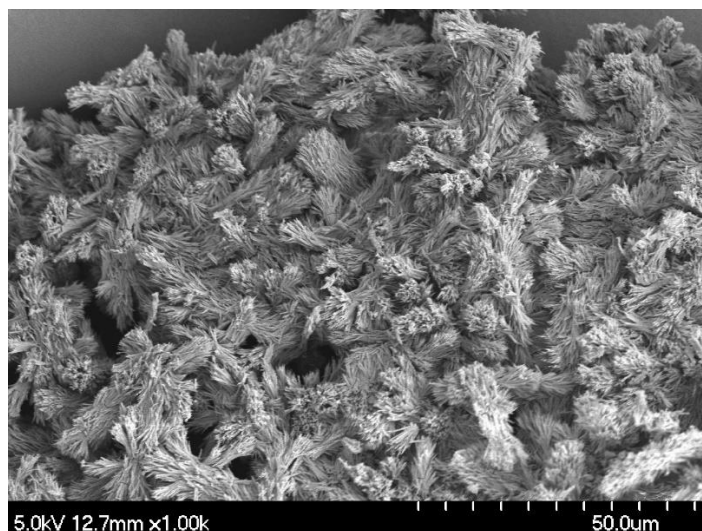


Figure 58: SEM image of solvothermally synthesised 4:1:1 zinc to copper to AZA.

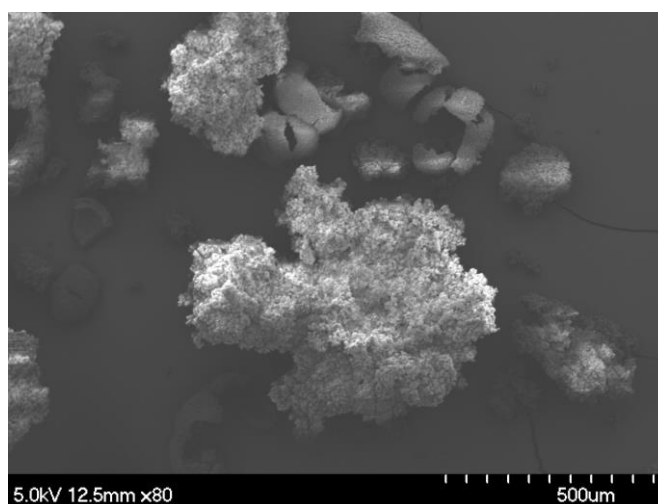


Figure 59: SEM image of solvothermally synthesised 5:1:1 zinc to copper to AZA.

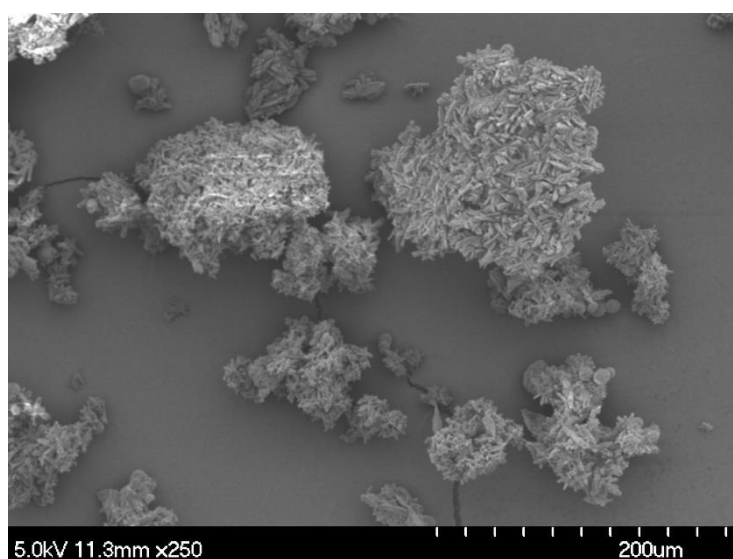


Figure 60: SEM image of solvothermally synthesised 6:1:1 zinc to copper to AZA.

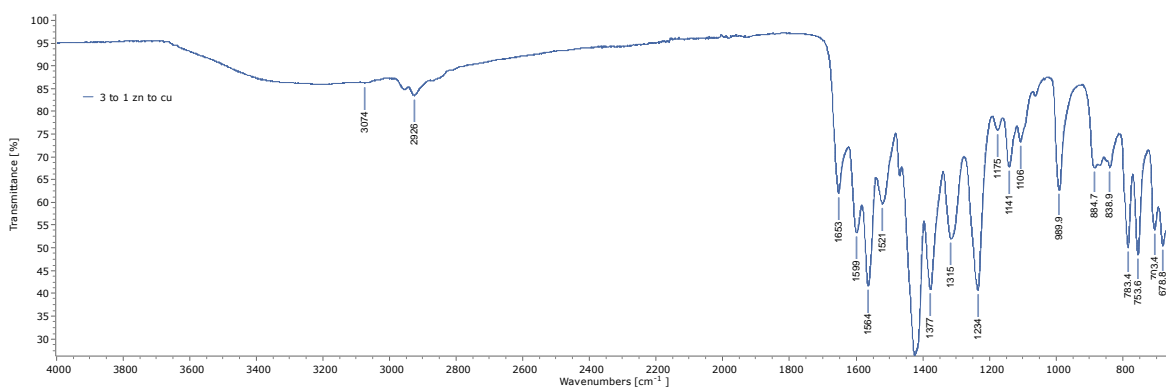


Figure 61: IR spectrum of mixed metal 3:1 zinc and copper MOF synthesised under reflux.

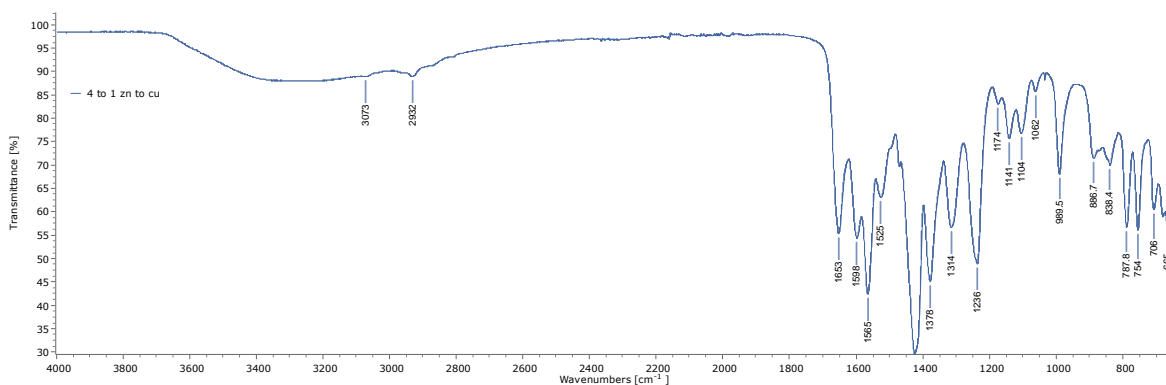


Figure 62: IR spectrum of mixed metal 4:1 zinc and copper MOF synthesised under reflux.

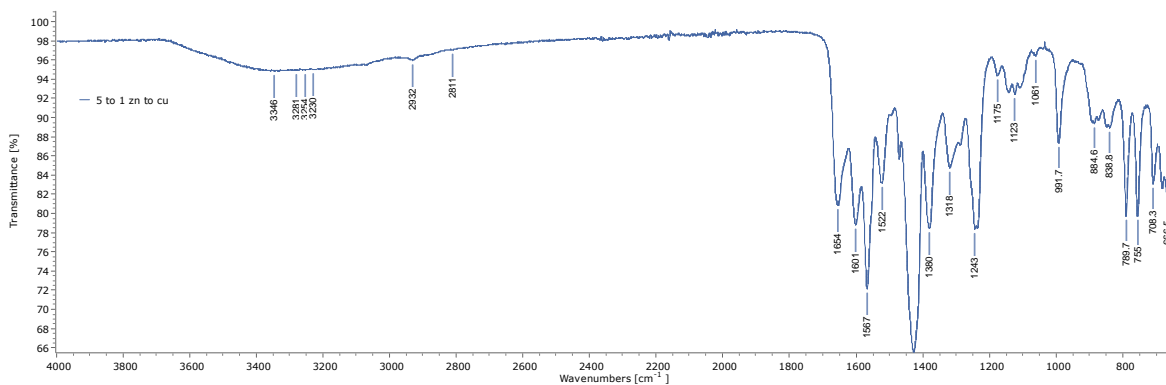


Figure 63: IR spectrum of mixed metal 5:1 zinc and copper MOF synthesised under reflux.

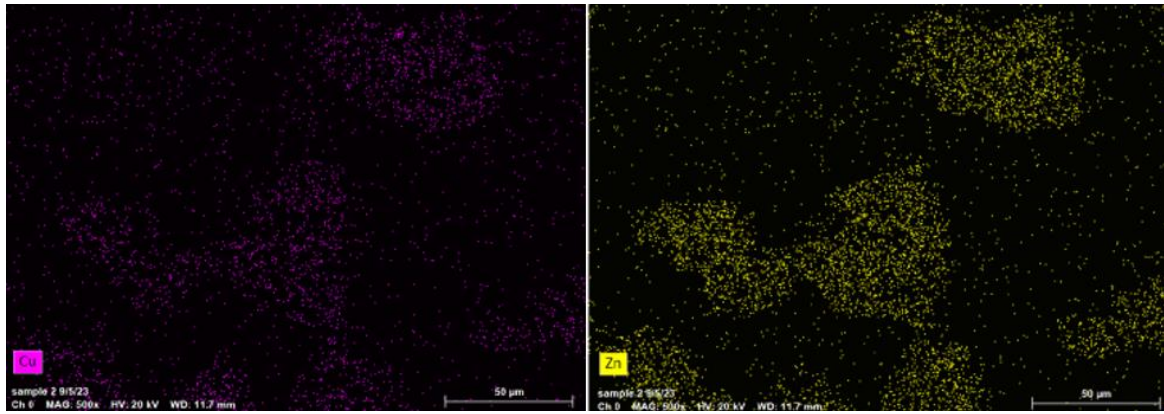


Figure 66: Elemental mapping of Microwave synthesised 3:1:1 zinc to copper to AZA, 1 hour.

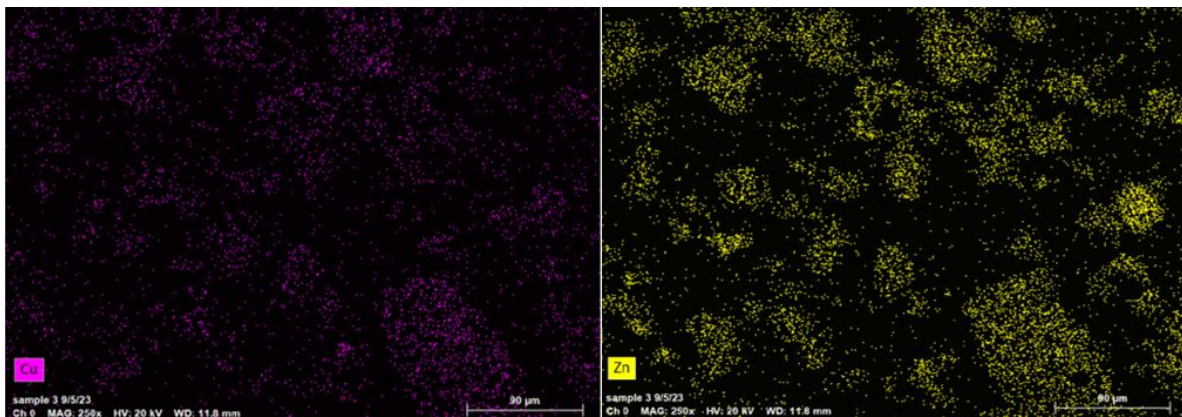


Figure 67: Elemental mapping of Microwave synthesised 3:1:1 zinc to copper to AZA, 1.5 hours.

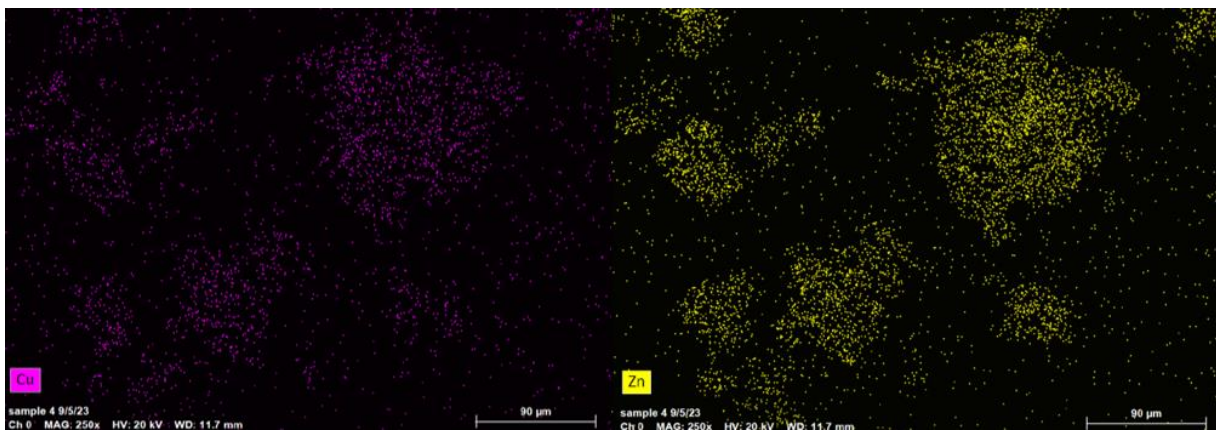


Figure 68: Elemental mapping of Microwave synthesised 3:1:1 zinc to copper to AZA, 2 hours.

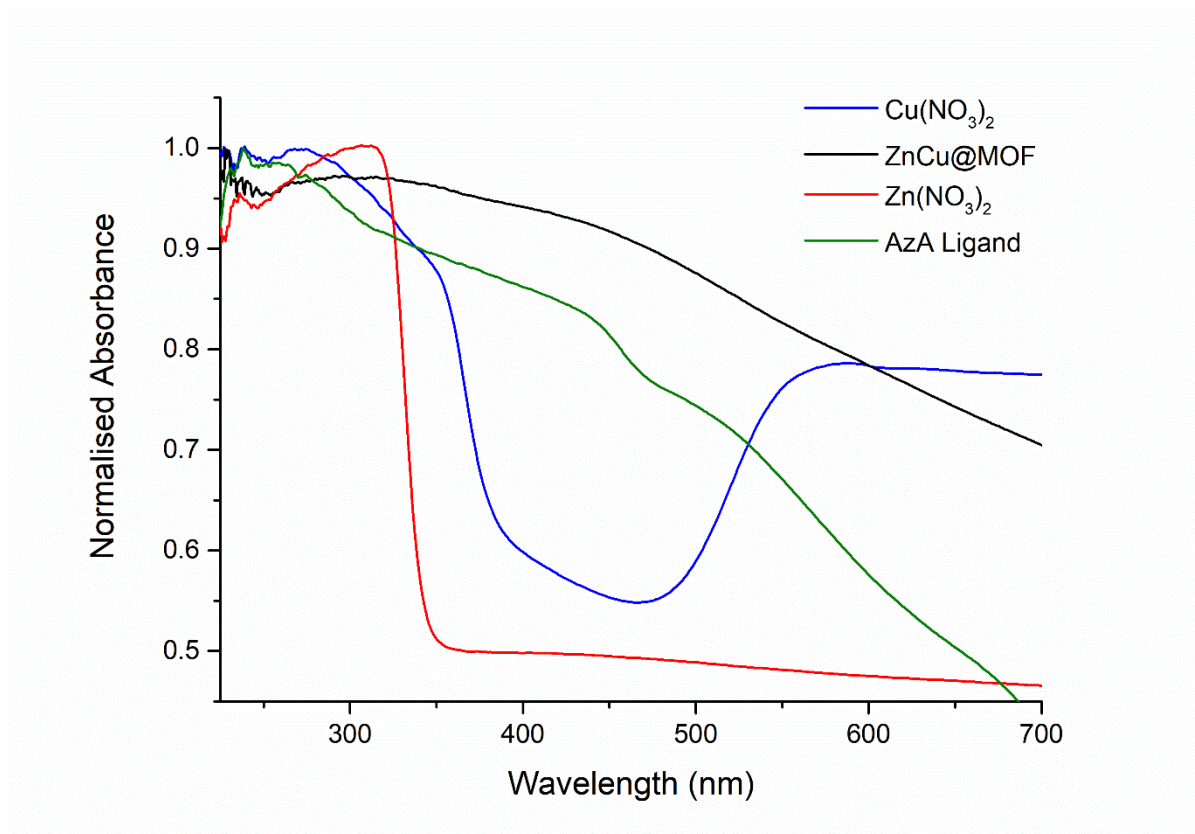


Figure 69: Solid state UV/Vis spectra carried out on the 3:1:1 zinc to copper to AZA 2 hour microwave synthesis, alongside that of the AZA ligand, and both metal sources.